AEDC-TR-78-45

Q.3

COMPARISON OF STORE TRAJECTORY AND AERODYNAMIC LOADS, AND MODEL FLOW-FIELD CHARACTERISTICS OBTAINED IN THE AEDC PWT/4T AND VKF/A WIND TUNNELS AT MACH NUMBER 1.63

D. W. Hill, Jr., J. T. Best, and R. H. Tolbert
ARO, Inc., a Sverdrup Corporation Company

PROPULSION WIND TUNNEL FACILITY
ARNOLD ENGINEERING DEVELOPMENT CENTER
AIR FORCE SYSTEMS COMMAND
ARNOLD AIR FORCE STATION, TENNESSEE 37389

February 1979

Final Report for Period 22 January — 15 February 1977

Prepared for

ARNOLD ENGINEERING DEVELOPMENT CENTER/DOTA
ARNOLD AIR FORCE STATION, TENNESSEE 37389

NOTICES
When U. S. Government drawings, specifications, or other data are used for any purpose other than a definitely related Government procurement operation, the Government thereby incurs no responsibility nor any obligation whatsoever, and the fact that the Government may have formulated, furnished, or in any way supplied the said drawings, specifications, or other data, is not to be regarded by implication or otherwise, or in any manner licensing the holder or any other person or corporation, or conveying any rights or permission to manufacture, use, or sell any patented invention that may in any way be related thereto.
Qualified users may obtain copies of this report from the Defense Documentation Center.
References to named commerical products in this report are not to be considered in any sense as an indorsement of the product by the United States Air Force or the Government.

This report has been reviewed by the Information Office (OI) and is releasable to the National Technical Information Service (NTIS). At NTIS, it will be available to the general public, including foreign nations.

APPROVAL STATEMENT

This report has been reviewed and approved.

John M. Rampy

JOHN M. RAMPY
Project Manager, Analysis and Evaluation Division
Directorate of Test Engineering

Approved for publication:

FOR THE COMMANDER

Robert W. Crossley

ROBERT W. CROSSLEY, Lt Colonel, USAF
Acting Director of Test Engineering
Deputy for Operations

REPORT DOCUMENTATION PAGE		READ INSTRUCTIONS BEFORE COMPLETING FORM
1. REPORT NUMBER AEDC-TR-78-45	2 GOVT ACCESSION NO.	3. RECIPIENT'S CATALOG NUMBER
4. TITLE (and Subtitle) COMPARISON OF STORE TRAJECTORY AND AERODYNAMIC LOADS, AND MODEL FLOW-FIELD CHARACTERISTICS OBTAINED IN THE AEDC PWT/4T AND VKF/A WIND TUNNELS AT MACH NUMBER 1.63		5. TYPE OF REPORT & PERIOD COVERED Final Report, 22 Jan. - 15 Feb. 1977 6. PERFORMING ORG. REPORT NUMBER
7. AUTHOR(s) D. W. Hill, Jr., J. T. Best, and R. H. Tolbert, ARO, Inc., a Sverdrup Corporation Company		8. CONTRACT OR GRANT NUMBER(s)
9 PERFORMING ORGANIZATION NAME AND ADDRESS Arnold Engineering Development Center Air Force Systems Command Arnold Air Force Station, Tennessee 37389		10. PROGRAM ELEMENT, PROJECT, TASK AREA & WORK UNIT NUMBERS Program Element 65807F
11 CONTROLLING OFFICE NAME AND ADDRESS Arnold Engineering Development Center/OIS Air Force Systems Command Arnold Air Force Station, Tennessee 37389		12. REPORT DATE February 1979 13. NUMBER OF PAGES 74
14. MONITORING AGENCY NAME & ADDRESS(if different from Controlling Office)		15. SECURITY CLASS. (of this report) UNCLASSIFIED 15a. DECLASSIFICATION/DOWNGRADING SCHEDULE N/A

16 DISTRIBUTION STATEMENT (of this Report)

Approved for public release; distribution unlimited.

17. DISTRIBUTION STATEMENT (of the abstract entered in Block 20, if different from Report)

18 SUPPLEMENTARY NOTES

Available in DDC.

19 KEY WORDS (Continue on reverse side if necessary and identify by block number)

wind tunnel tests
captive flight
models
predictions
trajectories
aerodynamic loading
flow fields
sampling probes

20. ABSTRACT (Continue on reverse side if necessary and identify by block number)

Tests were conducted in the VKF/A and PWT/4T wind tunnels at AEDC to obtain captive trajectory, aerodynamic loads, and flow-field data in order to assess the ability to reproduce trajectories from tunnel to tunnel. The data were obtained with a 0.05-scale generalized shape aircraft model, an ogive-cylinder store model, and conical flow survey probes at and near the centerline fuselage station pylon and the wing 1/3-semispan station pylon. The tests

DD FORM 1 JAN 73 1473 EDITION OF 1 NOV 65 IS OBSOLETE

20. ABSTRACT (Continued)

were conducted at a Mach number of 1.63 with aircraft model angle of attack set at zero. Generally, the trajectories obtained in the two wind tunnels compared well. There was very good agreement in the translational motion of the store trajectories, with only slight differences in the angular motion in selected cases.

PREFACE

The work reported herein was conducted by the Arnold Engineering Development Center (AEDC), Air Force Systems Command (AFSC), at the request of the Directorate of Test Engineering. Analysis and Evaluation Division (AEDC/DOTA). Mr. J. M. Rampy was the Air Force project manager. The test results presented were obtained by ARO, Inc., AEDC Division (a Sverdrup Corporation Company), operating contractor for the AEDC, AFSC, Arnold Air Force Station, Tennessee, under ARO Project Numbers P41C-L3A and V41A-M9A. Data analysis was completed on November 17, 1977, and the manuscript was submitted for publication on June 28, 1978.

CONTENTS

ILLUSTRATIONS

Figure

Figure Page

TABLES

1.0 INTRODUCTION

The Arnold Engineering Development Center (AEDC) Propulsion Wind Tunnel Facility (PWT) Aerodynamic Wind Tunnel (4T) captive trajectory system has been operational since 1968 (Ref. 1). The test capability of the von Kármán Gas Dynamics Facility (VKF) Supersonic Tunnel (A) has recently been expanded to include captive trajectory testing, and studies to evaluate this captive trajectory system have been reported in Ref. 2. This report presents the results of comparisons made between trajectories generated in Tunnel A and those obtained in Tunnel 4T using the same models and internal balance.

Predicting the trajectory of a store released from an aircraft requires information on the total forces and moments acting on the store. These input data are used with six-degree-of-freedom equations of motion (Refs. 1 and 2) to calculate the store trajectory. In general, static aerodynamic forces and moments are obtained from a store model that is tested in the wind tunnel. The accuracy of the predicted store trajectory is directly related to the accuracy of the experimentally determined aerodynamic coefficients. Consequently, agreement between Tunnel A and Tunnel 4T trajectories will be dependent upon reasonable comparability of the aerodynamic environment in the two wind tunnels. To assess this comparability, three types of test data were obtained in each facility: 1) online captive trajectory calculations, 2) store aerodynamic loads measurements, and 3) flow-field velocity vector measurements. Each type of data was taken both with and without a wing-body model in the wind tunnel.

Testing was accomplished at Mach number 1.63 for the captive trajectory and aerodynamic loads testing, and at Mach number 1.65 for the flow-field data. The aircraft angle of attack and sideslip angle were maintained at zero throughout the testing.

2.0 APPARATUS

2.1 TEST FACILITIES

The Aerodynamic Wind Tunnel (4T) is a closed-loop, continuous flow, variable density tunnel in which the Mach number can be varied from 0.1 to 1.3. Also, nozzle blocks can be installed to give nominal Mach numbers of 1.6 and 2.0. At all Mach numbers, the stagnation pressure can be varied from 300 to 3,700 psfa. The test section is 4 ft square and 12.5 ft long with perforated, variable porosity (0.5- to 10-percent open) walls. It is completely enclosed in a plenum chamber from which the air can be evacuated, allowing part of the tunnel airflow to be removed through the perforated walls of the test section.

Tunnel A is a continuous, closed-circuit, variable density supersonic wind tunnel with an automatically driven flexible-plate-type nozzle and a 40- by 40-in. test section. The tunnel can be operated at Mach numbers from 1.5 to 6 at maximum stagnation pressures from 4,200 to 28,800 psfa, respectively, and stagnation temperatures up to 750°R (M_∞ = 6). Minimum operating pressures range from about one-tenth to one-twentieth of the maximum at each Mach number. The tunnel is equipped with a model injection system which allows removal of the model from the test section while the tunnel remains in operation.

Isometric drawings of typical installations in the PWT/4T and VKF/A wind tunnels are shown in Figs. 1 and 2, respectively. For captive trajectory testing, two separate and independent support systems were used to support the models. The aircraft model was inverted in the test section and supported by an offset sting attached to the main model support system. The store model or conical probe was mounted from the captive trajectory support (CTS) system, which extends down from the tunnel top wall and provides store movement (six degrees of freedom) independent of the aircraft model. Schematic drawings showing some test section details and location of the models in each wind tunnel are shown in Figs. 3 and 4. A more complete description of the Tunnel A and Tunnel 4T test facilities can be found in Ref. 3.

2.2 TEST ARTICLES

The basic models used were provided by Nielsen Engineering and Research, Inc. The wing-body model, which represented a generalized aircraft shape, consisted of an ogive-cylinder-boattail fuselage with a swept wing (NACA 65A006 airfoil section), as shown in Fig. 5. The model had provisions for mounting pylons on the fuselage centerline and 1/3-semispan positions. The center of the wing pylon was located at the 40-percent chord position. For the flow-field testing, wedge-shape pylons, shown in Fig. 6, were mounted on both the fuselage centerline and 1/3-semispan locations. For the aerodynamic loads and trajectory testing, the wedge-shape pylon was mounted on the fuselage centerline and the swept-shape pylon, shown in Fig. 7, was mounted at the 1/3-semispan location. The store model used to obtain aerodynamic loads and trajectory data is shown in Fig. 8. The store model was an ogive-cylinder body with a cruciform-fin tail configuration.

The three-probe rake used in Tunnel A to obtain the flow-field data is shown in Fig. 9. The three conical probes with 40-deg apex angles were spaced 1.5 in. apart in the vertical plane. The 40-deg apex angle cone probe used in Tunnel 4T is shown in Fig. 10. Each of the probes had four equally spaced static pressure orifices around the surface of the cone and a total pressure orifice at the apex of the cone.

2.3 INSTRUMENTATION

A six-component, internal strain-gage balance was used to obtain store aerodynamic force and moment data. Translational and angular positions of the store were obtained from CTS analog inputs during the separation trajectories. The aircraft model angle of attack was determined using an internal, gravimetric angular position indicator. In Tunnel 4T, the pylons contained an optical sensor which enabled the store to be accurately positioned for launch. This sensor emits infrared radiation to the store and detects the reflected radiation. The signal of the reflected radiation is inversely proportional to the distance from the store to the sensor. The optical sensor was sensitive to store positions vertically and laterally with respect to the pylon surface. In Tunnel A, a precision optical level located outside the tunnel test section was used to assist in aligning the store with respect to the pylon surface.

3.0 TEST DESCRIPTION

3.1 TEST CONDITIONS

Wind tunnel nominal test conditions and a complete test summary are given in Tables 1 through 3. Store separation trajectory and aerodynamic loads data were obtained at Mach number 1.63. The flow-field data were obtained at Mach number 1.65. Tunnel conditions were held constant at the desired Mach number while the data were obtained.

To obtain a trajectory in Tunnel 4T, test conditions were established in the tunnel. Operational control of the CTS was then switched to the digital computer, which automatically set the wing-body model at the correct angle of attack, oriented the store model at a position corresponding to the carriage location (including adjustments to correct for sting deflections under load), and then controlled the store movement during the trajectory through commands to the CTS analog system (see block diagram, Fig. 1). In general, the Tunnel 4T trajectory program involves using a quadratic fit of the last three successive measured values of each static aerodynamic coefficient to predict the magnitude of the coefficients over the next time interval (Δt_p) of the trajectory. These predicted values are used to calculate the new position and attitude of the store at the end of the time interval. The equations of motion are evaluated over this time interval using an integration step size of $\Delta t = \Delta t_p/XINT$, where XINT is an integer specified as a program input. The CTS is then commanded to move the store model to this new position, and the aerodynamic loads are again measured. This process was repeated with a constant time interval until a complete trajectory had been obtained.

In Tunnel A, when the wing-body model was set at the desired angle of attack, the store model was manually driven to that angle and then moved near the carriage location. Then, its axial and vertical positions were checked and corrected optically, using the precision optical level. No lateral adjustments were made. Operational control was then switched to the digital computer for store movements during the trajectory calculation. The trajectory program in Tunnel A uses a linear extrapolation method for predicting aerodynamic coefficients over the successive time intervals, and the time interval over which the extrapolation is made is adjusted within the program based on comparisons of the predicted and measured values of each coefficient. Maximum and minimum time intervals and allowable coefficient extrapolation tolerances are program inputs.

3.2 DATA ACQUISITION

In Tunnels A and 4T, a digital computer was programmed to solve the six-degree-of-freedom equations and to calculate the angular and linear displacements of the store relative to the pylon.

When the wind tunnel data are applied to the calculations of the full-scale store trajectories, the measured forces and moments are reduced to coefficient form and then applied with proper full-scale store dimensions and flight dynamic pressure. A scale factor (model to full scale) of 0.05 was used for the simulation of trajectories during these tests; i.e., the full-scale trajectory coordinates were computed and then the tunnel coordinates for positioning the store were determined by multiplying the full-scale values by 0.05. Dynamic pressure was calculated using a flight velocity equal to the free-stream velocity component plus the components of store velocity relative to the wing-body and a density corresponding to the simulated altitude.

The initial portion of each launch trajectory incorporated simulated ejector forces in addition to the measured aerodynamic forces acting on the store. The ejector force, shown in Fig. 11, was considered to act at an angle, ω_m, to the pylon mounting surface. Other full-scale parameters used in the trajectory calculations are listed in Table 1.

3.3 CORRECTIONS

During the acquisition of trajectories and store aerodynamic loads data, deflections of the balance and sting caused by aerodynamic forces on the store model were accounted for in the data reduction program to calculate true store-model positions and angles. Corrections were also made for model weight tares to calculate the net aerodynamic forces on the store model.

Airloads on the conical pressure probes were not measured, and the deflections were not considered large enough to be accounted for in the determination of the probe position.

3.4 PRECISION OF DATA

Uncertainties in the basic tunnel parameters, total pressure (p_t), total temperature (T_t), and Mach number (M_∞), were estimated from repeat calibrations of the instrumentation and from repeatability and uniformity of the test section flow during tunnel calibration. These uncertainties were used to estimate uncertainties in other free-stream properties.

			Uncertainty, Percent					
Tunnel	M_∞	P_T	ΔM_∞	Δp_t	ΔT_t	Δq_∞	Δp_∞	ΔRe
A	1.63	2,707	1.0	0.2	0.5	0.4	3.6	0.9
↓	1.63	2,016	↓	↓	↓	↓	↓	↓
↓	1.65	2,707	↓	↓	↓	↓	↓	↓
4T	1.63	2,670	0.5	0.2	0.1	0.3	1.2	0.6
↓	1.63	2,000	↓	↓	↓	↓	↓	↓
↓	1.65	2,670	↓	↓	↓	↓	↓	↓

The balance uncertainties, based on a 95-percent confidence level, were combined with the uncertainties in the tunnel parameters, assuming a Taylor series error propagation to estimate the precision of the aerodynamic coefficients. The maximum estimated uncertainties are given as follows:

		Uncertainty					
Tunnel	p_t	ΔC_N	ΔC_Y	ΔC_A	ΔC_ℓ	ΔC_m	ΔC_n
A	2,044	0.019	0.019	0.024	0.010	0.070	0.070
A	2,721	0.015	0.015	0.018	0.018	0.052	0.052
4T	1,800	0.012	0.012	0.010	0.005	0.020	0.010
4T	2,670	0.006	0.006	0.007	0.004	0.015	0.014

The estimated uncertainties in store model and probe positioning from the ability of the CTS to set on a specified value were ±0.050 in. (model scale) in X, Y, and Z, and ±0.15 deg in pitch and yaw. The estimated uncertainty in the wing-body angle of attack was ±0.05 deg. From review of data repeatability and accuracy of pressure measurement, the estimated uncertainties in α_{xy} and α_{xz} are ±0.25 deg.

The trajectory data are subject to error from several sources including tunnel conditions, balance measurements, computer inputs, and CTS positioning control. Typical

uncertainties in the full-scale position data resulting from balance precision limitations are presented below. These values are conservative in that they were determined by assuming that the balance measurement errors accumulate as a bias uncertainty in the trajectory calculations. All calculated uncertainties are based on a 95-percent confidence level. The following are maximum uncertainties in the full-scale position data for Tunnels 4T and Tunnel A.

		Uncertainties					
M_∞	I_{yy}, I_{zz}, slug-ft^2	t, sec	ΔX, ft	ΔY, ft	ΔZ, ft	Δθ, deg	ΔΨ, deg
1.63	700	0.4	0.02	0.02	0.02	0.1	0.1
1.63	70	0.4	0.02	0.02	0.02	1.5	1.0

4.0 RESULTS AND DISCUSSION

Three types of test data were obtained in each facility: 1) online captive trajectory calculations, 2) store aerodynamic loads measurements, and 3) flow-field velocity vector measurements. Each type of data was taken both with and without a wing-body model in the wind tunnel. Summaries of the test conditions and data obtained are given in Tables 1 through 3. Selected flow-field and store loads data are presented herein to show comparisons between the two wind tunnels. Trajectories obtained in both tunnels are also presented to show the net effect of the differences in flow-field aerodynamics and integration technique on the calculated store motion. All aerodynamic loads and trajectory data were obtained with the store model rolled to ϕ_m = 45 deg (see Fig. 8) so that the fins were in an "X" configuration. All data were obtained with the wing-body model at zero angle of attack.

4.1 FLOW-FIELD DATA

Flow-field measurements beneath the wing-body centerline pylon and 1/3-semispan pylon are presented in Figs. 12 and 13, respectively. The upwash (α_{xz}) and sidewash (α_{xy}) flow angles are measured with respect to the wind tunnel axial centerline. The upwash and sidewash angles are presented as a function of wing-body model fuselage station (FS) location for various buttock line (BL) and waterline (WL) positions. On each figure, the FS location of the pylon is identified. The upwash and sidewash angles show the same trends in the Tunnel A and Tunnel 4T measurements. Significant differences occur only when the probe is in the vicinity of the pylon; WL = 2.88 for the centerline pylon (Fig. 12) and WL = 1.37 for the 1/3-semispan pylon (Fig. 13). The differences may be attributable to the inability to position the probe in the same location relative to the wing-body aircraft model or to differences in the flow-field environment. As would be expected, the flow angles decreased as distance from the wing-body model increased.

The repeatability of the flow-field data in Tunnel 4T for Reynolds numbers of 3.8 and 5.0 million per foot is shown in Fig. 14. Differences in local flow angle of as much as 1 deg can be seen in Fig. 14. These differences are not considered to be the result of the small change in Reynolds number but could be caused by the repeatability in positioning the probe.

4.2 FREE-STREAM AERODYNAMIC DATA

The variation of the free-stream aerodynamic coefficients with store angle of attack, θ, and yaw angle, ψ, are shown in Fig. 15 for the ogive-cylinder model. The store is statically stable, with a static margin of approximately 1.7 calibers at $\theta = 0$. For negative angles of attack (Fig. 15a), there is a slight difference between the Tunnel A and Tunnel 4T measurements of normal-force and pitching-moment coefficients. The differences may be a function of the model location in the tunnel at which the data were obtained, since the Tunnel A data show some sensitivity to the vertical position (Z_T = 0 and 3 in.). The side-force and yawing-moment coefficient data (Fig. 15b) agree very well between Tunnel A and Tunnel 4T for both plus and minus ψ values and are insensitive to tunnel location.

4.3 AERODYNAMIC DATA IN THE AIRCRAFT FLOW FIELD

The aerodynamic characteristics of the ogive-cylinder store in the flow field of the aircraft are presented in Figs. 16 and 17. In each figure, store aerodynamic data from Tunnel A and Tunnel 4T are presented for comparison and are plotted versus Z_p for variations in X_p, Y_p, θ, and ψ.

Aerodynamic coefficient data in the flow field beneath the centerline pylon position are shown in Fig. 16. The side-force and yawing-moment coefficients show no sensitivity to changes in store position and attitude. This is to be expected since the data were obtained in the wing-body model plane of symmetry. The aerodynamic coefficients obtained in Tunnels A and 4T show good agreement.

Aerodynamic coefficients beneath the 1/3-semispan pylon position are presented in Fig. 17. The comparison of the coefficients obtained in Tunnels A and 4T shows good agreement in all coefficients except the pitching-moment and yawing-moment coefficients. The pitching-moment coefficient (Fig. 17a) agrees well at the carriage position, but between Z_p = 3 and 5 there is a difference of approximately 0.5. The yawing-moment coefficient shows differences of approximately 0.10 at and near the carriage position but agrees well for $Z_p > 2$. These differences in coefficients might be attributed to the differences in the flow-field environment of the store and/or the ability to position the store at the same location relative to the wing-body model. Aerodynamic

coefficients for other X_p and Y_p positions are presented in Figs. 17b through i. These data show the same trends in pitching-moment and yawing-moment coefficient as described above, except that for θ = -15 deg (Fig. 17g) a maximum difference of 0.8 in pitching-moment coefficient occurs near Z_p = 4.0. The effect of these differences in pitching-moment and yawing-moment coefficient on the trajectories from tunnel to tunnel is described in Section 4.4.

4.4 SEPARATION TRAJECTORY DATA

The separation trajectories were simulations of motion in the free-stream flow field and releases from the centerline and 1/3-semispan pylon stations of the wing-body model. Data showing the linear displacements of the store relative to the carriage position and the angular displacements relative to the flight-axis system are presented as functions of full-scale trajectory time. Positive X, Y, and Z displacements (as seen by the pilot) are forward, to the right, and down, respectively. Positive changes in θ and ψ (as seen by the pilot) are nose up and nose to the right, respectively. The full-scale store parameters used in the trajectory calculations are listed in Table 1. In all the trajectories, the store rolling motion was specified to be zero. In the simulation of the trajectories, the aircraft motion was unaccelerated and in level flight at a simulated pressure altitude of 40,000 feet. A scale factor (model to full scale) of 0.05 was assumed in the calculations.

The trajectories obtained in the free stream for the ogive-cylinder store are presented in Fig. 18. The trajectory data are presented to show variations with and without ejector force (Figs. 18a and b), and with the ejector line of action specified at 0 or 90 deg (Figs. 18c and d) to provide pitch motion or yaw motion, respectively. In all cases, the translational motions of the trajectories obtained in Tunnels A and 4T agree very well, but the angular motions show slight differences. The largest difference in pitch or yaw motion in Fig. 18 is approximately 1 deg. This difference falls within the uncertainties, as discussed in Section 3.4. The repeatability of the Tunnel A trajectory shown in Fig. 18c is excellent. The differences in the trajectory angular motions between Tunnels A and 4T may be attributable to a combination of the differences in store free-stream characteristics (Fig. 15) and to nonuniformities in the respective airstreams. The trajectories obtained from the centerline pylon station of the wing-body are presented in Fig. 19. The trajectory data are presented for variations in ejector moment arm (Figs. 19a and b) and for variations in the integration time interval (Fig. 19a). The translational and angular motions of the store agree extremely well between Tunnel A and Tunnel 4T. The effect of increasing the integration interval was to increase the nose-down pitch motion slightly ($\approx$ 0.5 deg). The differences in the angular motions were more pronounced when an integration interval of 0.020 sec was used in 4T. As the time interval, Δt_p, is increased, the prediction of coefficients (Section 3.2) will become less accurate as a result of

nonlinear flow field, thus producing deviations in the calculated angular and translational motions. An integration interval of 0.010 sec appears to give satisfactory results in the trajectory integration process for these models. A schlieren photograph obtained in Tunnel A showing the wing-body model flow field with the store at the beginning and end of a centerline pylon trajectory is shown in Fig. 20. This photograph shows the complexity of the wing-body model flow-field environment, which consists of multiple oblique shocks which would make measured flow characteristics and store reactions very sensitive to probe and store location.

The trajectories obtained from the 1/3-semispan pylon station of the wing-body model are presented in Fig. 21. The trajectory data are presented for variations in ejector moment arm and the ejector force line of action. The comparisons between Tunnels A and 4T trajectory data show good agreement in the translational and pitch motions, but the Tunnel 4T trajectories show as much as 2 deg more nose-outboard (negative) yaw motion (Figs. 21a through 21e). The differences from tunnel to tunnel in pitching-moment and yawing-moment coefficient data obtained in the aircraft flow field, as discussed in Section 4.3, do not appear to have a significant effect on the angular motion of the store. The direction in yaw motion is consistent with the direction of offsets in the yawing-moment coefficient, C_n, as shown in Figs. 17a and d. These data also indicate that an integration interval of 0.010 sec will give an acceptable integrated motion. The slight variation of Reynolds number in Fig. 21e is assumed to have little effect on the trajectory. The repeatability of a Tunnel 4T trajectory from the 1/3-semispan pylon station is shown in Fig. 22. The only difference occurred in the pitch motion amplitude, and was approximately 0.25 deg.

5.0 CONCLUDING REMARKS

A comparison of Tunnel A and Tunnel 4T wind tunnel data was made to assess the ability to reproduce online captive trajectory calculations from tunnel to tunnel. To assess this comparability, three types of test data were obtained in each facility: 1) online captive trajectory calculations, 2) store aerodynamic loads measurements, and 3) flow-field velocity vector measurements. Each type of data was taken both with and without a wing-body model at a nominal Mach number of 1.6.

Overall, there was good agreement between trajectories from Tunnel A and Tunnel 4T with and without the presence of the wing-body model. The translational motion of the trajectories agreed very well, with only slight differences in angular motion (2 deg) in selected cases. The differences in angular motion were the result of variations in the flow-field environment of the store in each tunnel. This was evidenced by small

the differences in both store aerodynamic loads and flow-field velocity vector data. The differences in the tunnel-to-tunnel aerodynamic loads and flow-field velocity vector measurements might be attributable to the small uncertainties in positioning the store model or probe in the same location relative to the wing-body model. In an aircraft flow field where there are multiple shocks and strong flow-field gradients, the aerodynamic loads or flow-field velocity vectors measured could be very sensitive to small changes in the store or probe location.

REFERENCES

1. Christopher, J. P. and Carleton, W. E. "Captive-Trajectory Store-Separation System of the AEDC-PWT 4-Foot Transonic Tunnel." AEDC-TR-68-200 (AD839743), September 1968.

2. Billingsley, J. P., Burt, R. H., and Best, J. T. "Store Separation Testing Techniques at the Arnold Engineering Development Center, Volume III: Description and Validation of Captive Trajectory Store Separation Testing in the von Kármán Facility." AEDC-TR-79-1.

3. Test Facilities Handbook (Tenth Edition). "Propulsion Wind Tunnel Facility, Vol. 4" and "von Kármán Gas Dynamics Facility, Vol. 3." Arnold Engineering Development Center, May 1974.

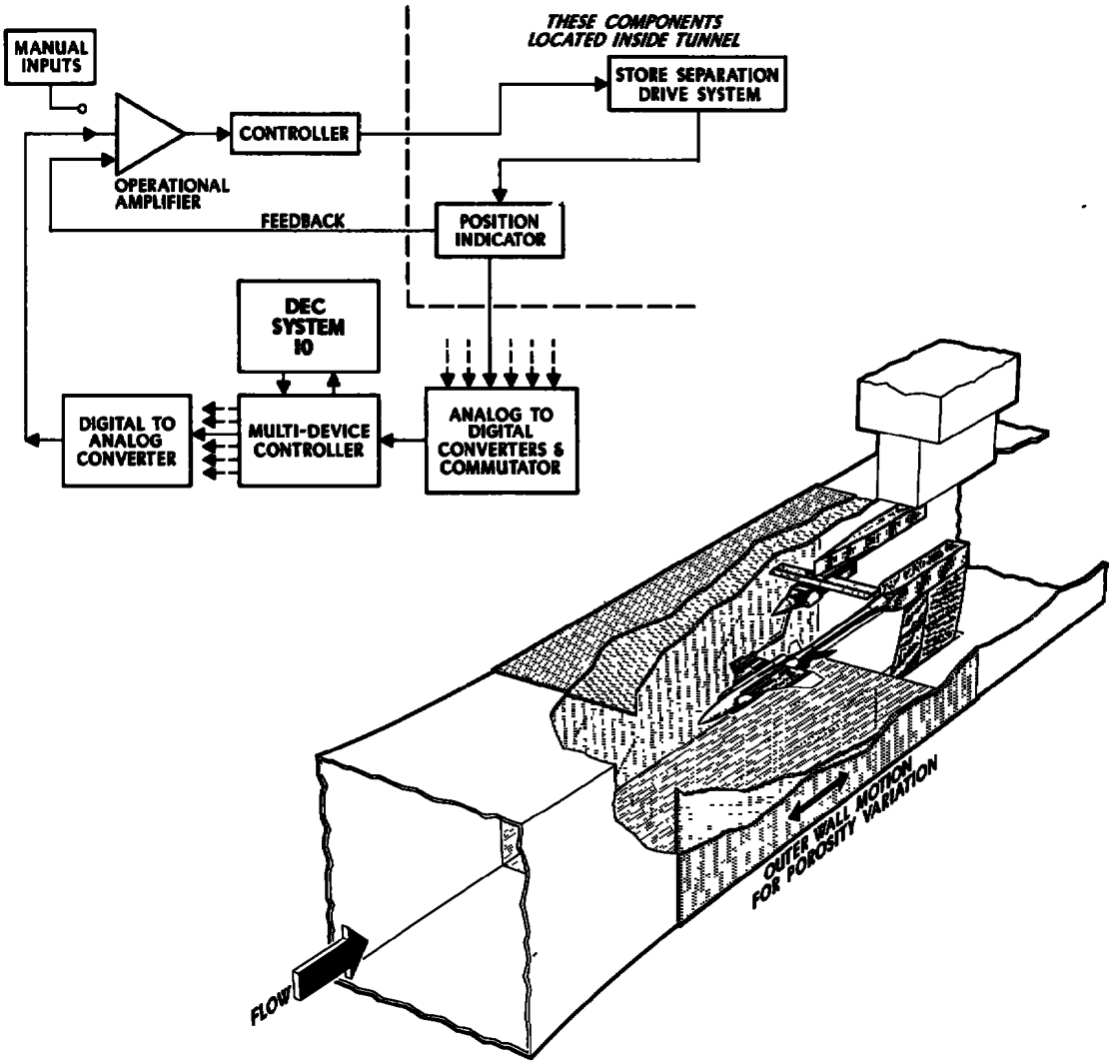

Figure 1. Typical tunnel 4T store separation installation and block diagram of the computer control loop.

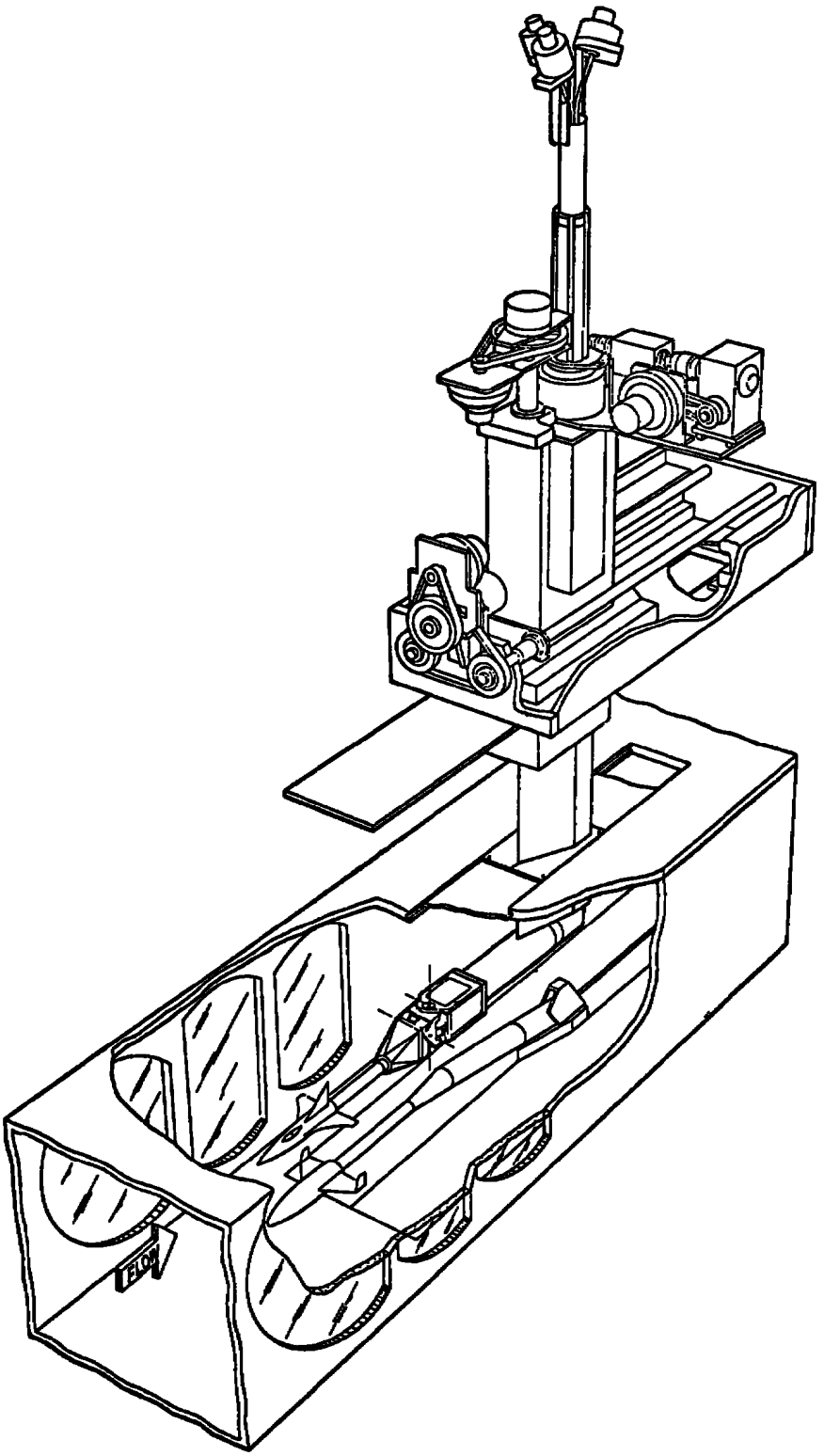

Figure 2. Typical Tunnel A store separation installation.

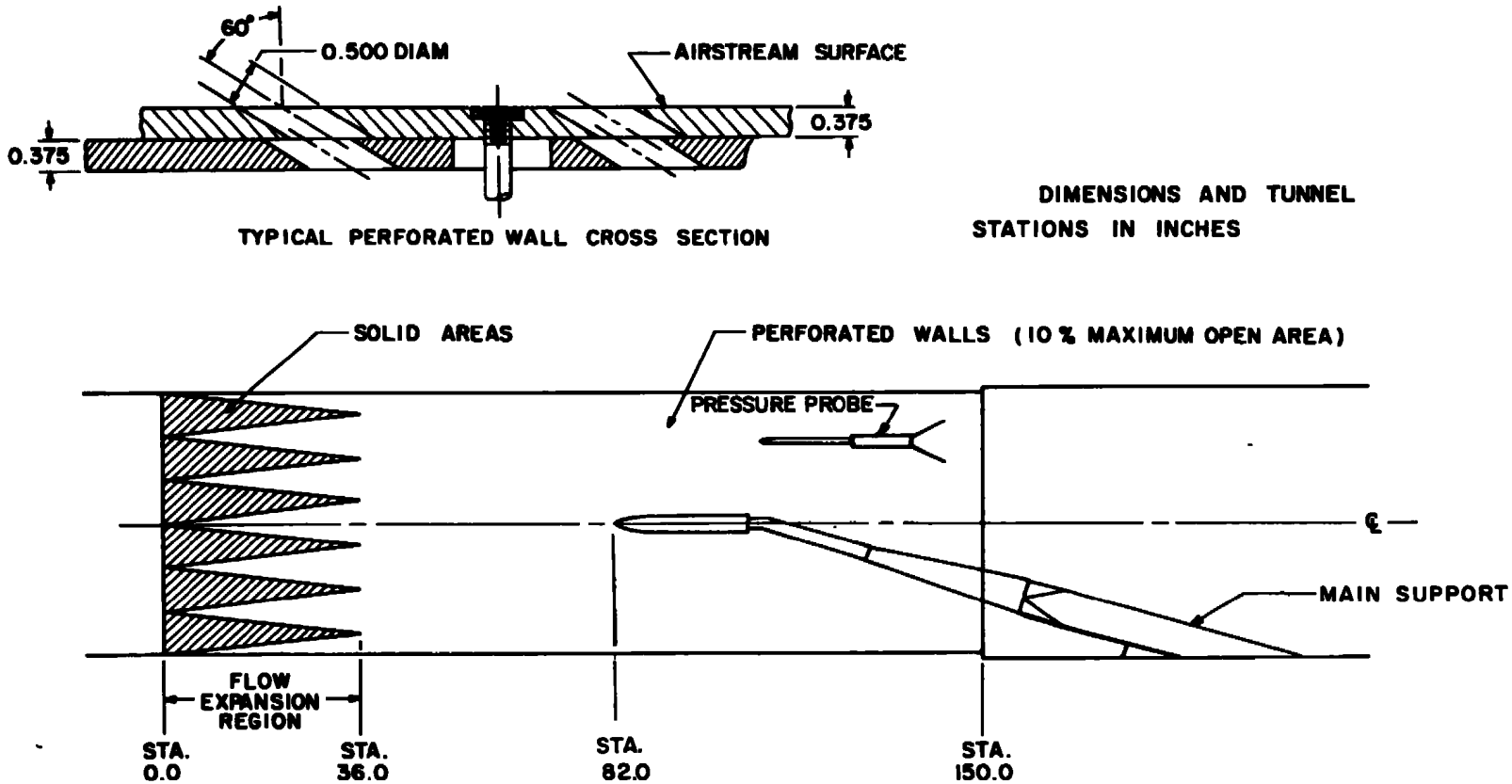

Figure 3. Tunnel 4T test section showing pressure probe and wing-body model location.

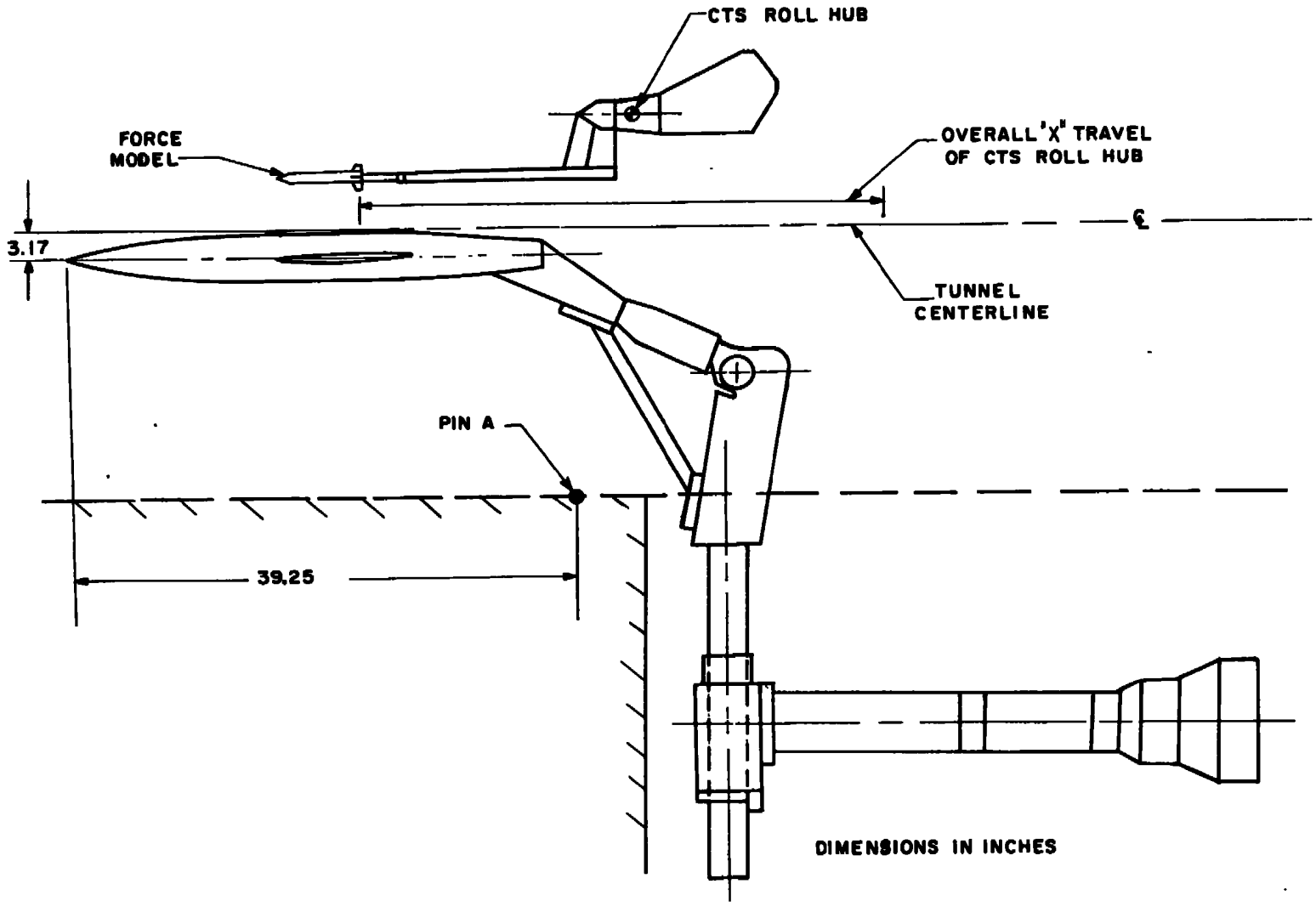

Figure 4. Tunnel A test section showing force model and wing-body location.

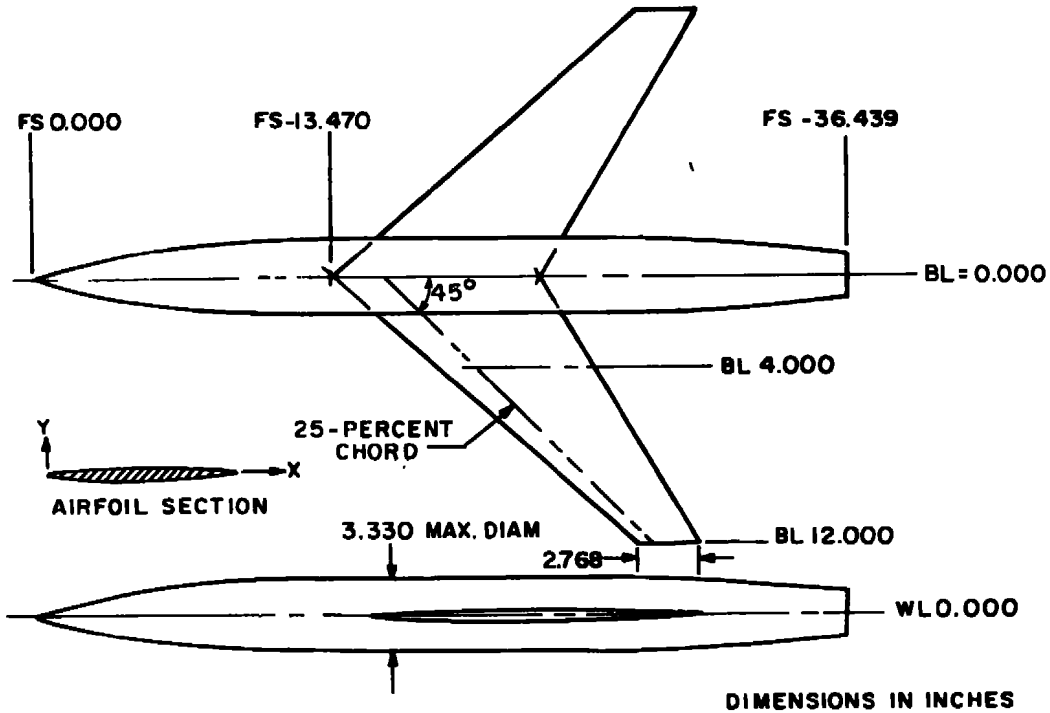

BODY COORDINATES

STATION PERCENT LENGTH	RADIUS PERCENT LENGTH
0.00	0.00
3.28	0.91
6.57	1.71
9.86	2.41
13.15	3.00
16.43	3.50
19.72	3.90
23.01	4.21
26.29	4.43
29.58	4.53
32.00	4.57
75.34	4.57
76.69	4.54
79.98	4.38
83.26	4.18
86.55	3.95
89.84	3.72
93.13	3.49
96.41	3.26
100.00	3.02

AIRFOIL COORDINATES

X, % CHORD SEE SEC.	Y, % CHORD SEE SEC.
0.00	0.000
0.50	0.464
0.75	0.563
1.25	0.718
2.50	0.981
5.00	1.313
7.50	1.591
10.00	1.824
15.00	2.194
20.00	2.474
25.00	2.687
30.00	2.842
35.00	2.945
40.00	2.996
45.00	2.992
50.00	2.925
55.00	2.793
60.00	2.602
65.00	2.364
70.00	2.087
75.00	1.775
80.00	1.437
85.00	1.083
90.00	0.727
95.00	0.370
100.00	0.013
L.E RADIUS 0.229% CHD	
T.E RADIUS 0.014% CHD	

Figure 5. Details and dimensions of wing-body model.

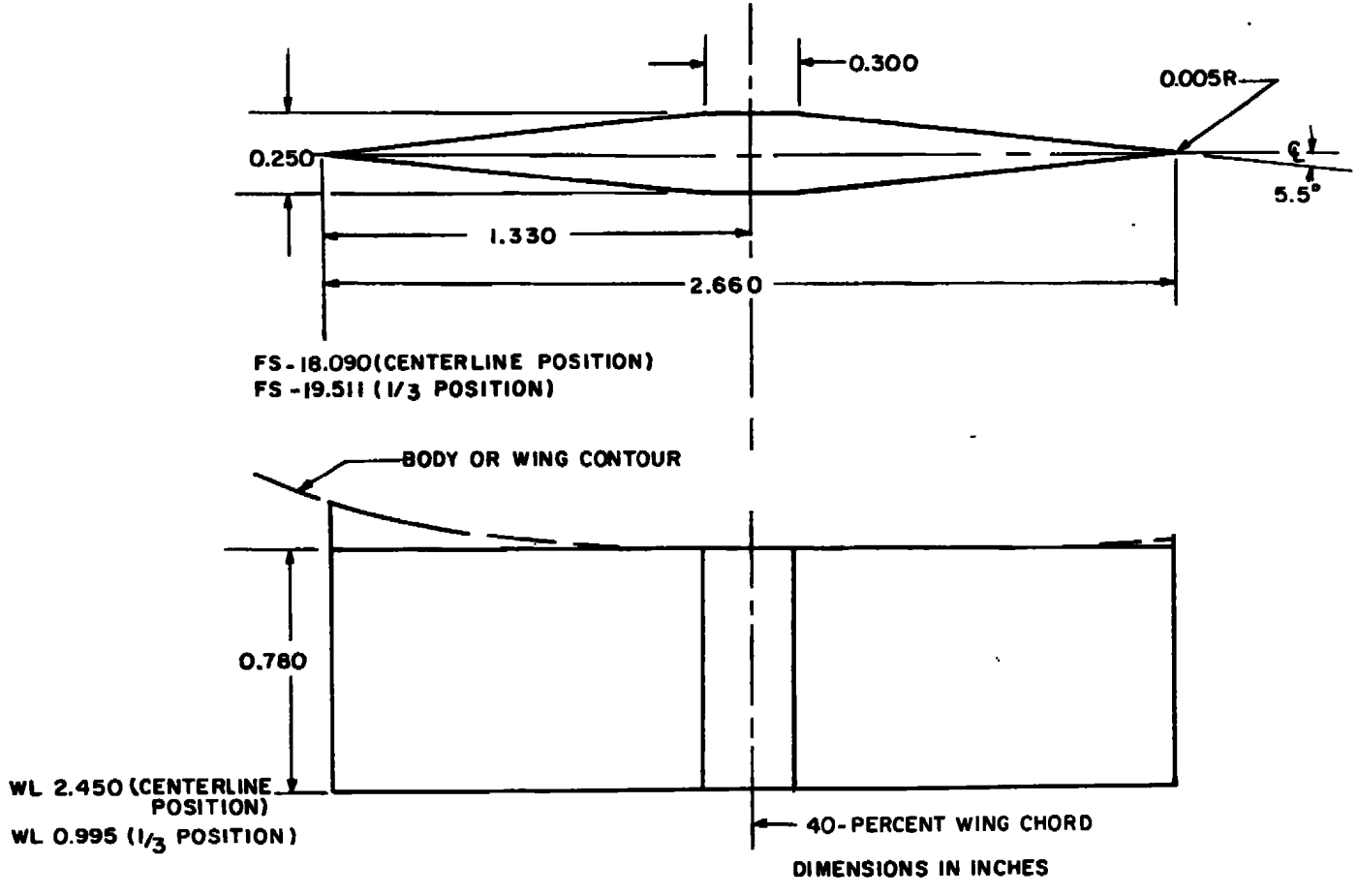

Figure 6. Details and dimensions of wedge-shape pylon.

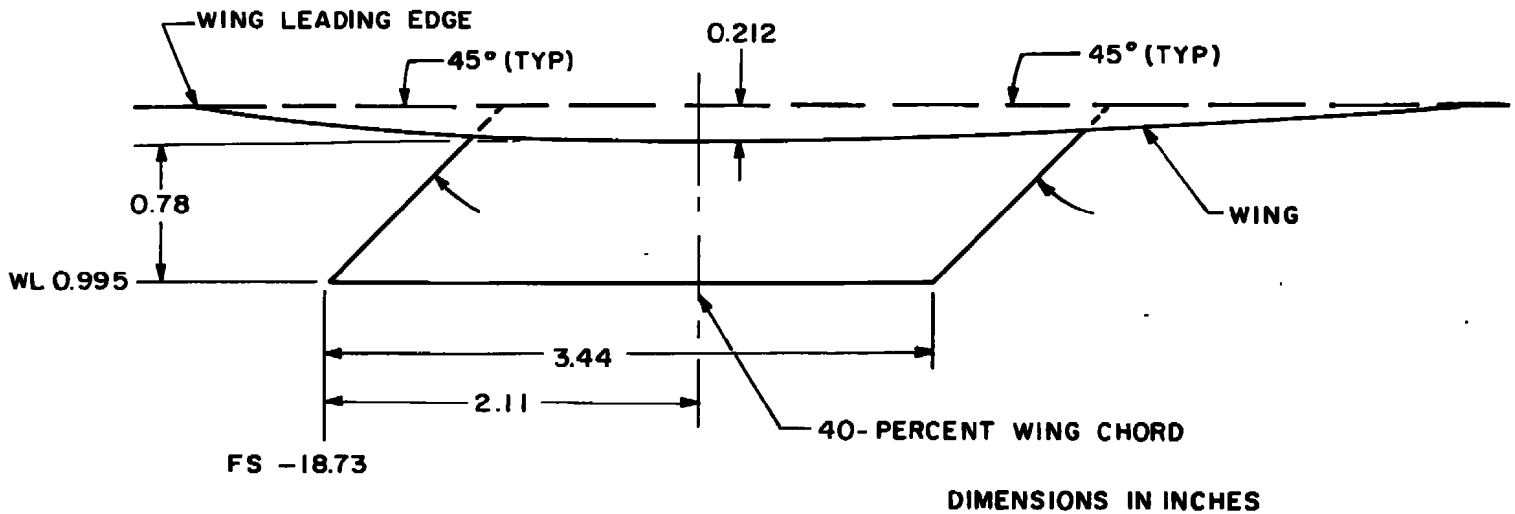

Figure 7. Details and dimensions of swept-shape pylon.

CG LOCATION AT CARRIAGE POSITION		
	℄ PYLON	1/3-SEMISPAN PYLON
FS	-19.42	-20.84
BL	0	-4.00
WL	2.875	1.42

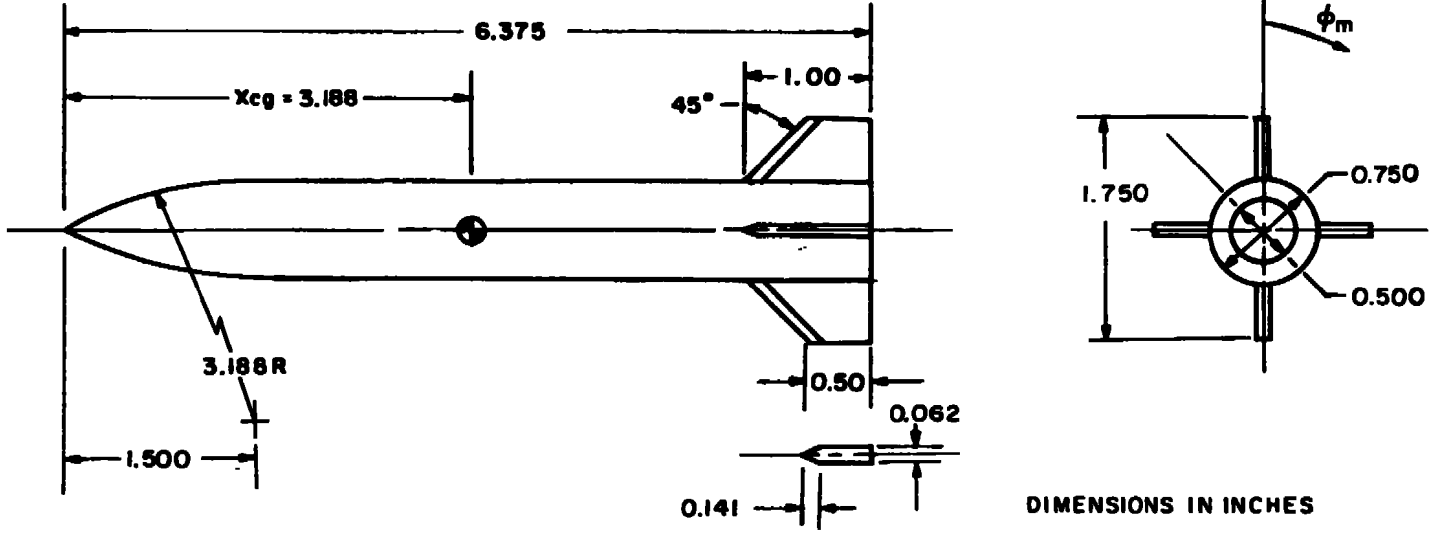

Figure 8. Details and dimensions of ogive-cylinder force model.

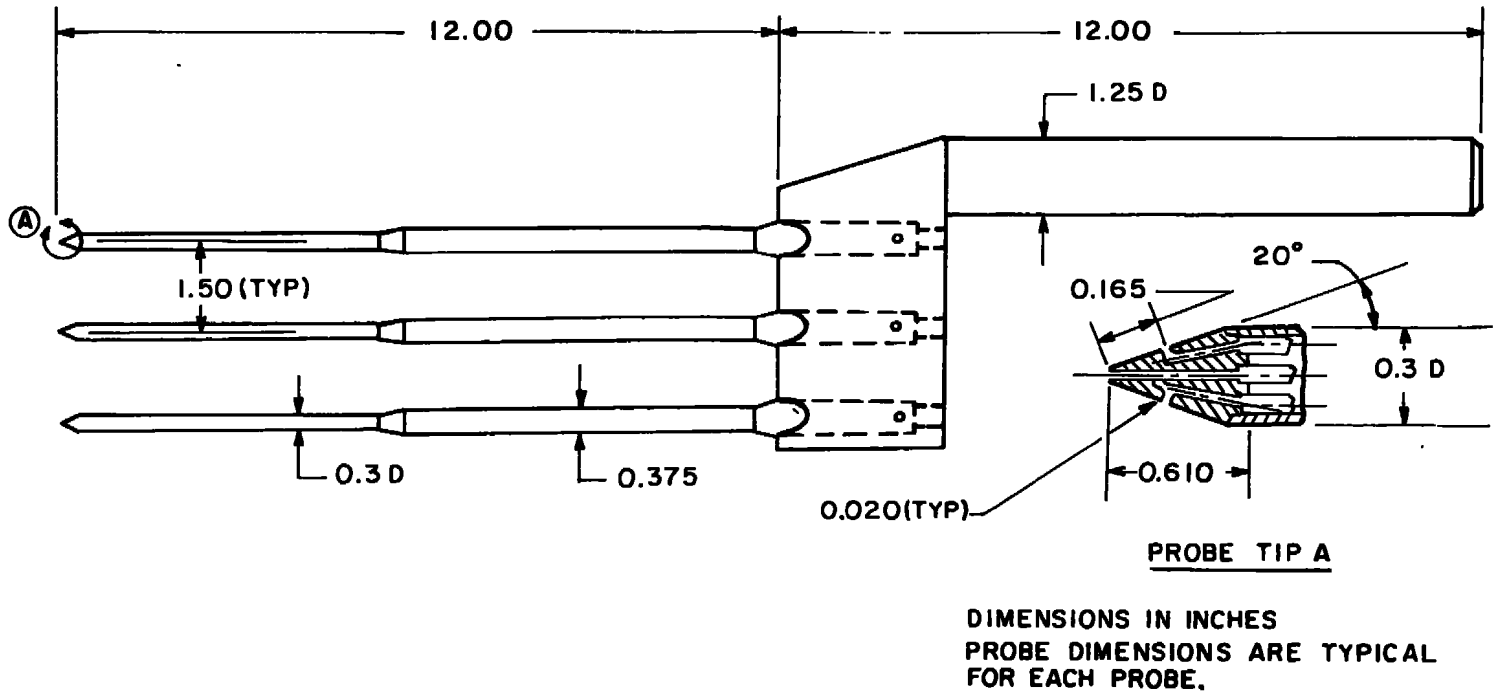

Figure 9. Details and dimensions of Tunnel A 40-deg cone pressure probe rake.

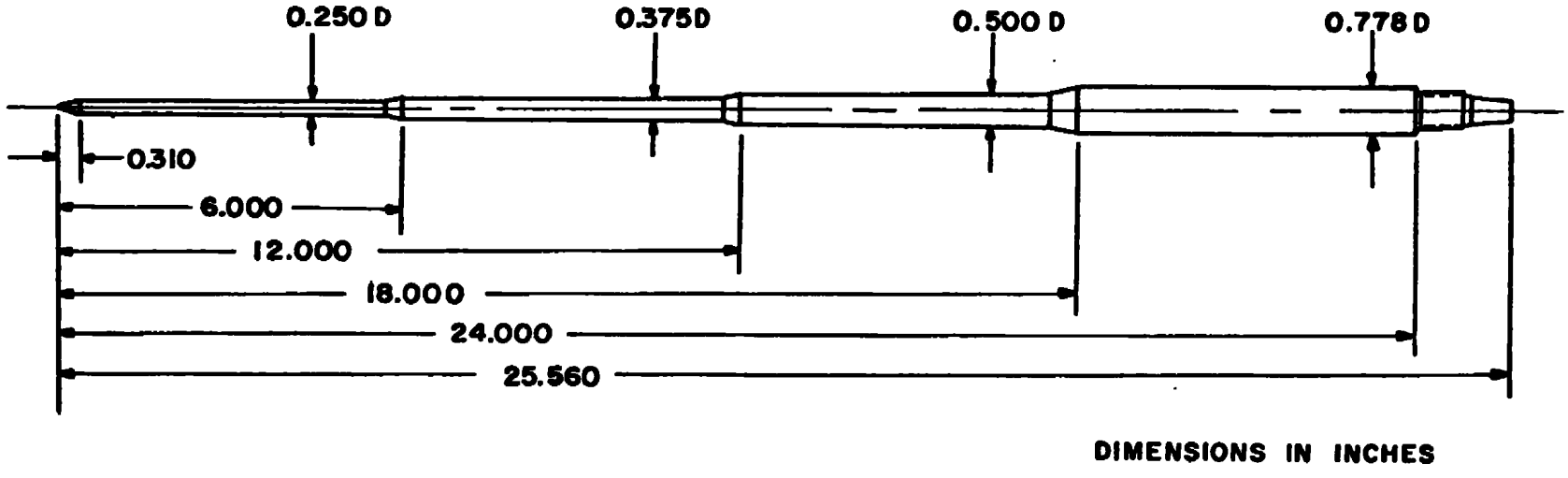

a. General details

Figure 10. Details and dimensions of the Tunnel 4T 40-deg cone pressure probe.

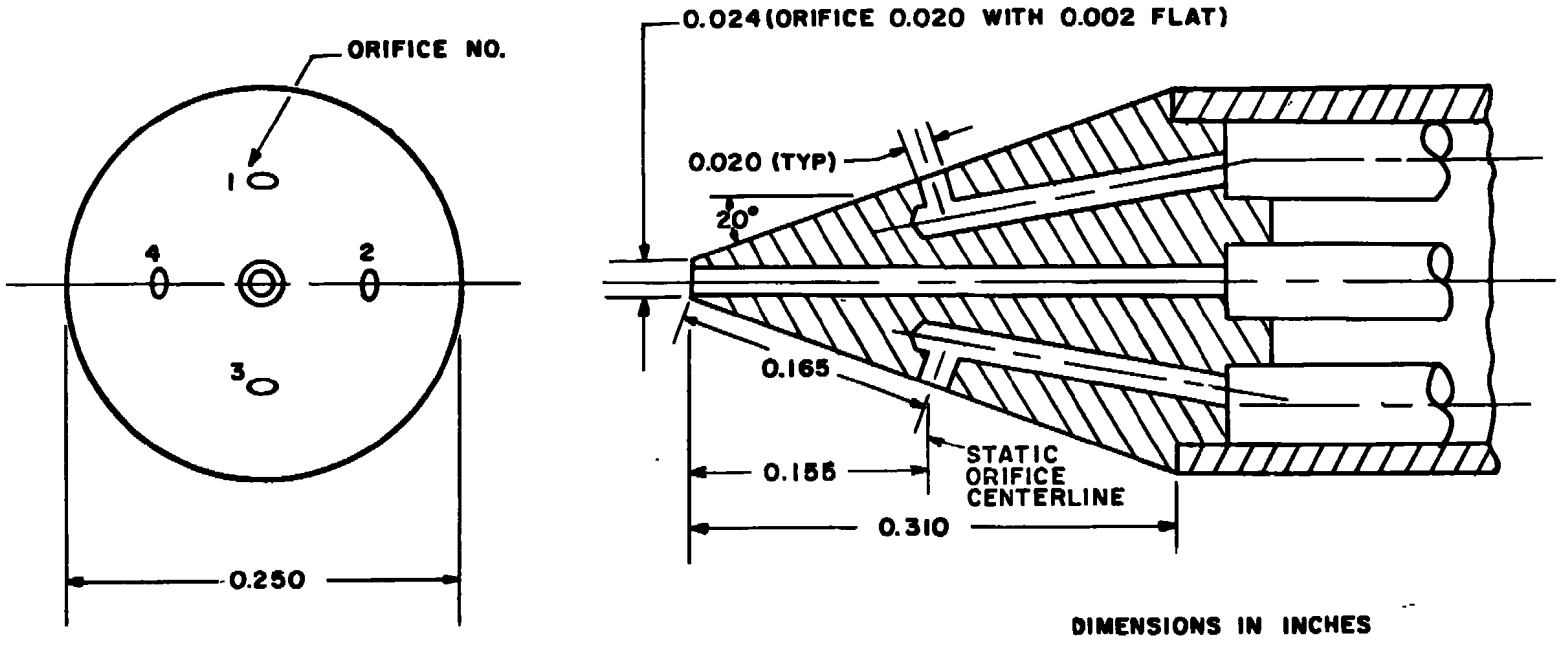

b. Probe tip details

Figure 10. Concluded.

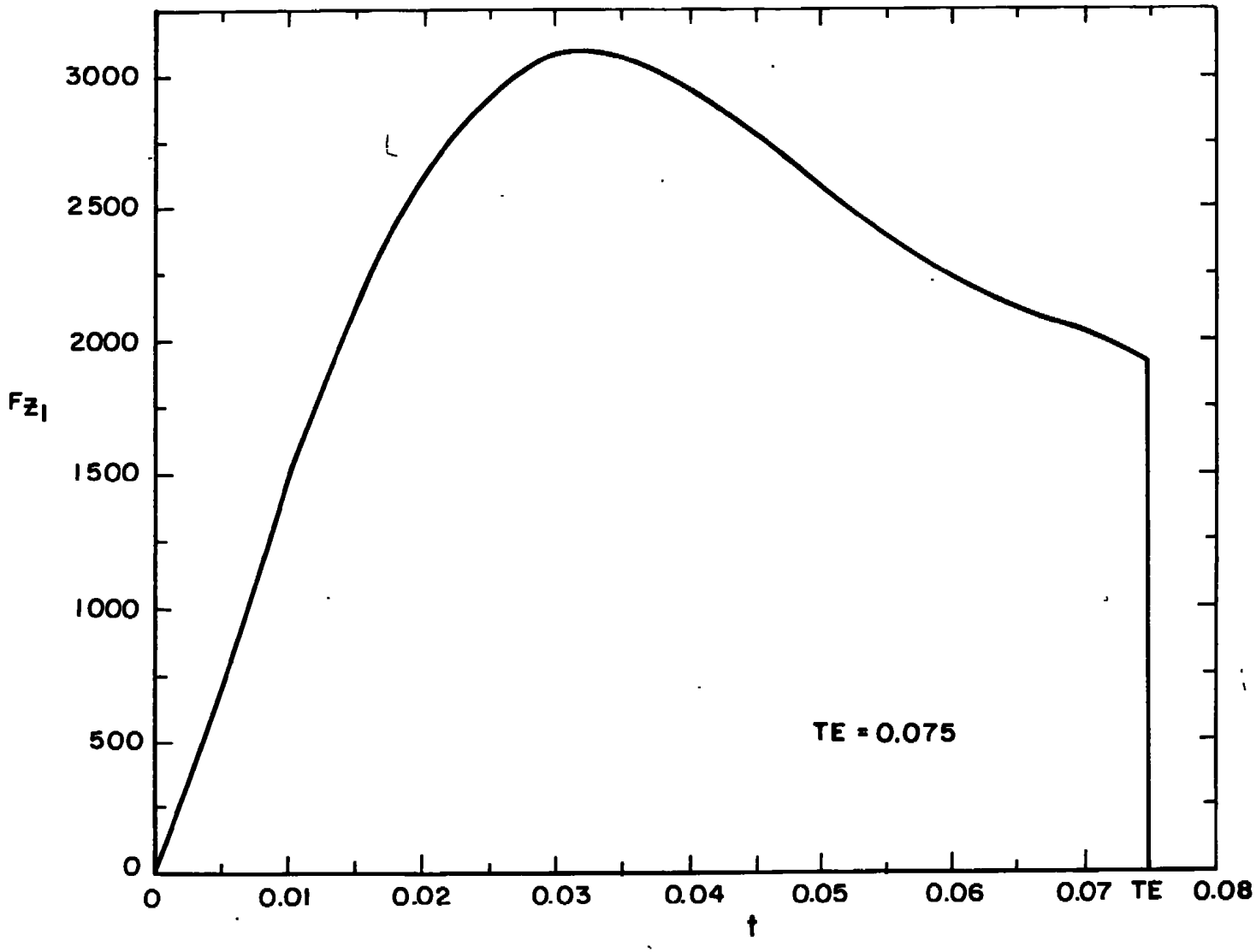

Figure 11. Simulated ejector force function.

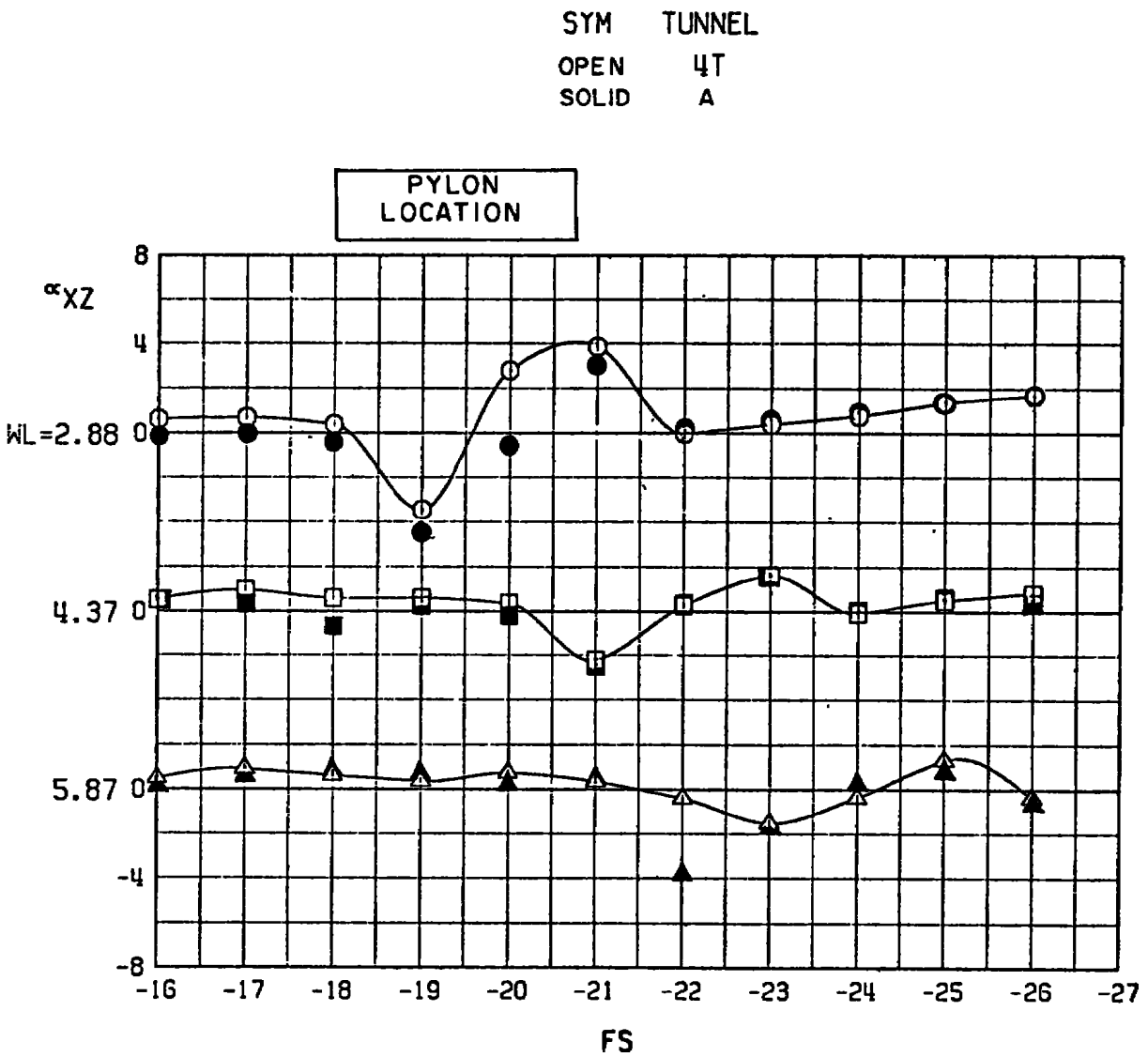

a. Upwash angle, BL = 0

Figure 12. Flow-field measurements beneath the centerline pylon station, M_∞ = 1.65, Re/ft = 5.0 x 10^{-6}.

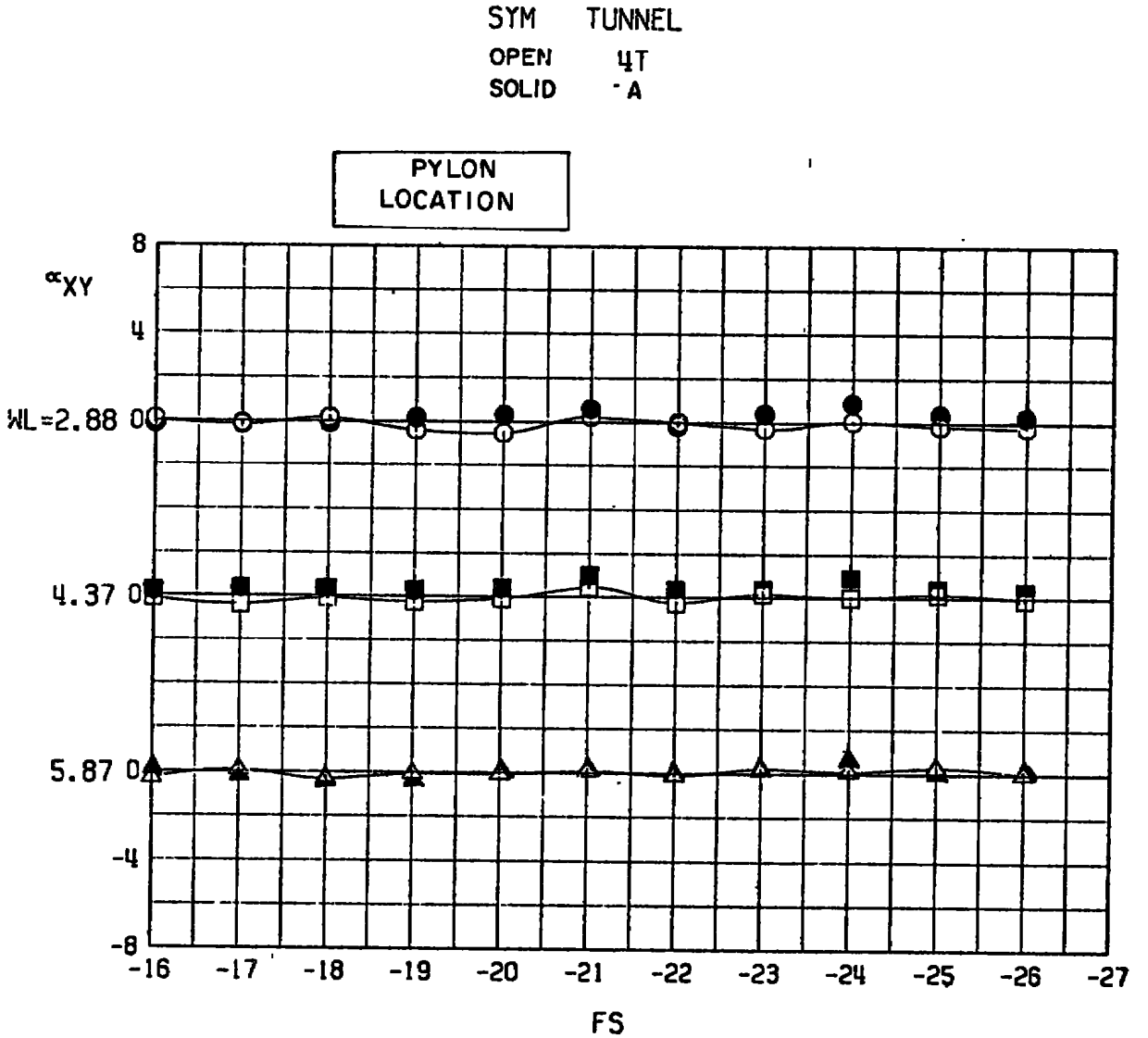

b. Sidewash angle, BL = 0
Figure 12. Concluded.

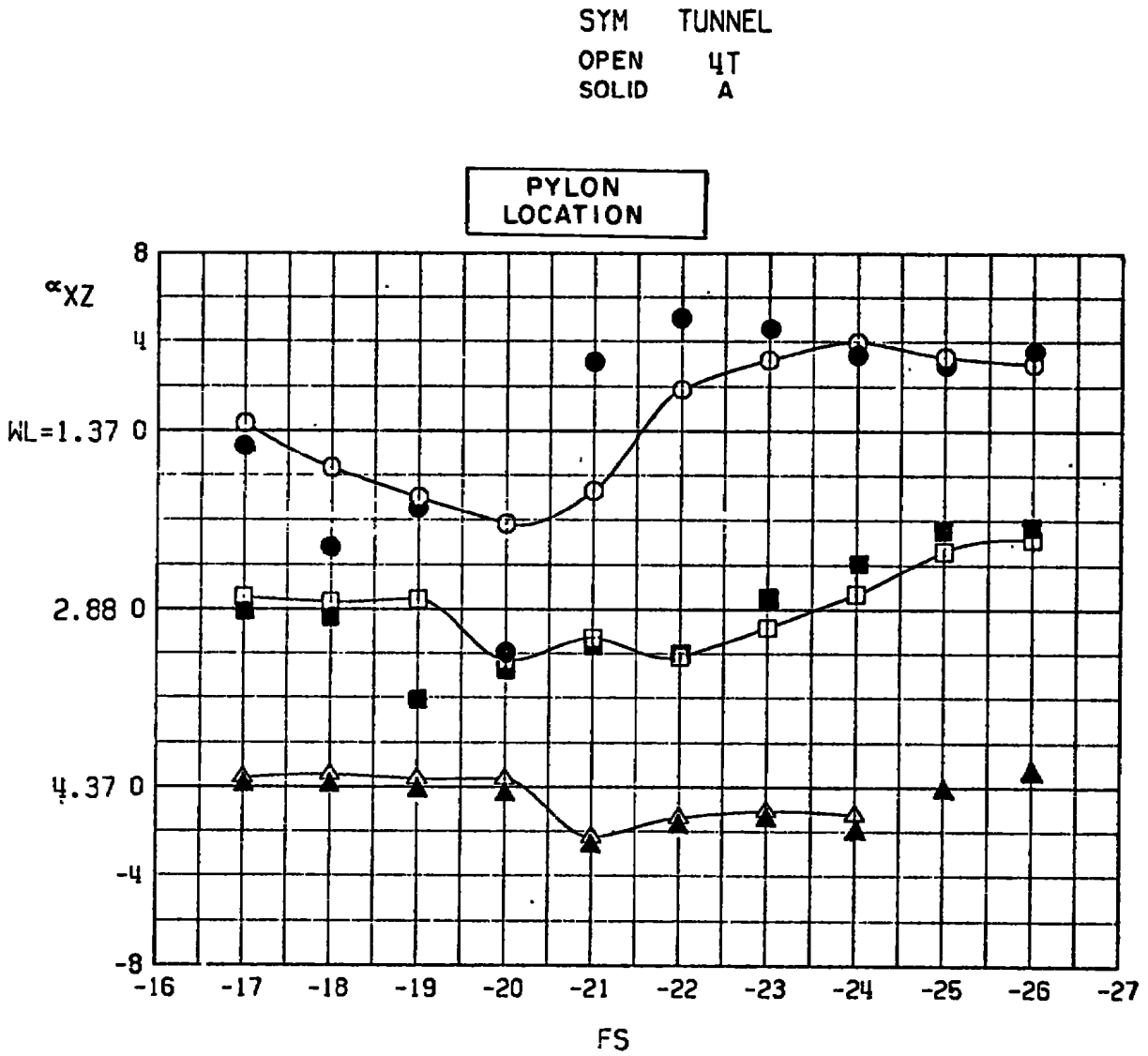

a. Upwash angle, BL = 4.0 in.

Figure 13. Flow-field measurements beneath the 1/3-semispan pylon station, M_∞ = 1.65, Re/ft = 5.0 x 10^{-6}.

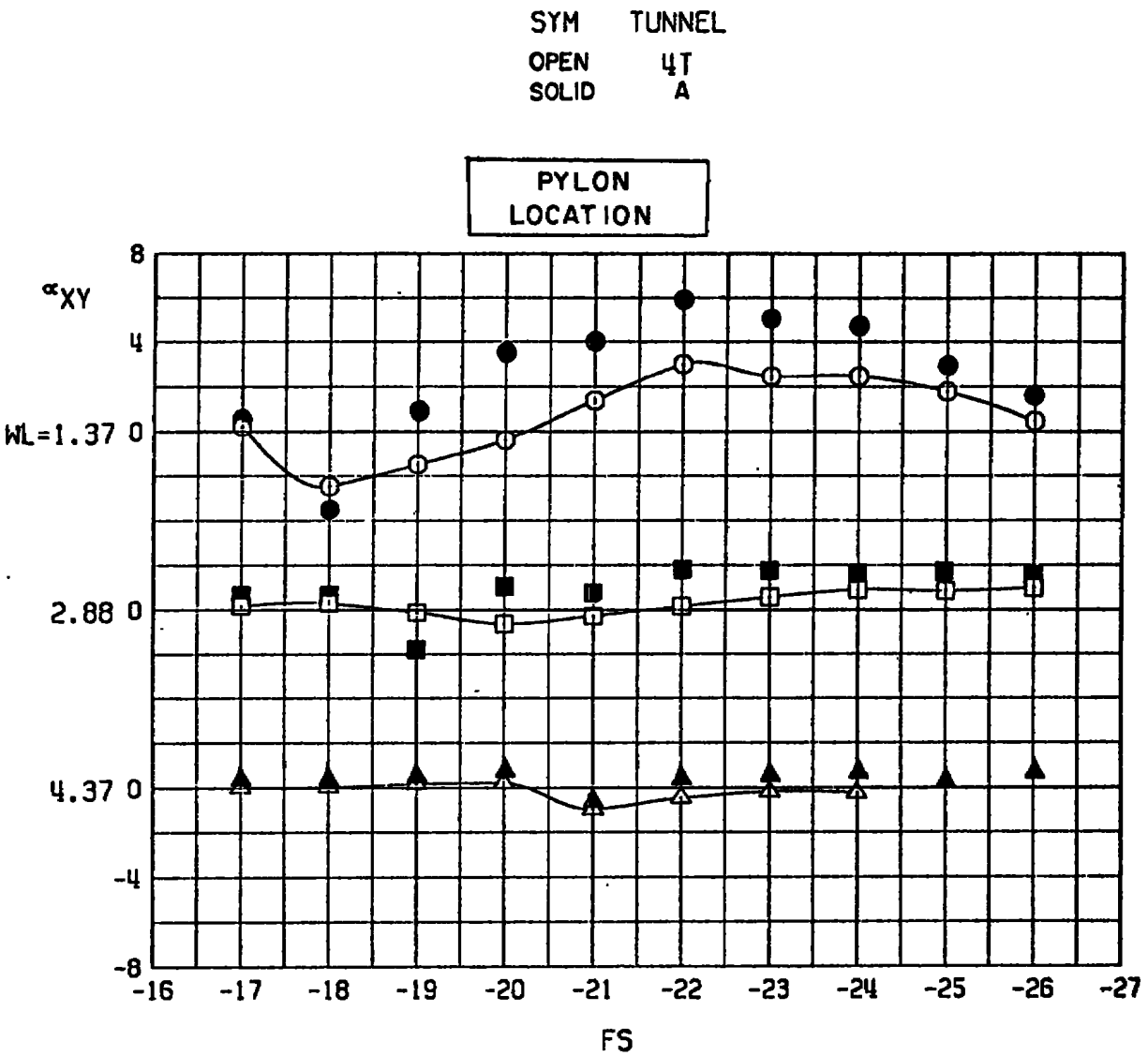

b. Sidewash angle, BL = -4.0 in.
Figure 13. Continued.

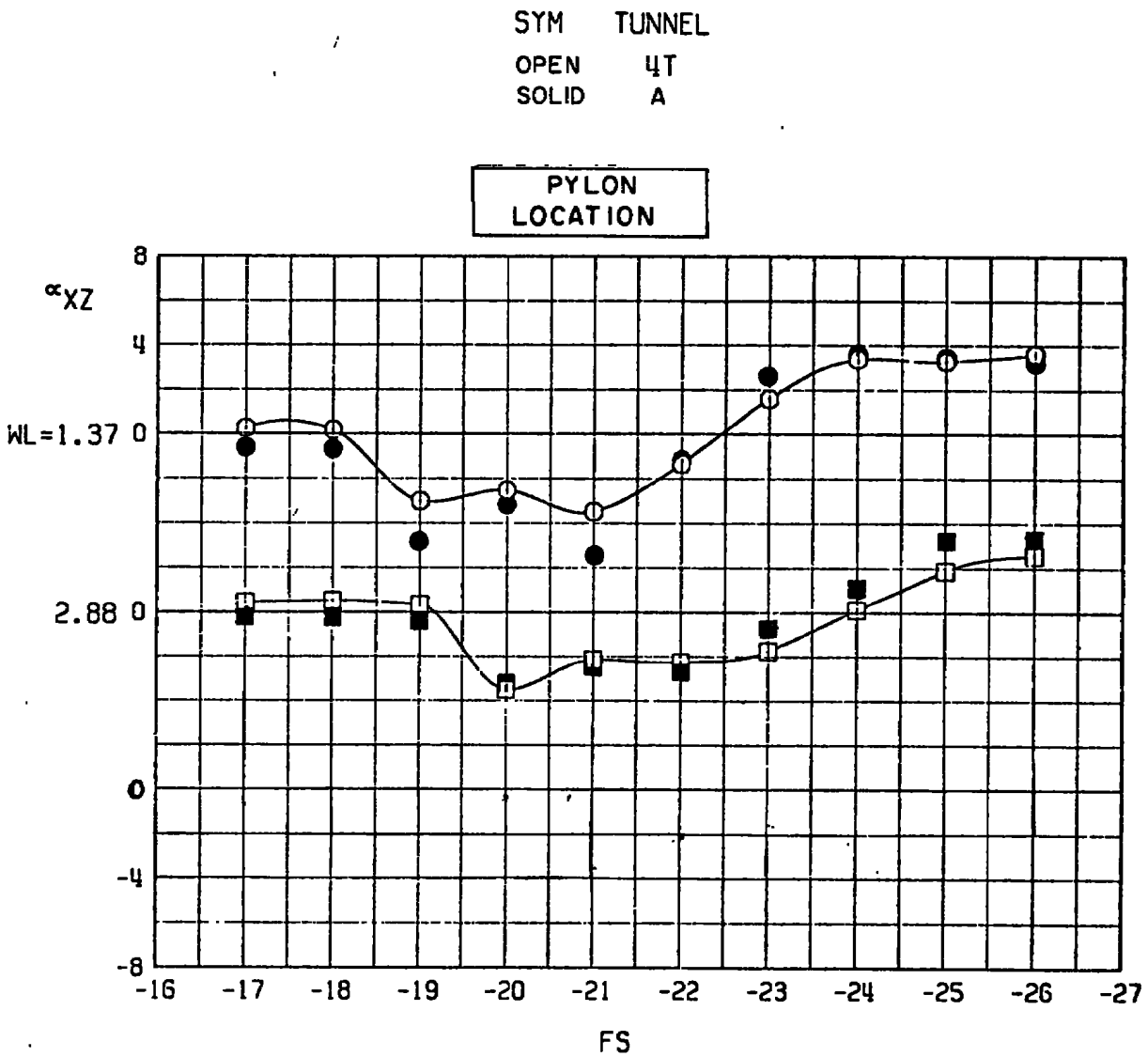

c. Upwash angle, BL = -4.75 in.

Figure 13. Continued.

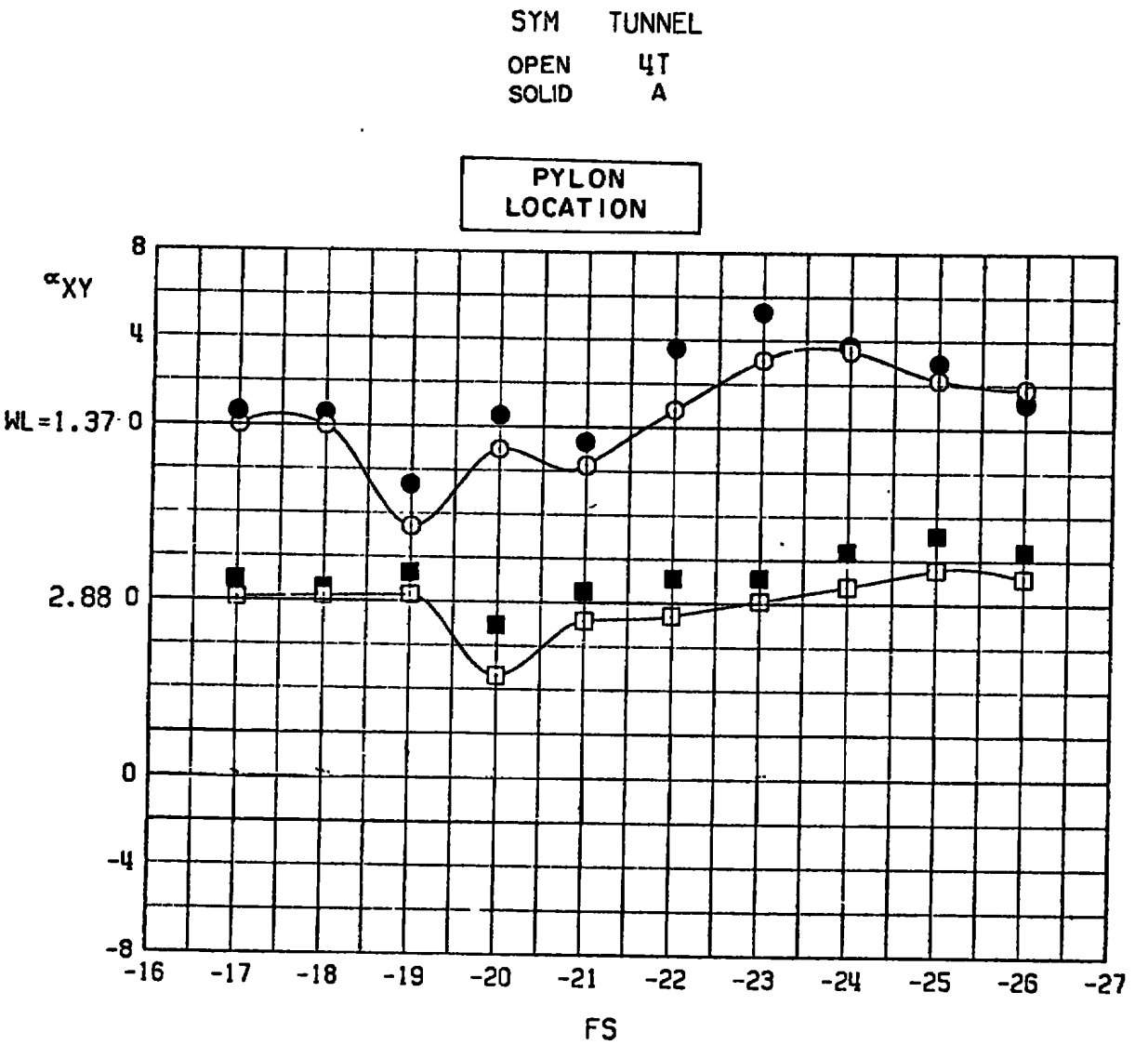

d. Sidewash angle, BL = -4.75 in.
Figure 13. Concluded.

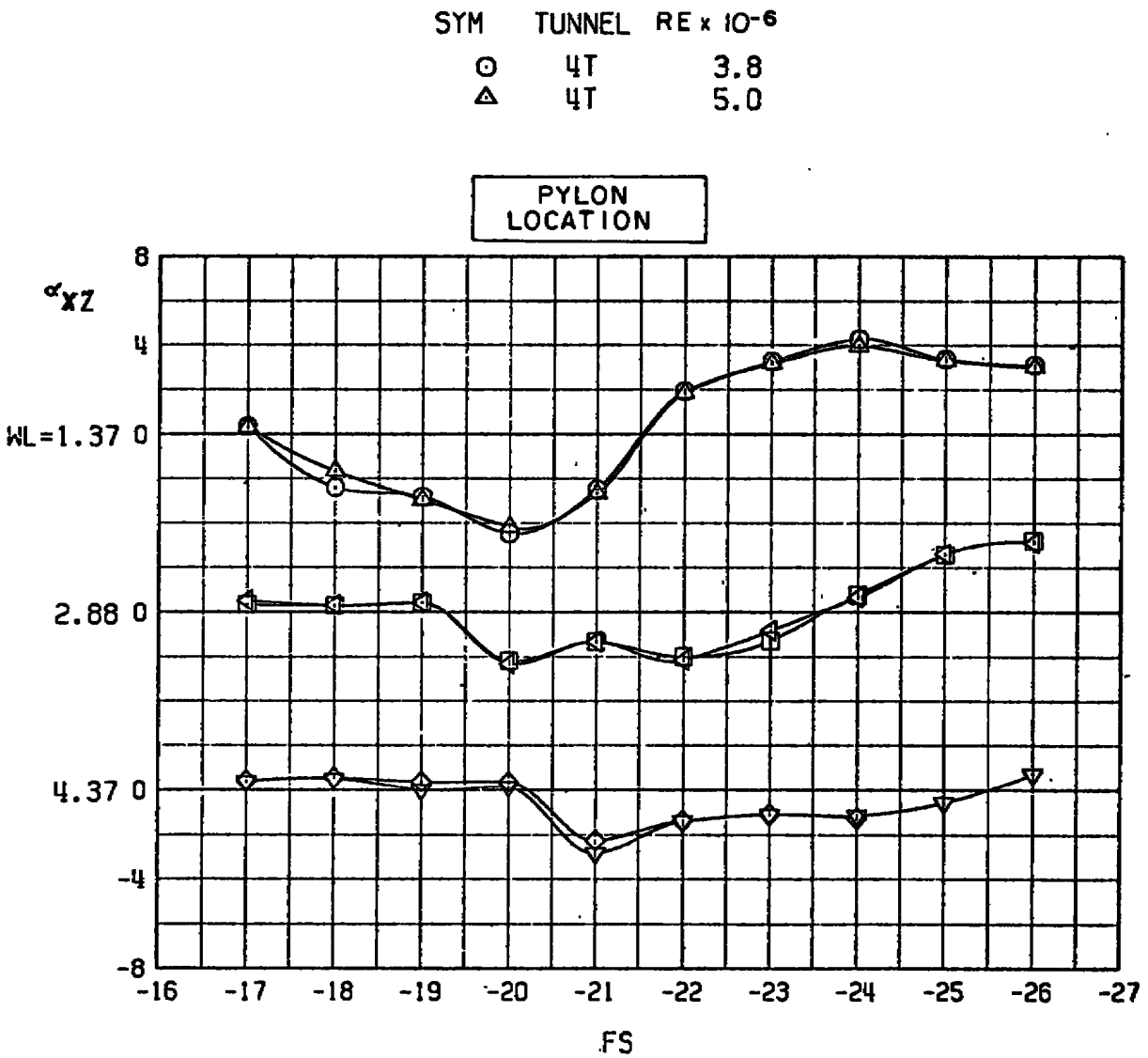

a. Upwash angle, BL = -4.0 in.

Figure 14. Repeatability of flow-field measurements beneath the 1/3-semispan pylon station, M_∞ = 1.65.

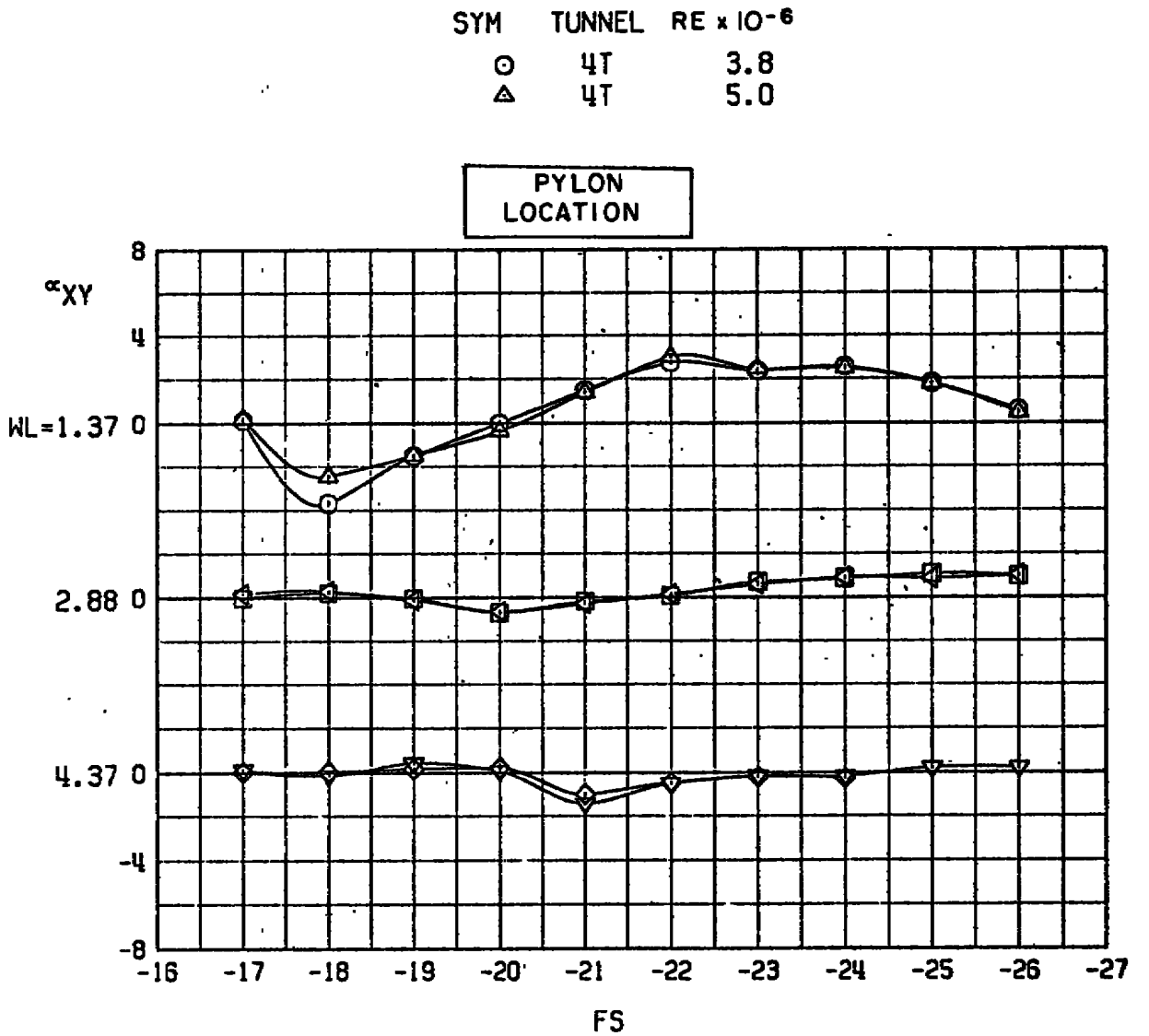

b. Sidewash angle, BL = -4.0 in.
Figure 14. Continued.

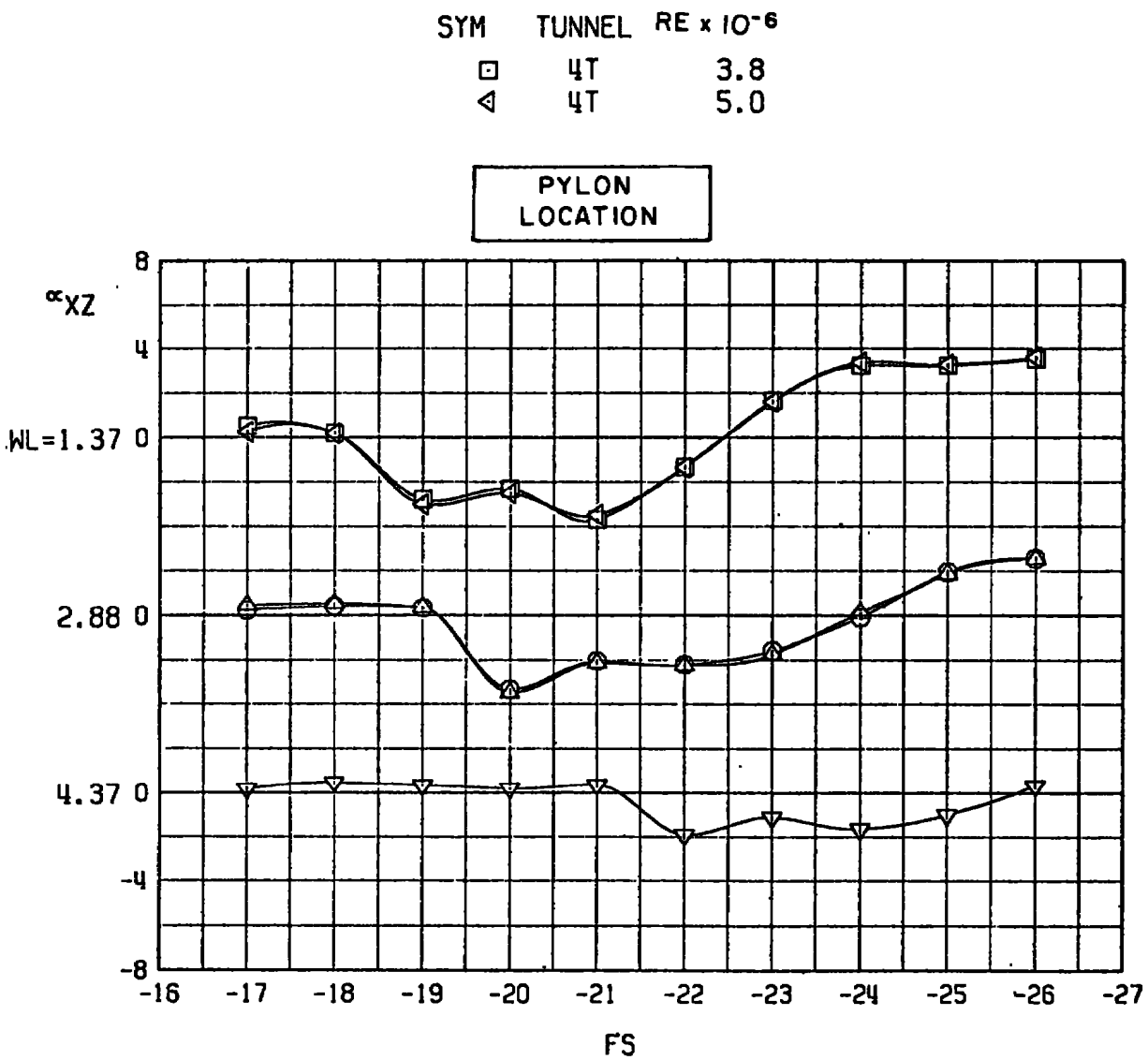

c. Upwash angle, Bl = -4.75 in.
Figure 14. Continued.

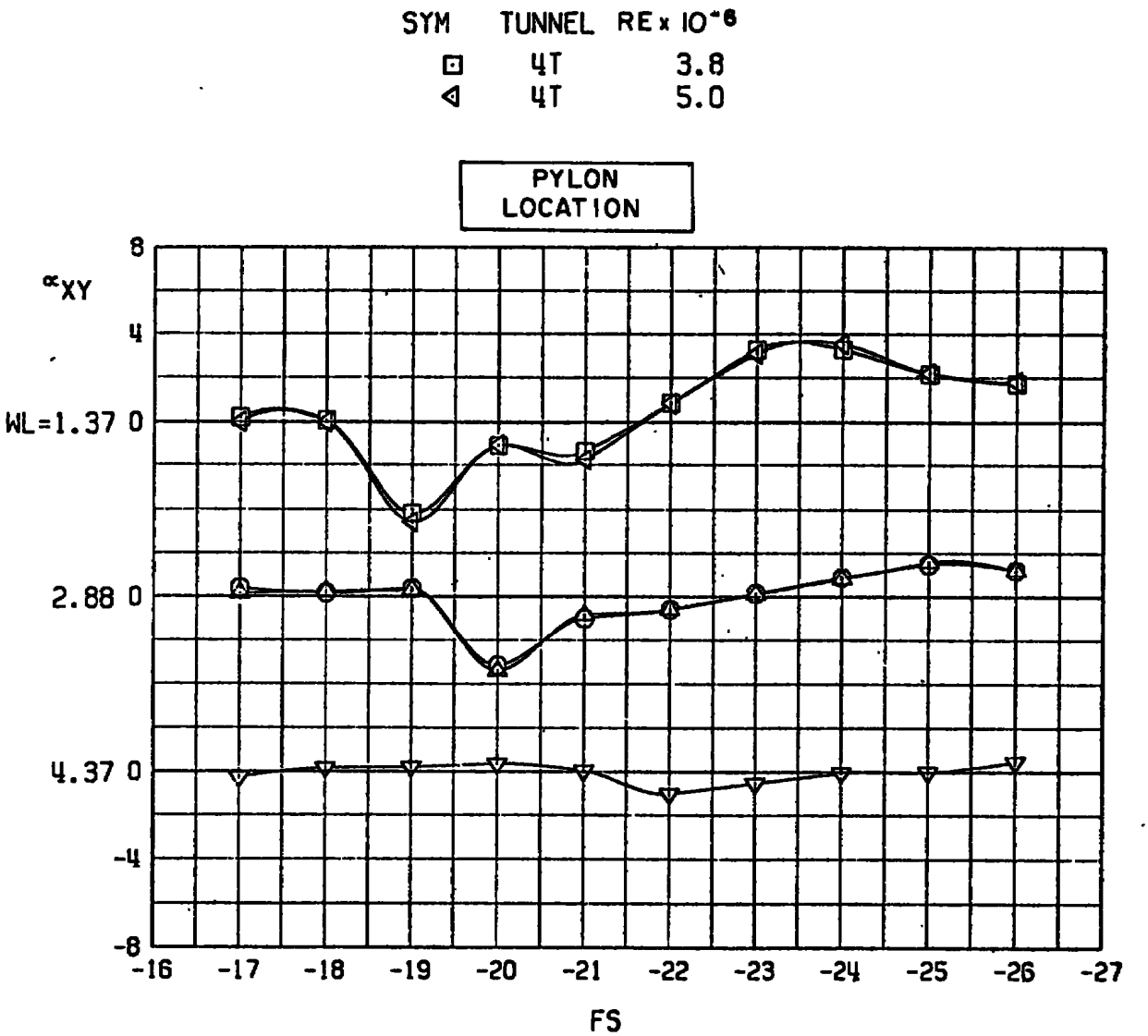

d. Sidewash angle, BL = -4.75 in.

Figure 14. Concluded.

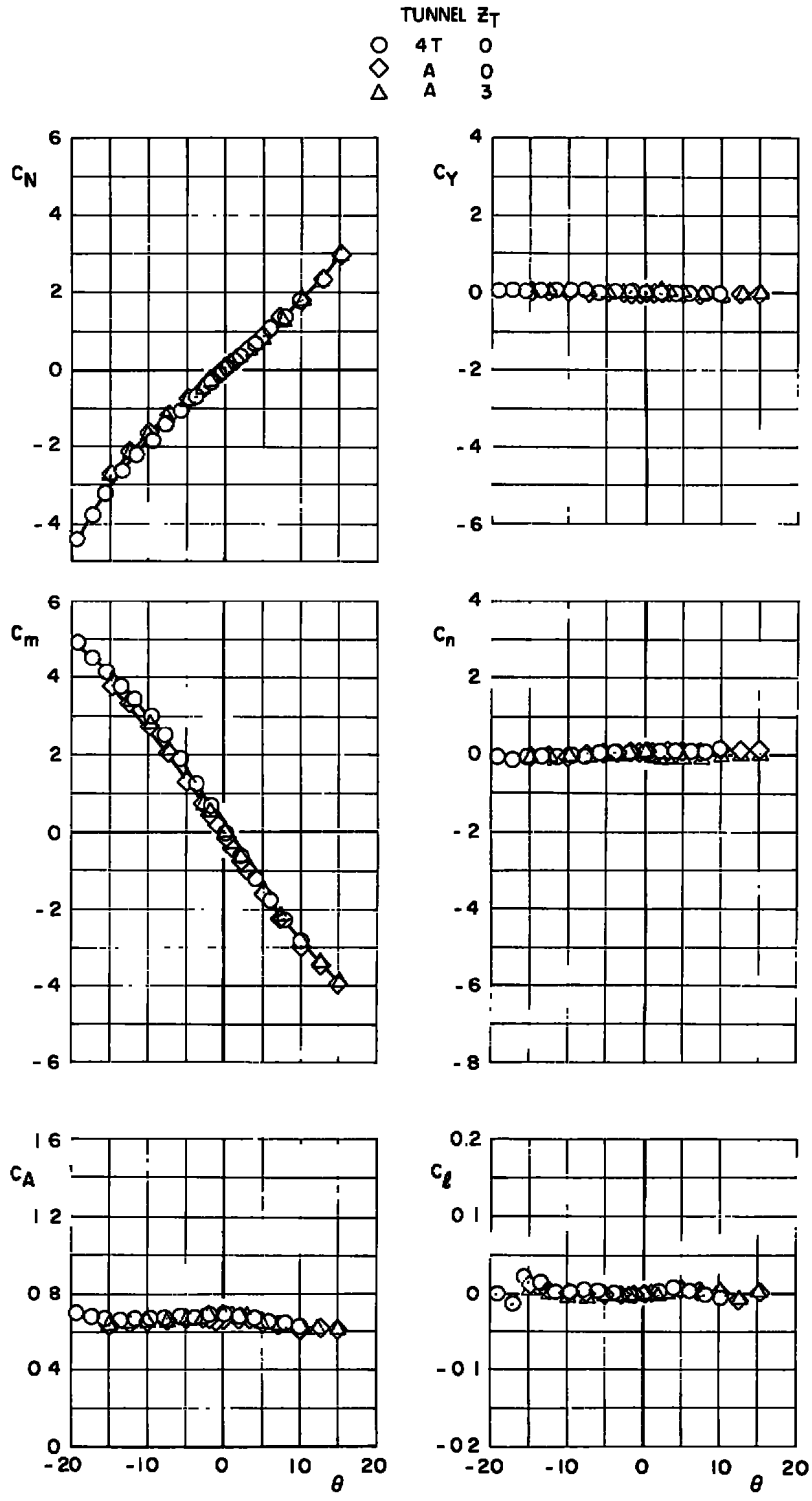

a. $\psi = 0$

Figure 15. Free-stream static stability characteristics of the ogive-cylinder store, $M_\infty = 1.63$, Re/ft = 5.0×10^6.

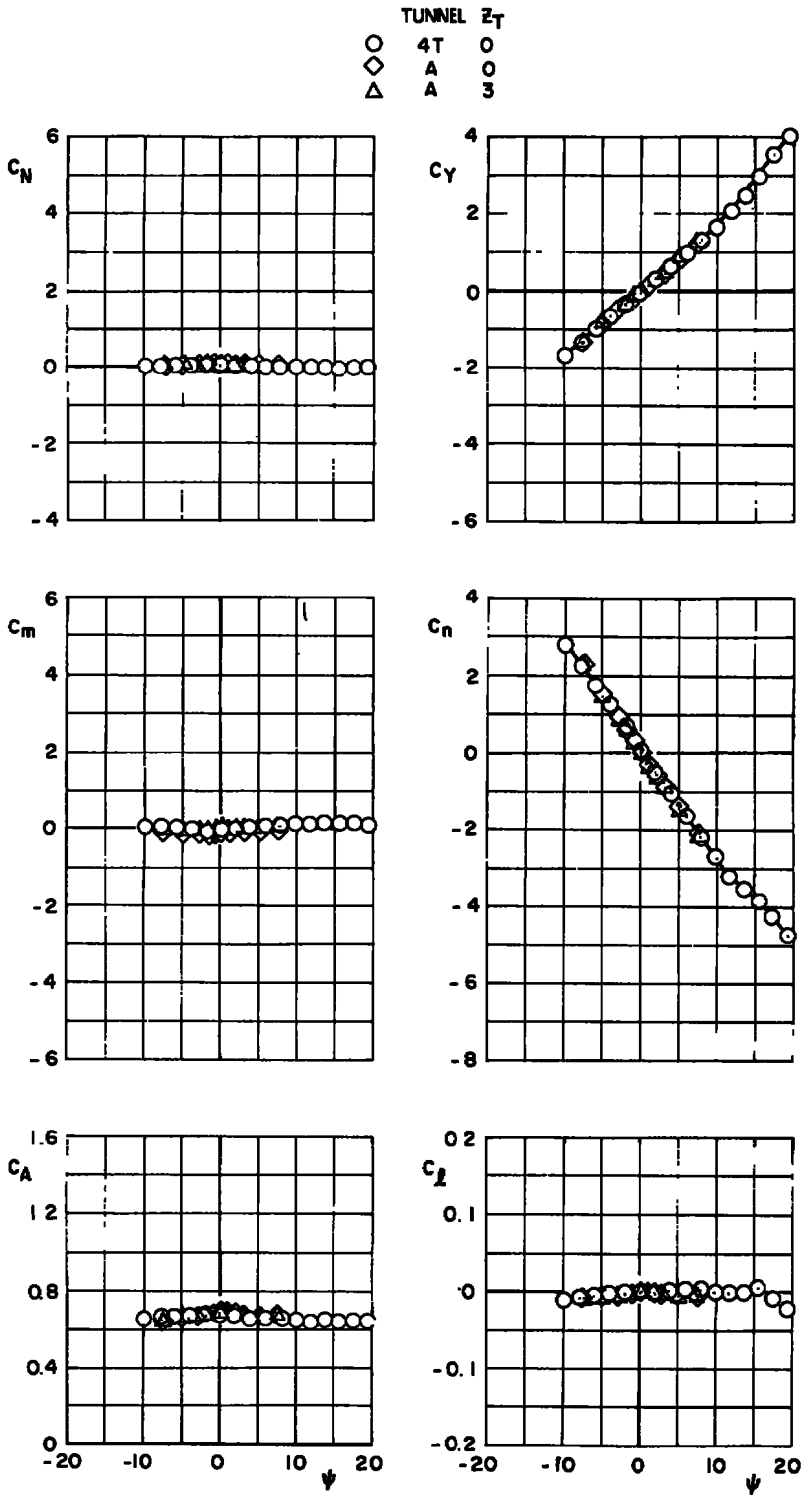

b. $\theta = 0$

Figure 15. Concluded.

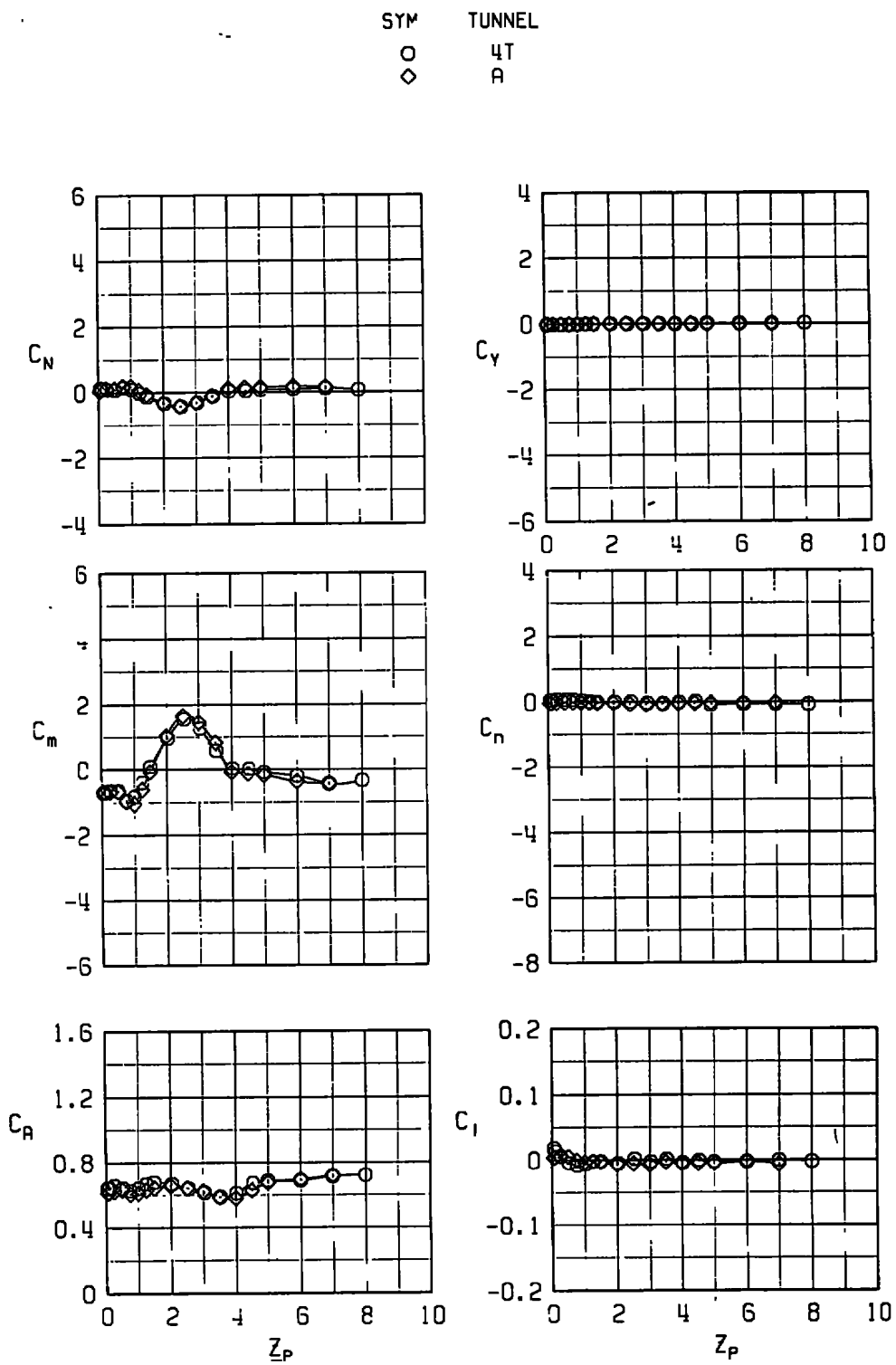

a. $X_p = 0$, $Y_p = 0$, $\theta = 0$, $\psi = 0$

Figure 16. Aerodynamic coefficients in the flow field beneath the centerline pylon station, $M_\infty = 1.63$, Re/ft = 5.0×10^6.

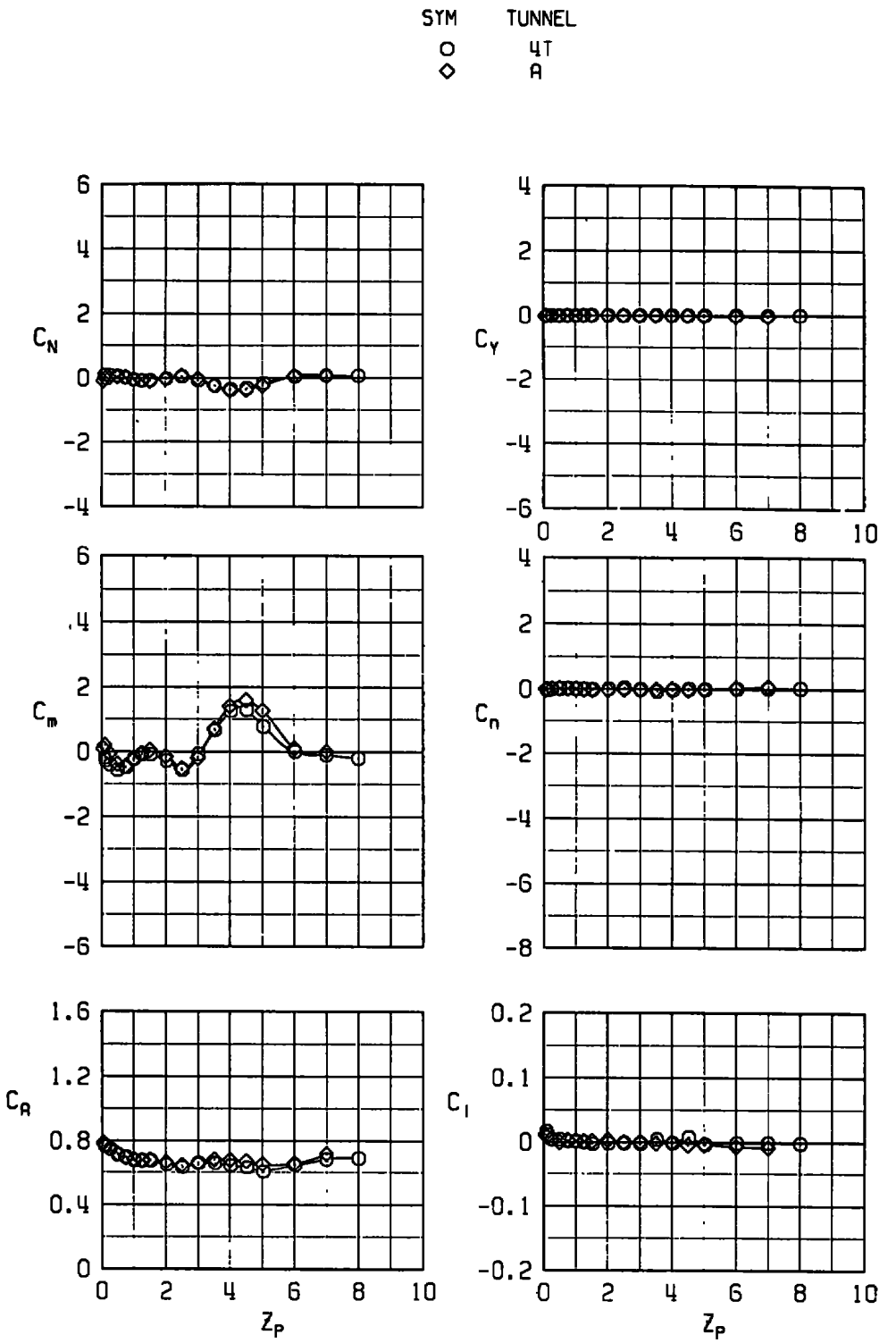

b. X_p = -2.0 in., Y_p = 0, θ = 0, ψ = 0

Figure 16. Continued.

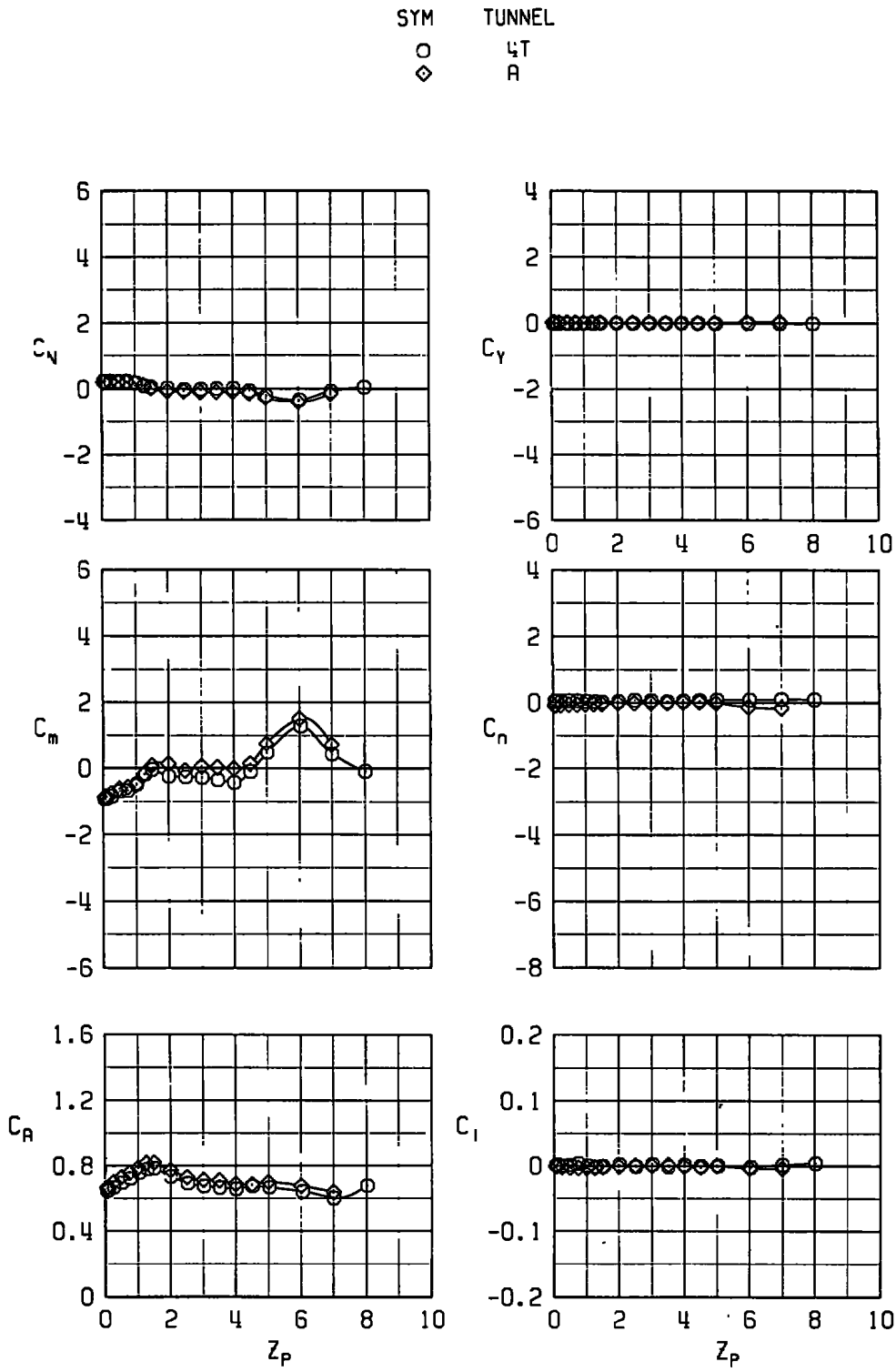

c. X_p = -4.0 in., Y_p = 0, θ = 0, ψ = 0

Figure 16. Continued.

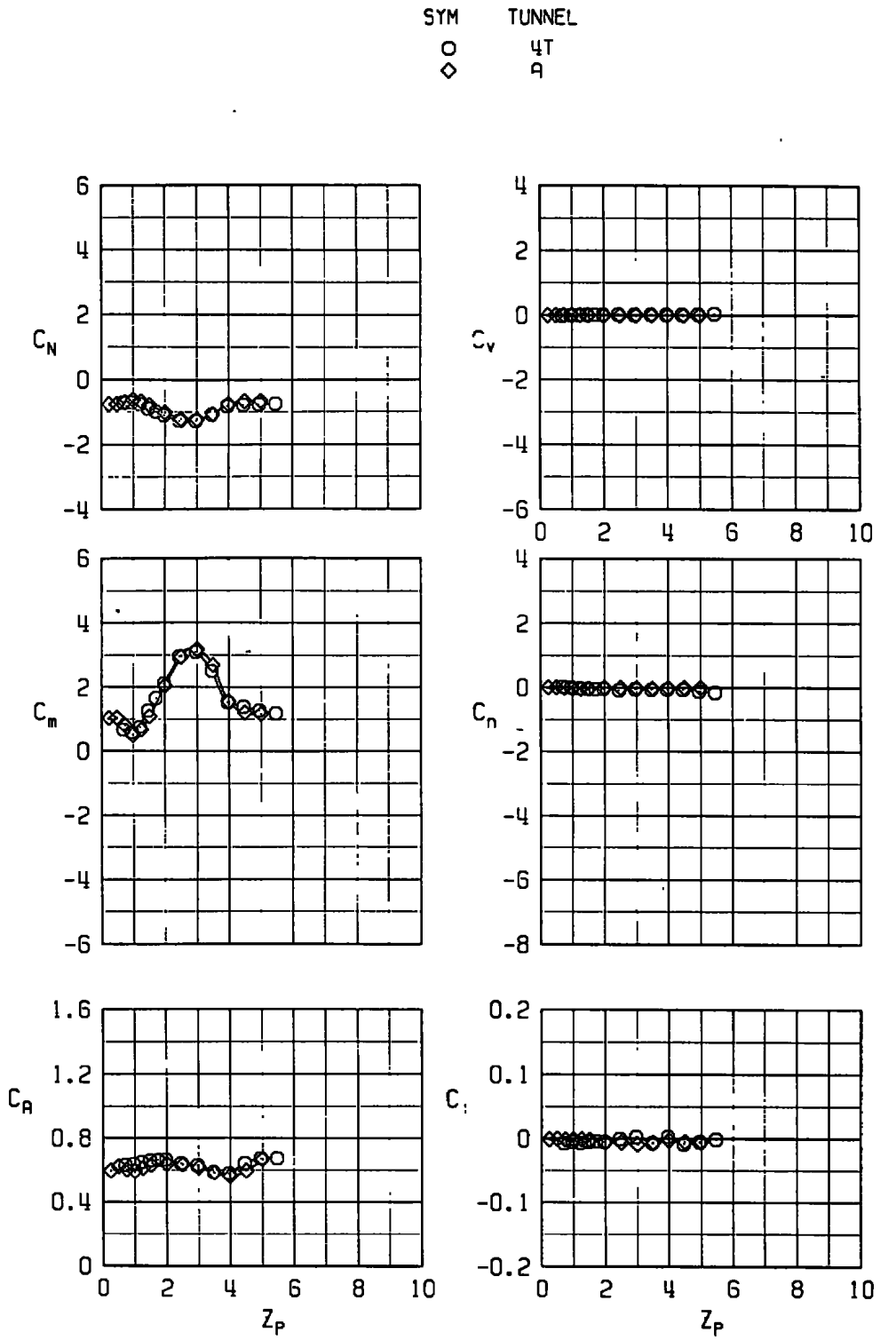

d. X_p = 0, Y_p = 0, θ = -5.0 deg, ψ = 0

Figure 16. Concluded.

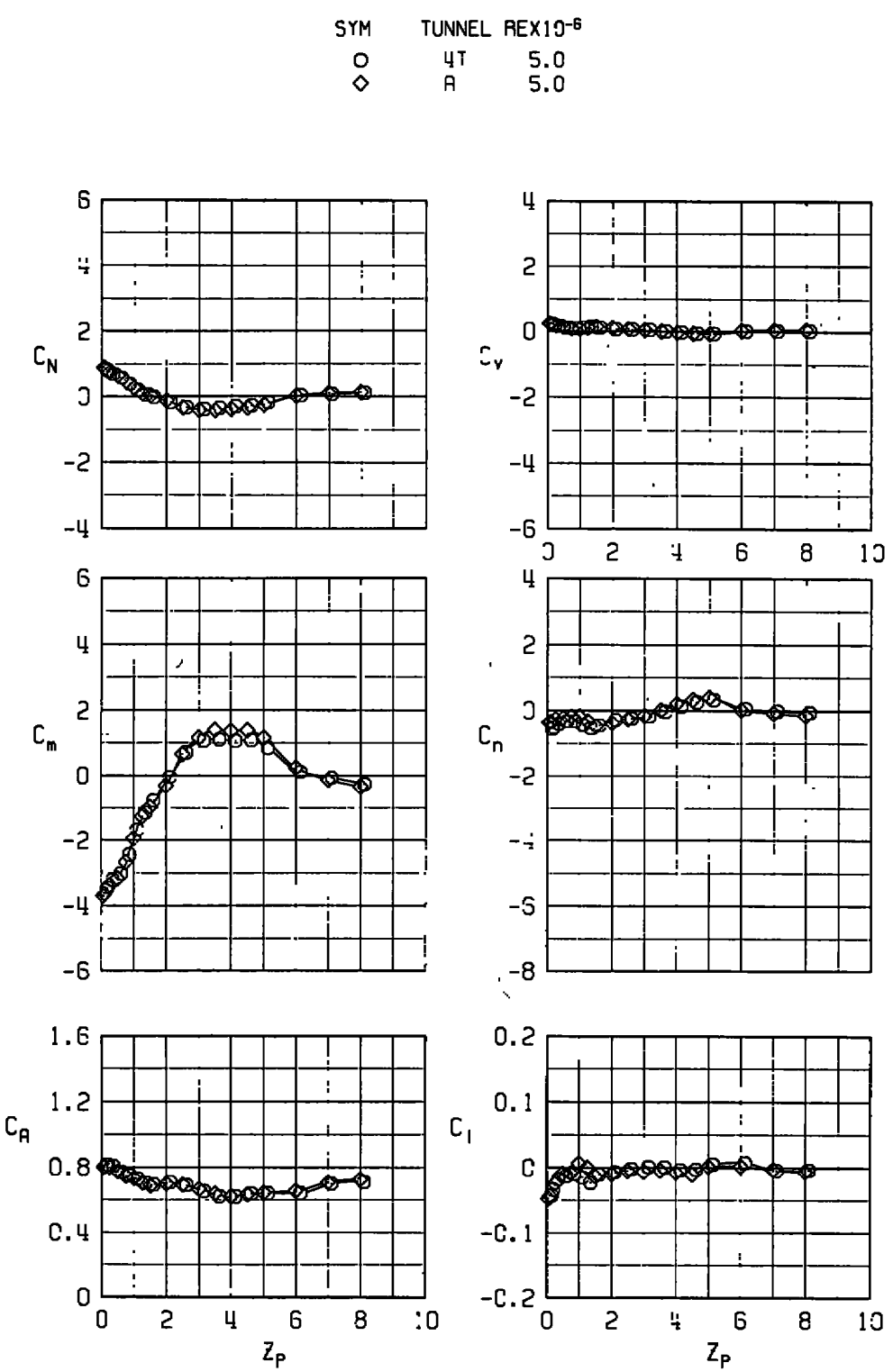

a. $X_p = 0$, $Y_p = 0$, $\theta = 0$, $\psi = 0$

Figure 17. Aerodynamic coefficients in the flow field beneath the 1/3-semispan pylon station, $M_\infty = 1.63$.

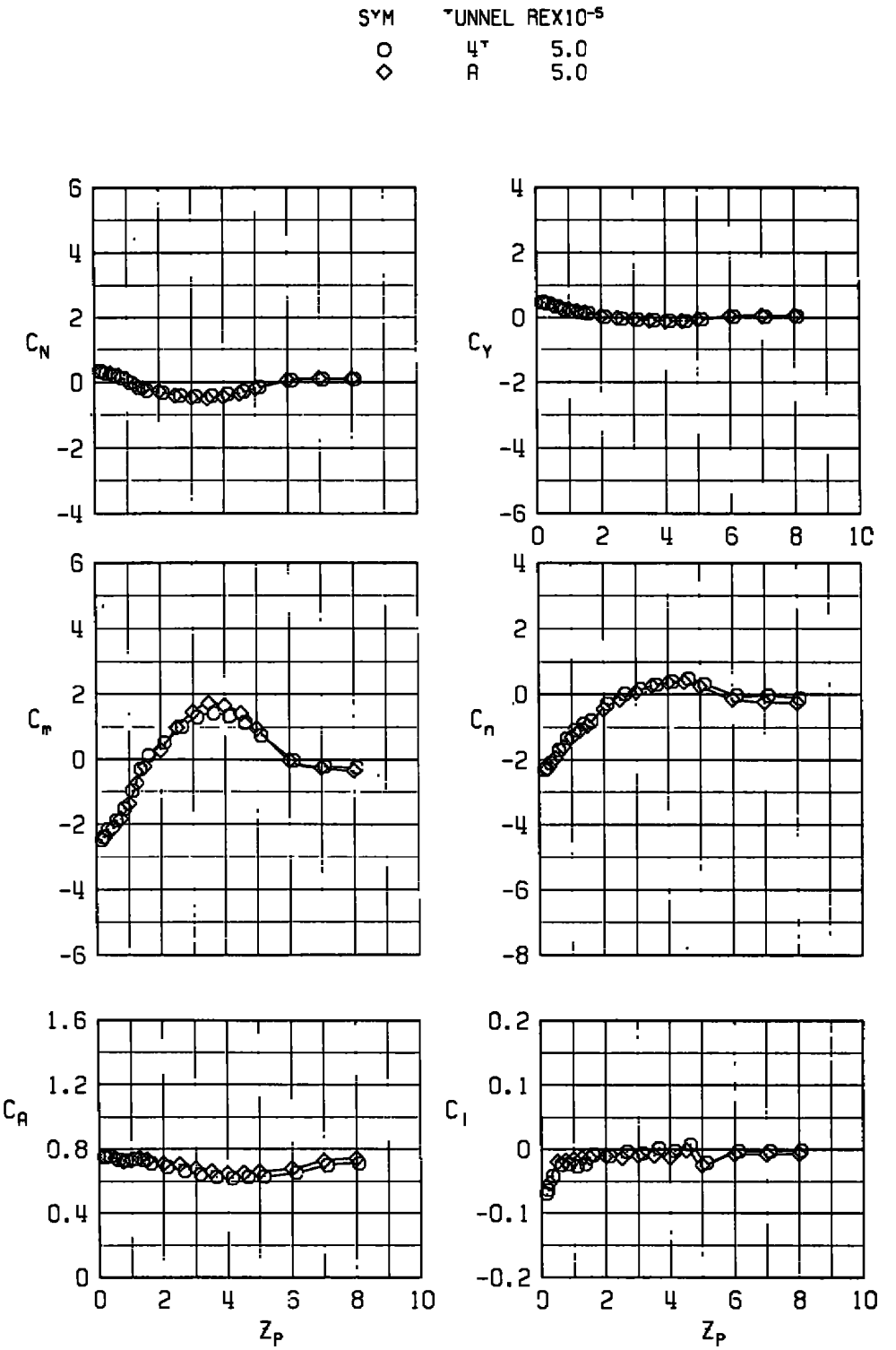

b. X_p = 0, Y_p = -1 in., θ = 0, ψ = 0
Figure 17. Continued.

SYM	TUNNEL	REX10^{-6}
○	4T	5.0
◇	A	5.0

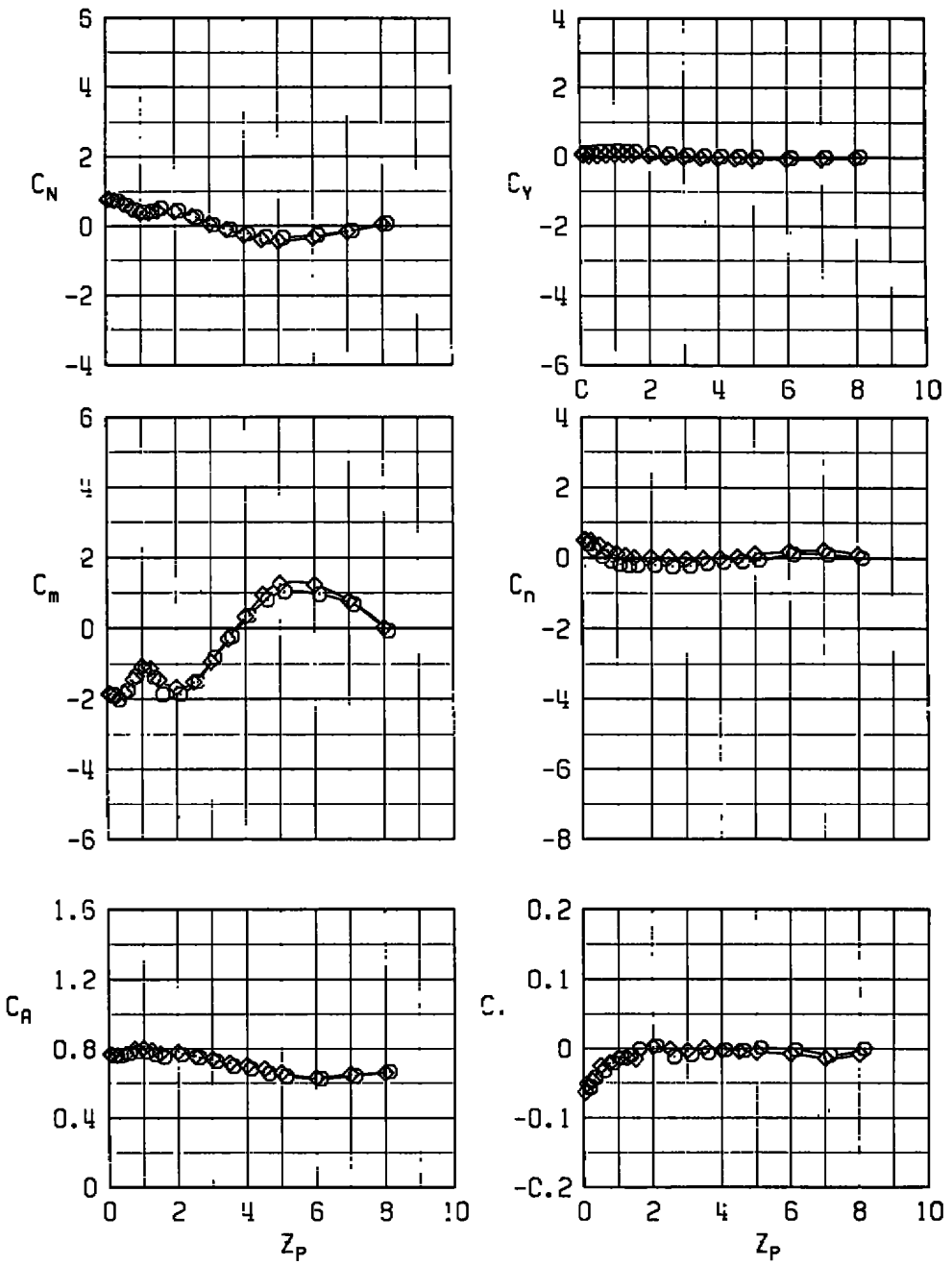

c. X_p = -2.0 in., Y_p = 0, θ = 0, ψ = 0

Figure 17. Continued.

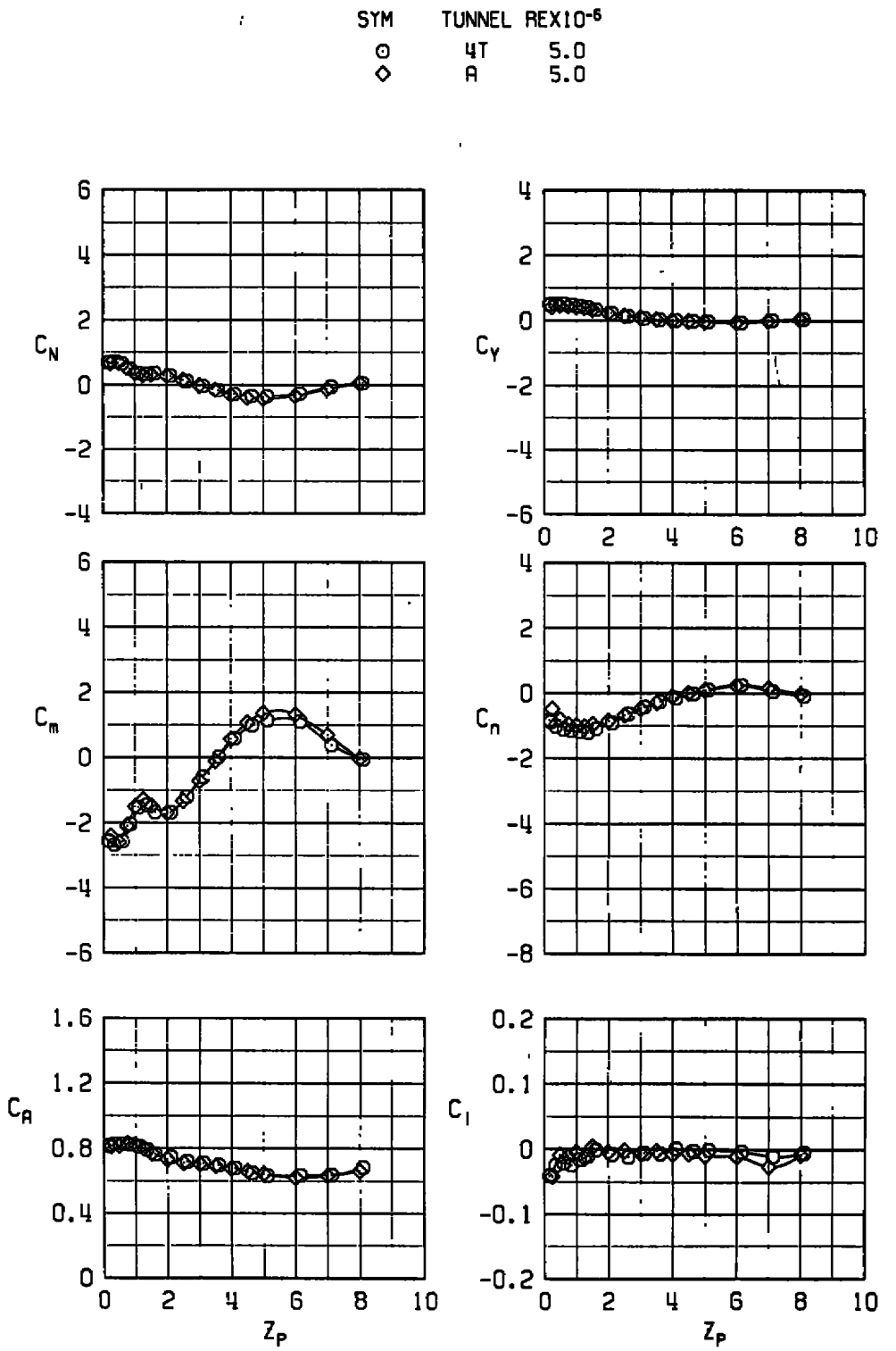

d. X_p = -2.0 in., Y_p = -1.0 in., θ = 0, ψ 0
Figure 17. Continued.

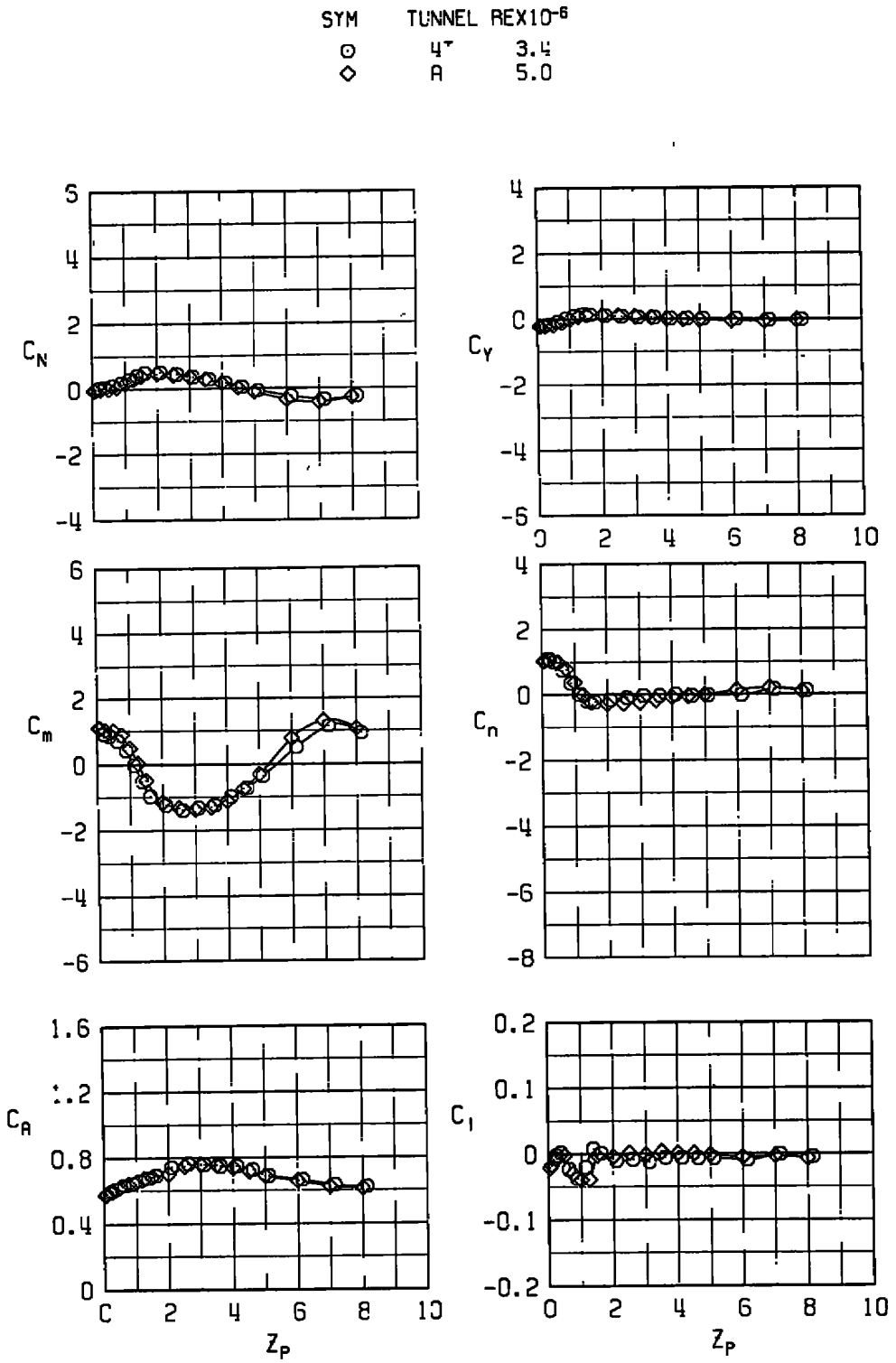

e. X_p = -4.0 in., Y_p = 0, θ = 0, ψ = 0

Figure 17. Continued.

SYM	TUNNEL	REX10^{-6}
○	4T	3.4
◇	A	5.0

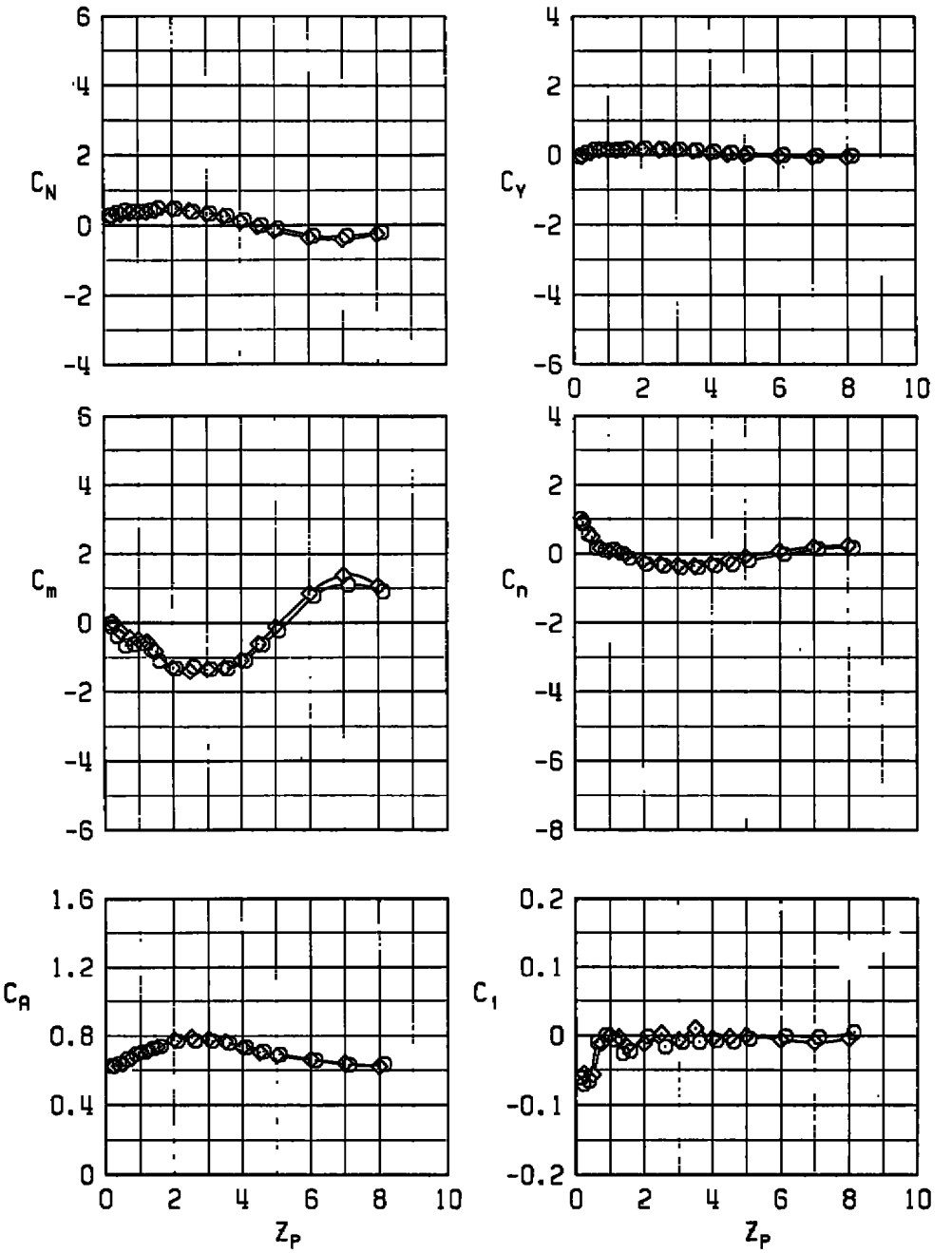

f. X_p = -4.0 in., Y_p = -1.0 in., θ = 0, ψ = 0
Figure 17. Continued.

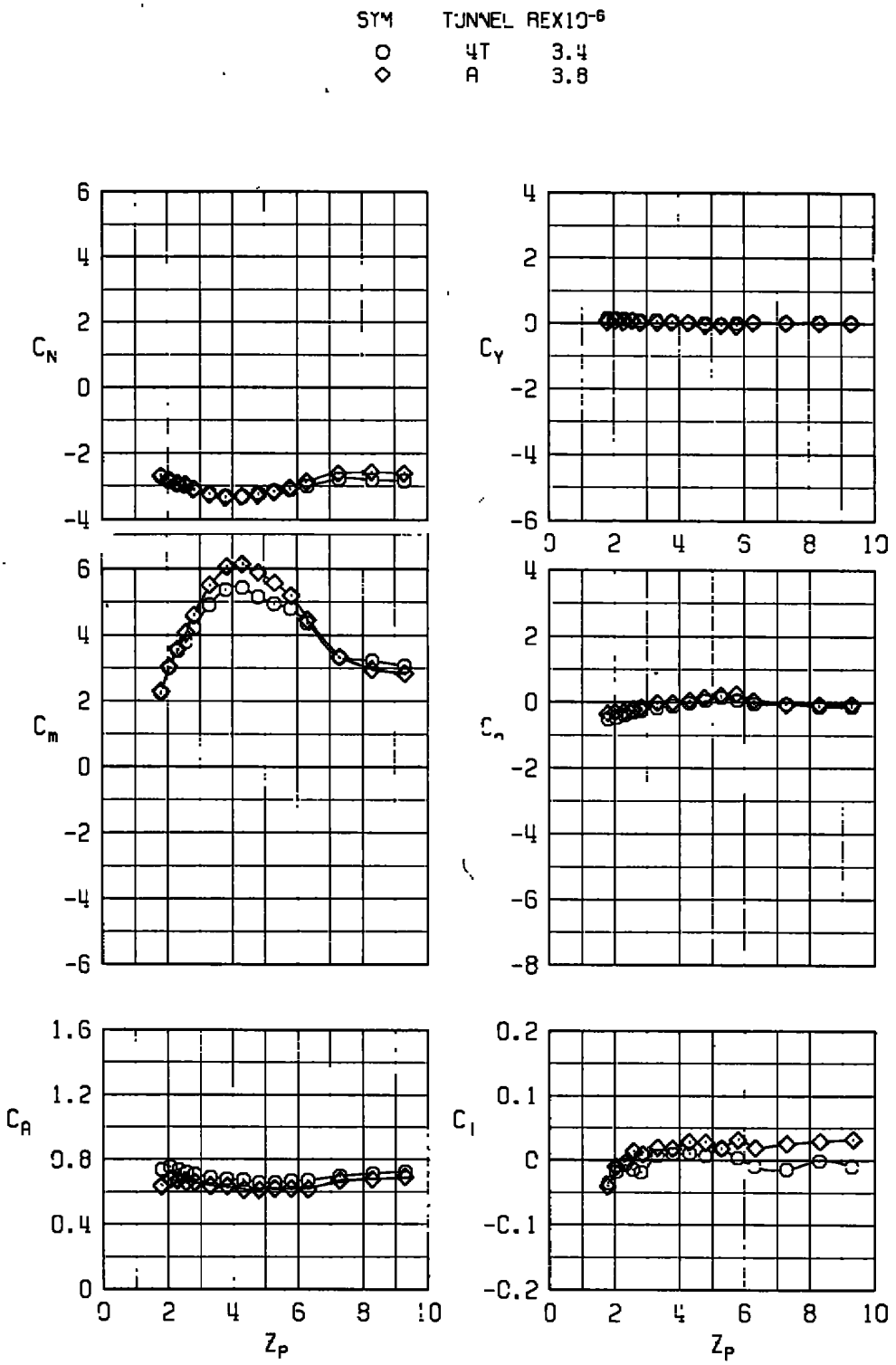

g. X_p = -0.15 in., Y_p = 0, θ = -15 deg, ψ = 0
Figure 17. Continued.

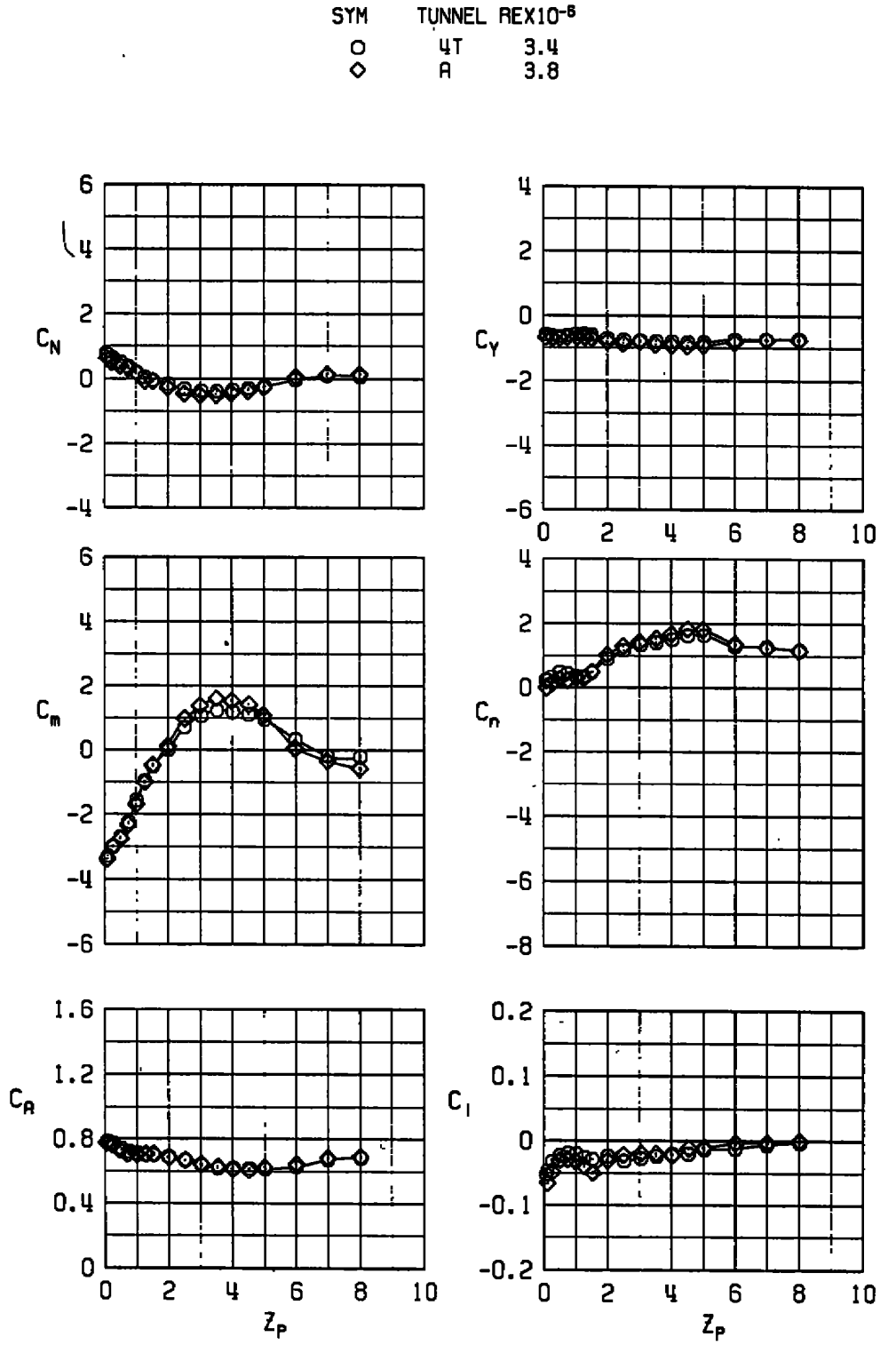

h. $X_p = 0$, $Y_p = -0.45$ in., $\theta = 0$, $\psi = 0$

Figure 17. Continued.

SYM	TUNNEL	REX10^{-6}
○	4T	3.4
◇	A	3.8

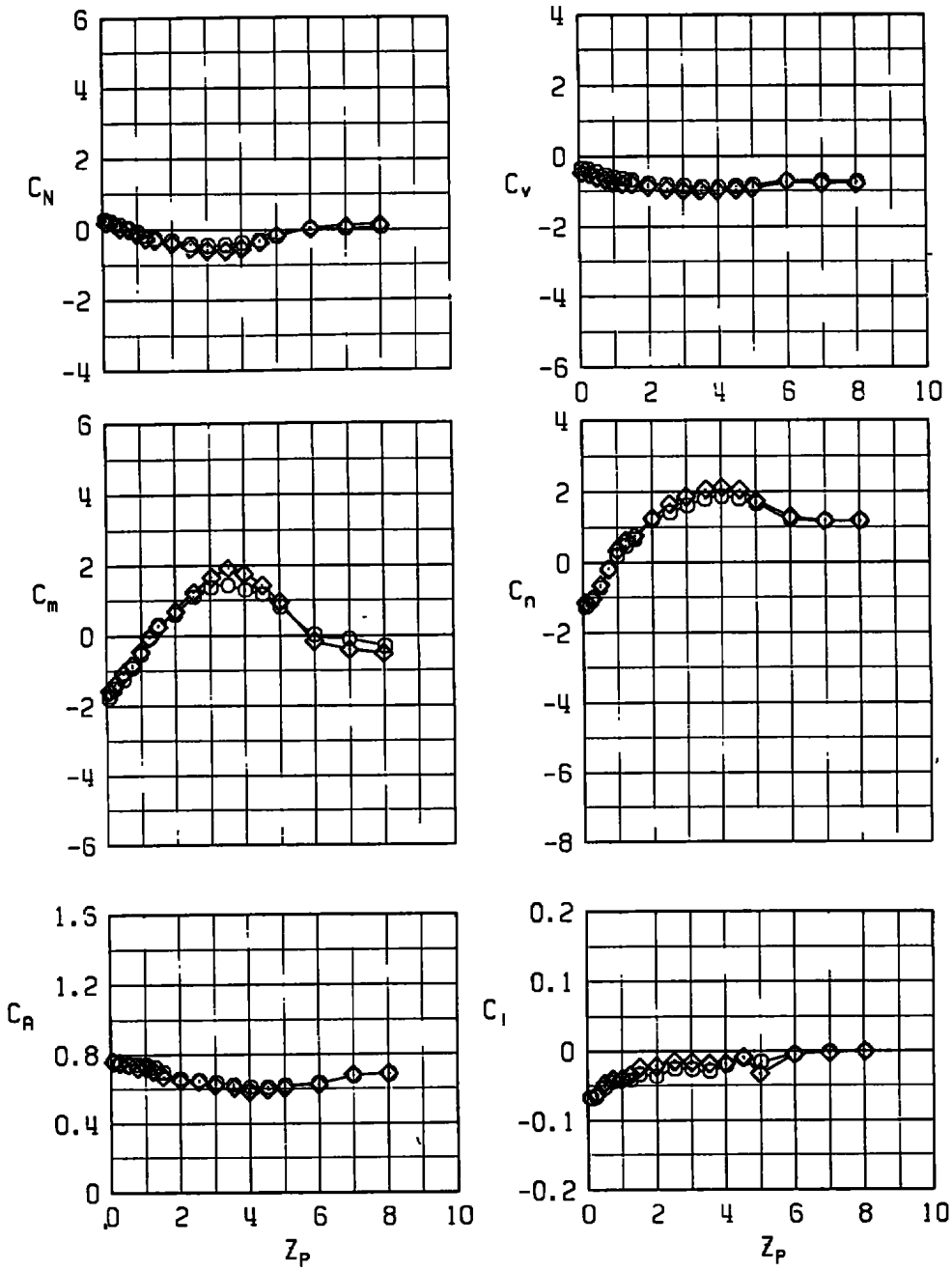

i. $X_p = 0$, $Y_p = -1.45$ in., $\theta = 0$, $\psi = -5.0$ deg
Figure 17. Concluded.

SYM	TUNNEL	ΔT_p	TRAJ
⊙	4T	0.010	2
◇	A	0.010	2

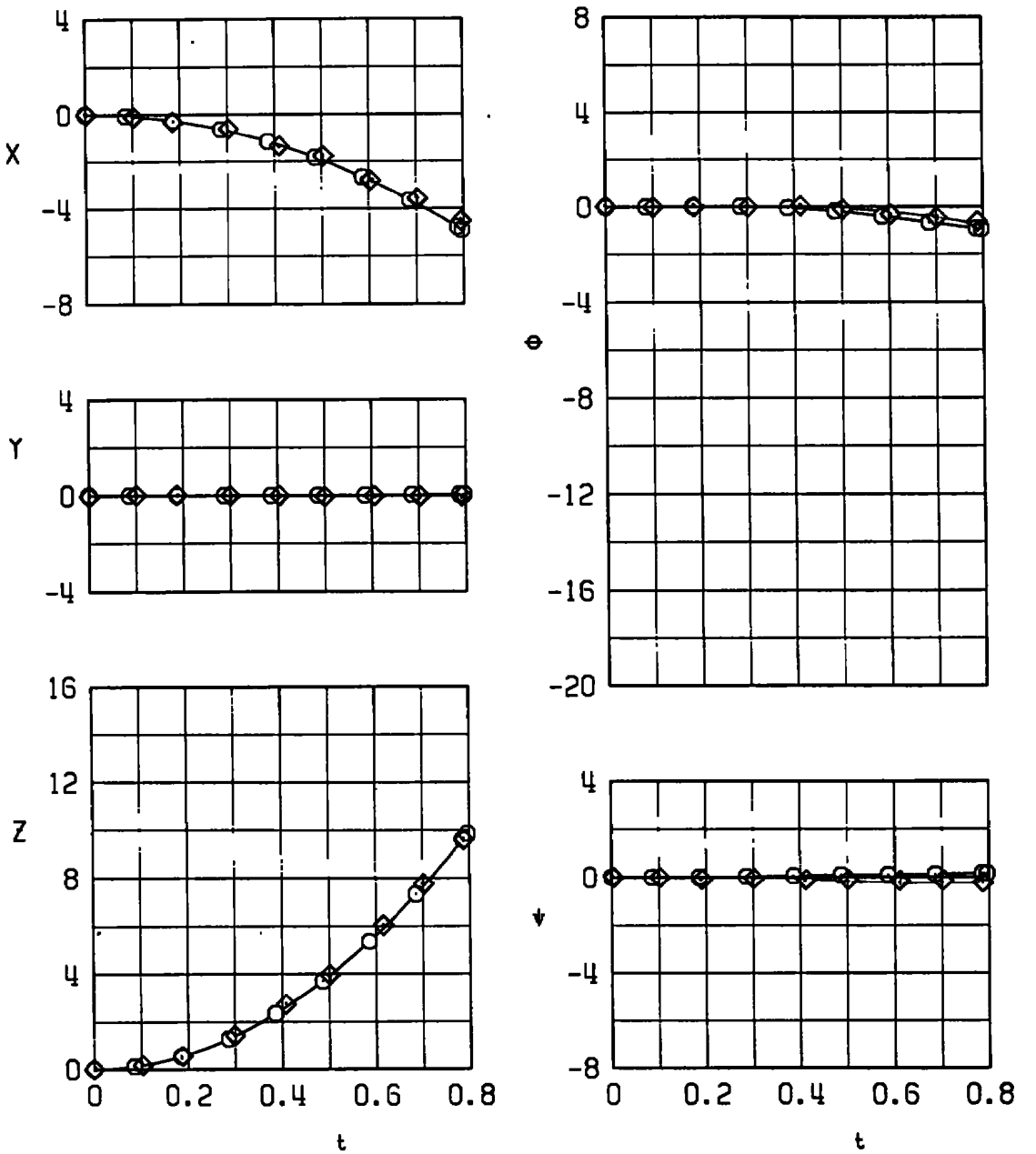

a. Without ejector force

Figure 18. Free-stream trajectories, M_∞ = 1.63.

SYM	TUNNEL	REX10^{-6}	ΔT_p	TRAJ
⊙	4T	5.0	0.002	I
⊡	4T	5.0	0.020	I
◇	A	5.0	TABLE I	I

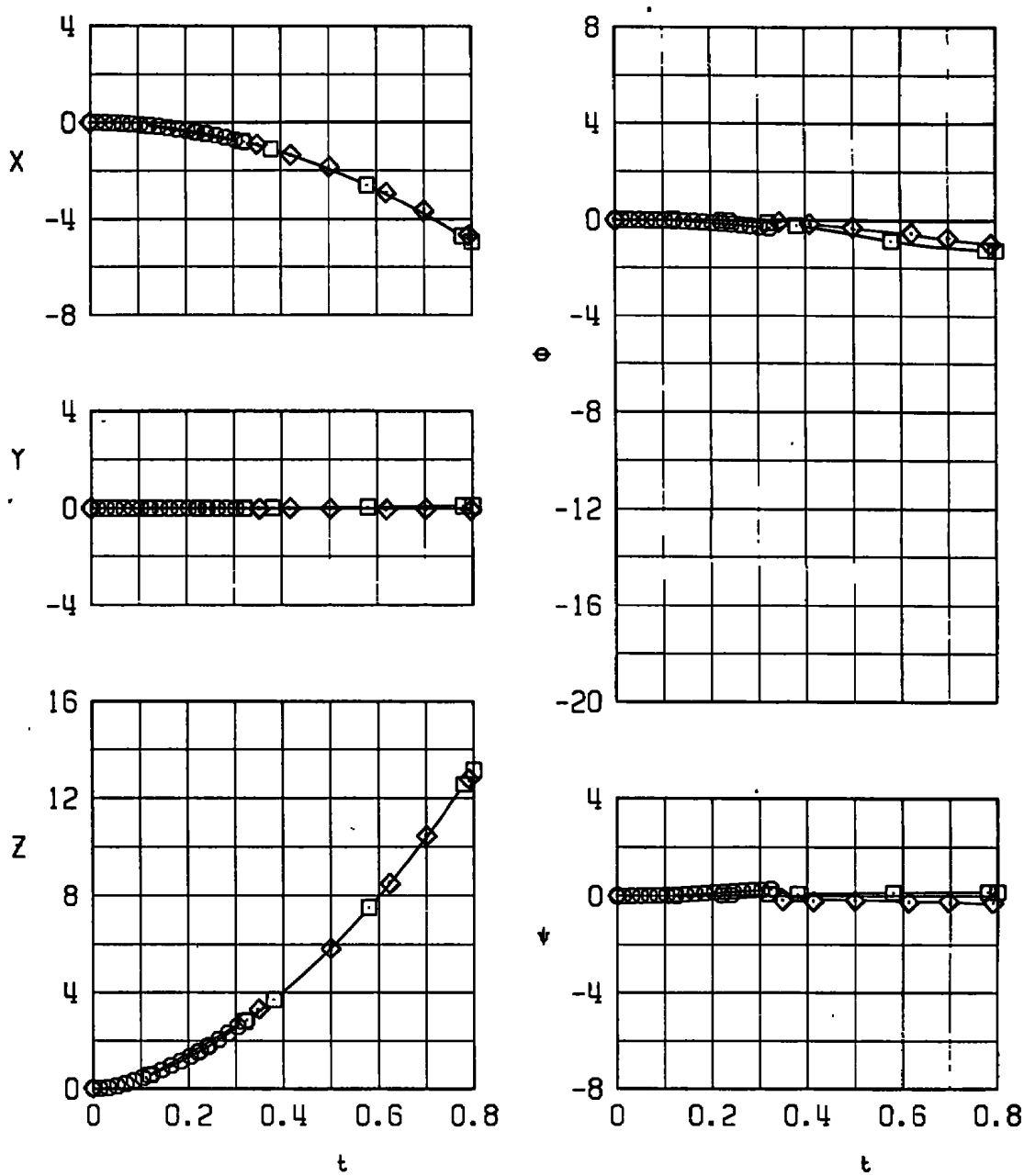

b. With ejector force: $X_{L_1} = 0$, $\omega_m = 0$
Figure 18. Continued.

SYM	TUNNEL	REX10^{-6}	ΔT_p	TRAJ
⊙	4T	3.5	0.010	3
▽	A	3.8	TABLE I	3
◇	A	3.8	TABLE I	3

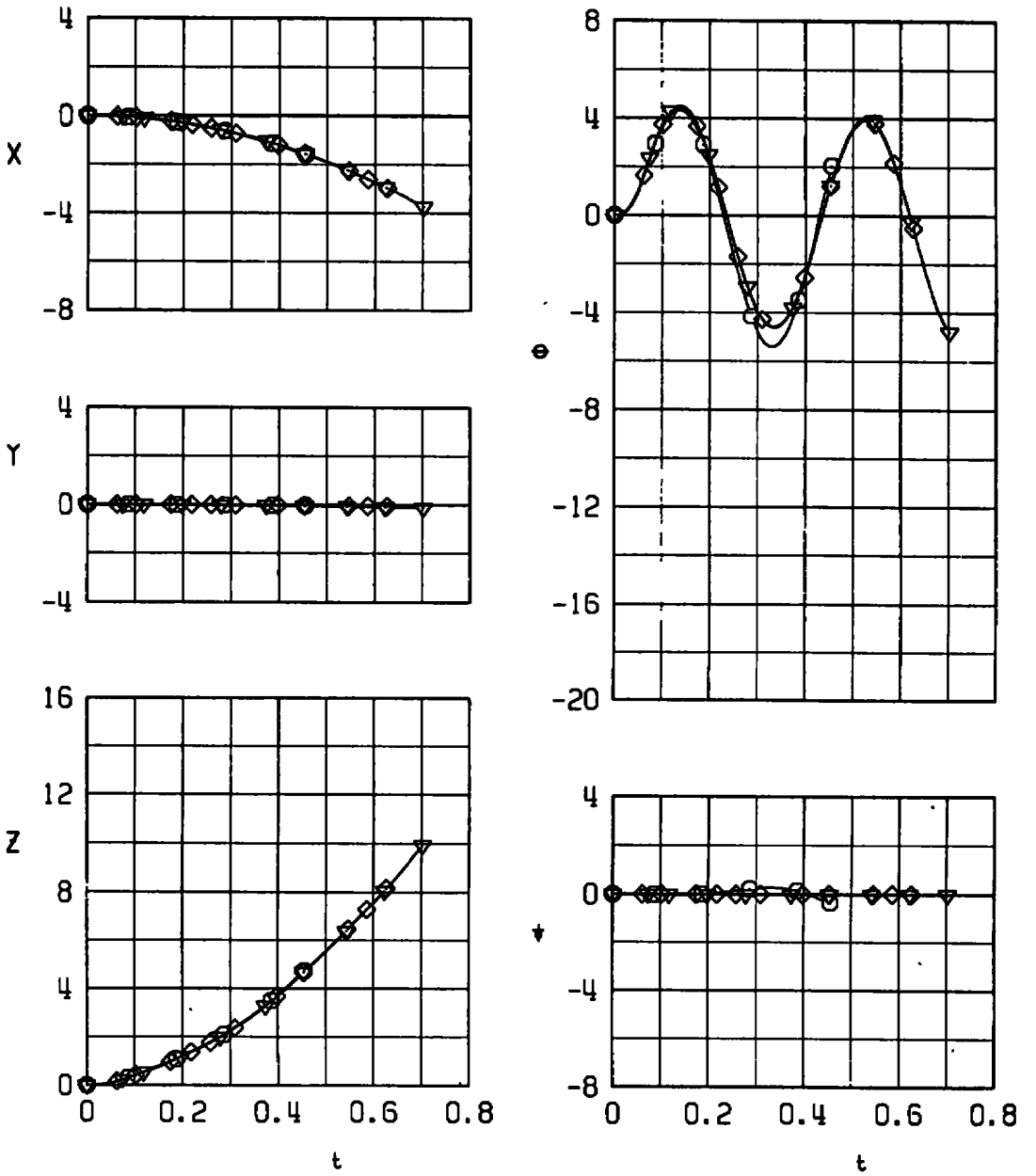

c. With ejector force: X_{L_1} = 0.50 ft, ω_m = 0
Figure 18. Continued.

SYM	TUNNEL	REX10^{-6}	ΔT_p	TRAJ
⊙	4T	3.5	0.010	4
◇	A	3.8	TABLE I	4

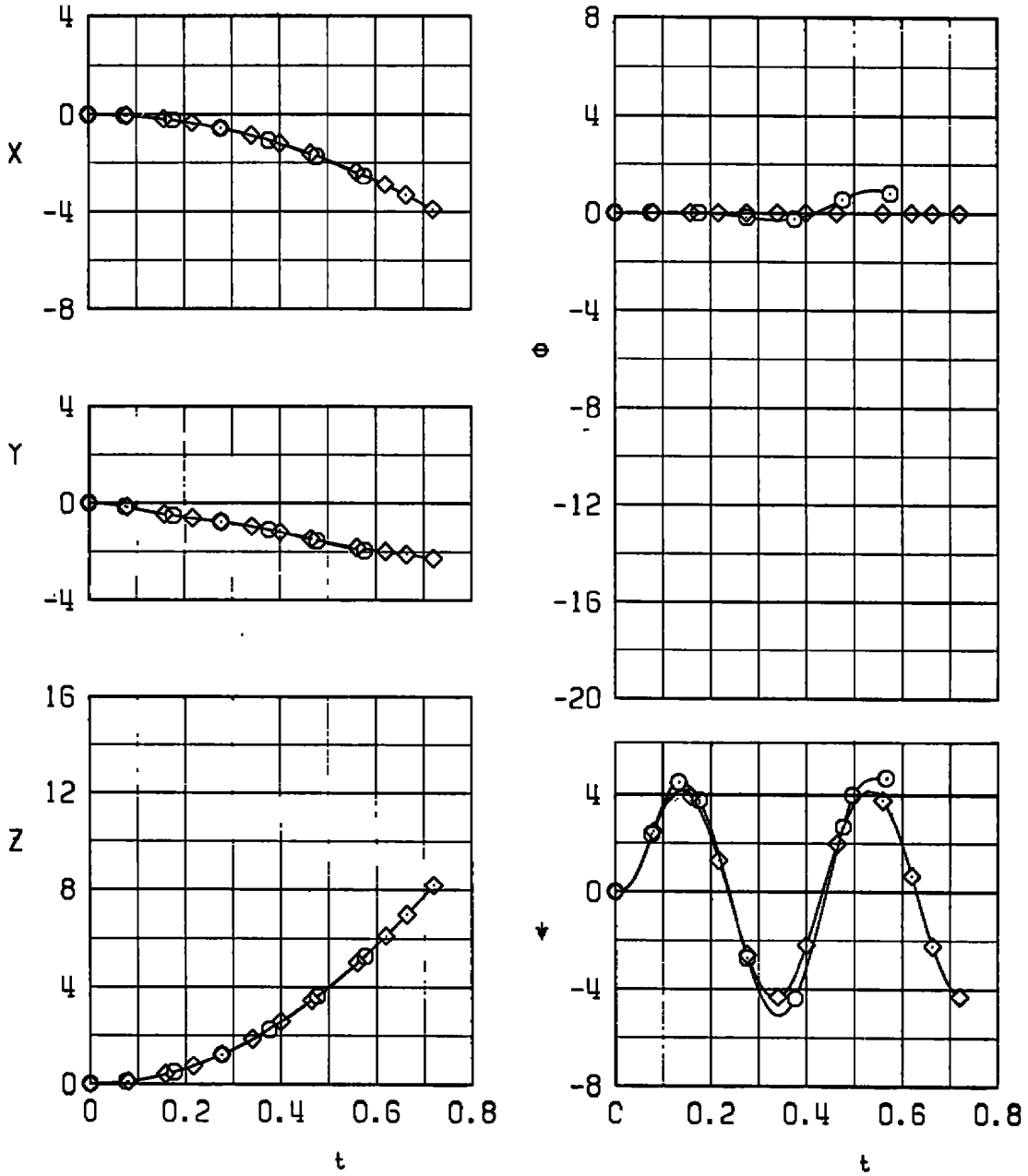

d. With ejector force: X_{L_1} = -0.50 ft, ω_m = 90 deg
Figure 18. Concluded.

SYM	TUNNEL	REX10^{-6}	ΔT_p	TRAJ
⊙	4T	5.0	0.004	5
⊡	4T	5.0	0.010	5
△	4T	5.0	0.020	5
◇	A	5.0	TABLE I	5

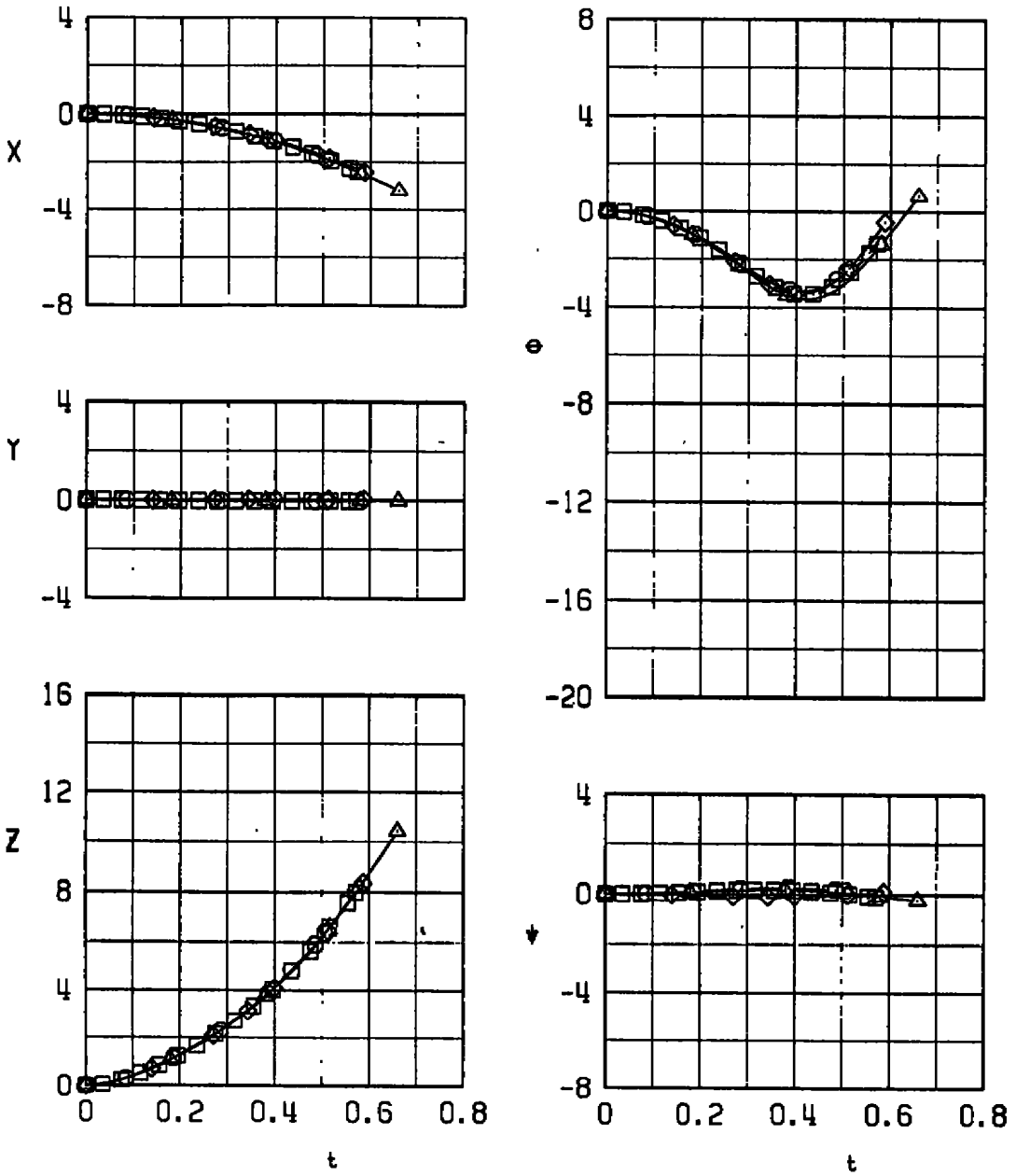

a. $X_{L_1} = 0$, $\omega_m = 0$

Figure 19. Separation trajectories from the centerline pylon station, $M_\infty = 1.63$.

SYM	TUNNEL	REX10^{-6}	ΔT_p	TRAJ
⊡	4T	5.0	0.010	6
◇	A	3.8	TABLE I	6

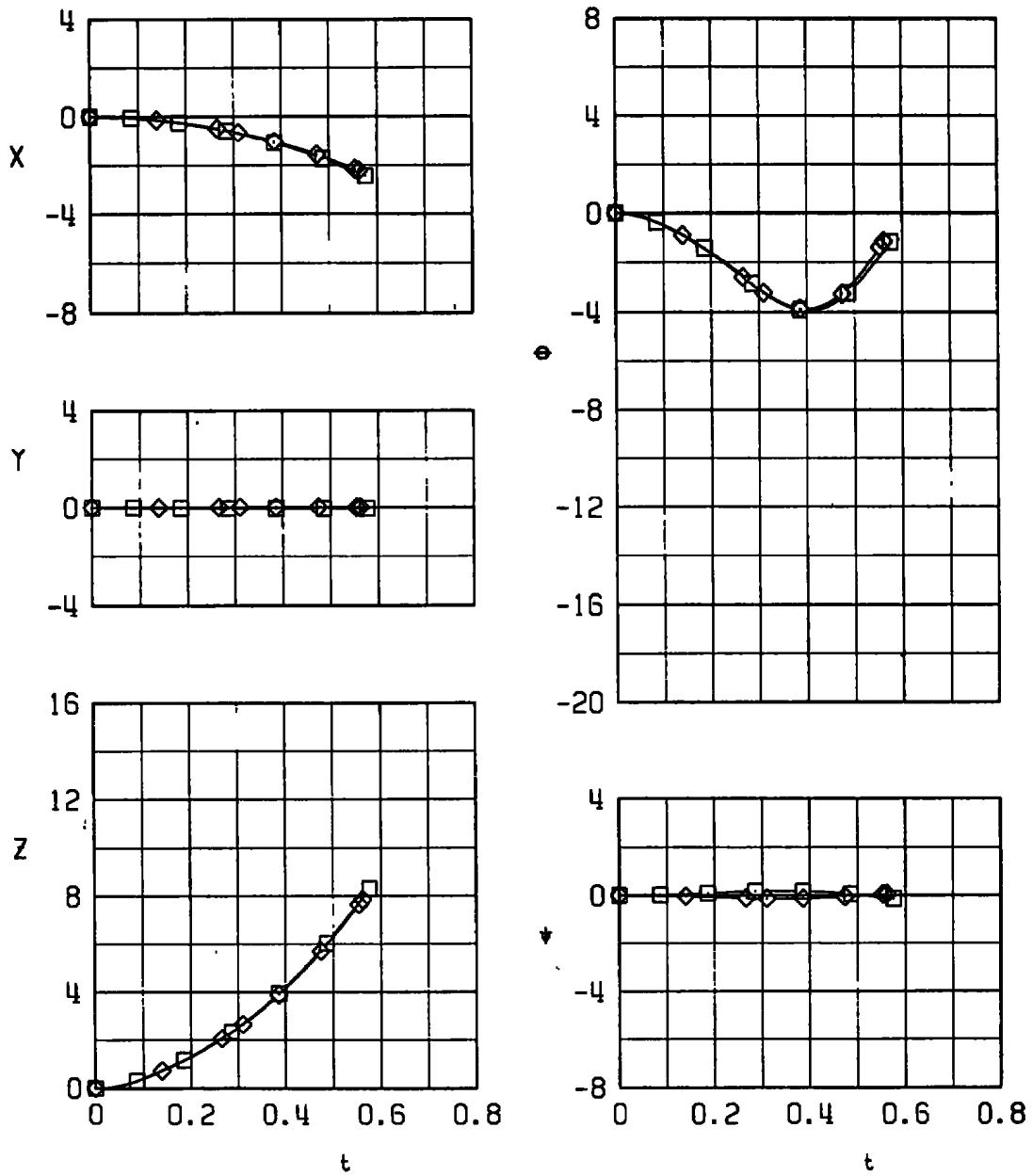

b. X_{L_1} = 0.20 ft, ω_m = 0
Figure 19. Concluded.

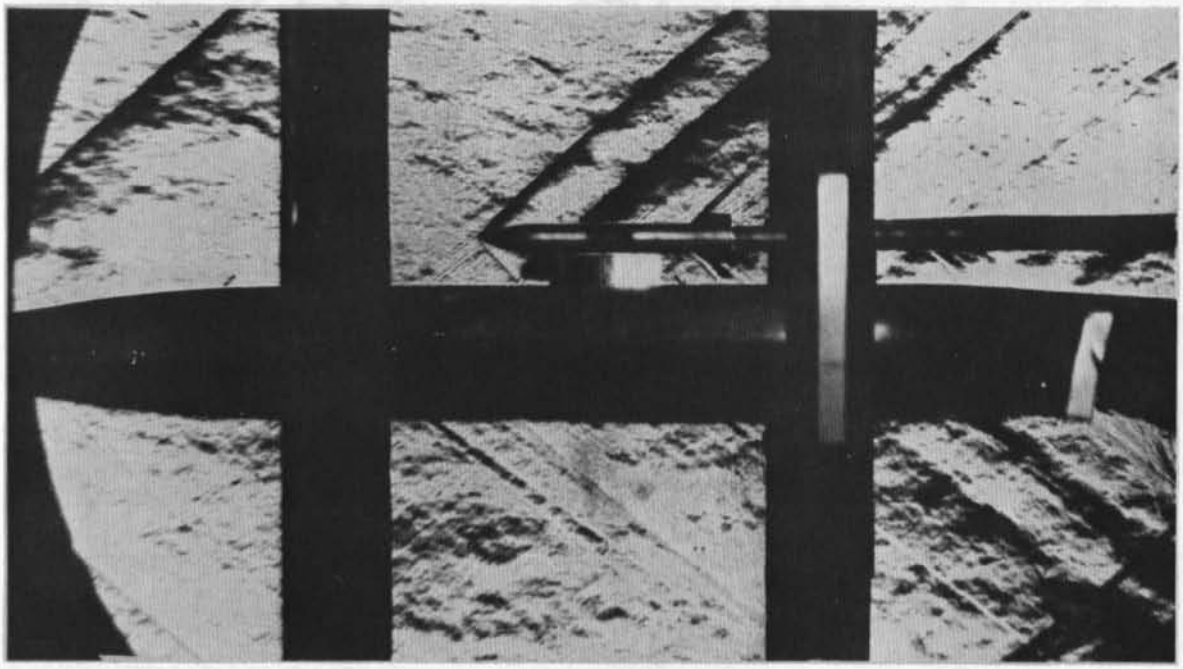

a. Carriage position

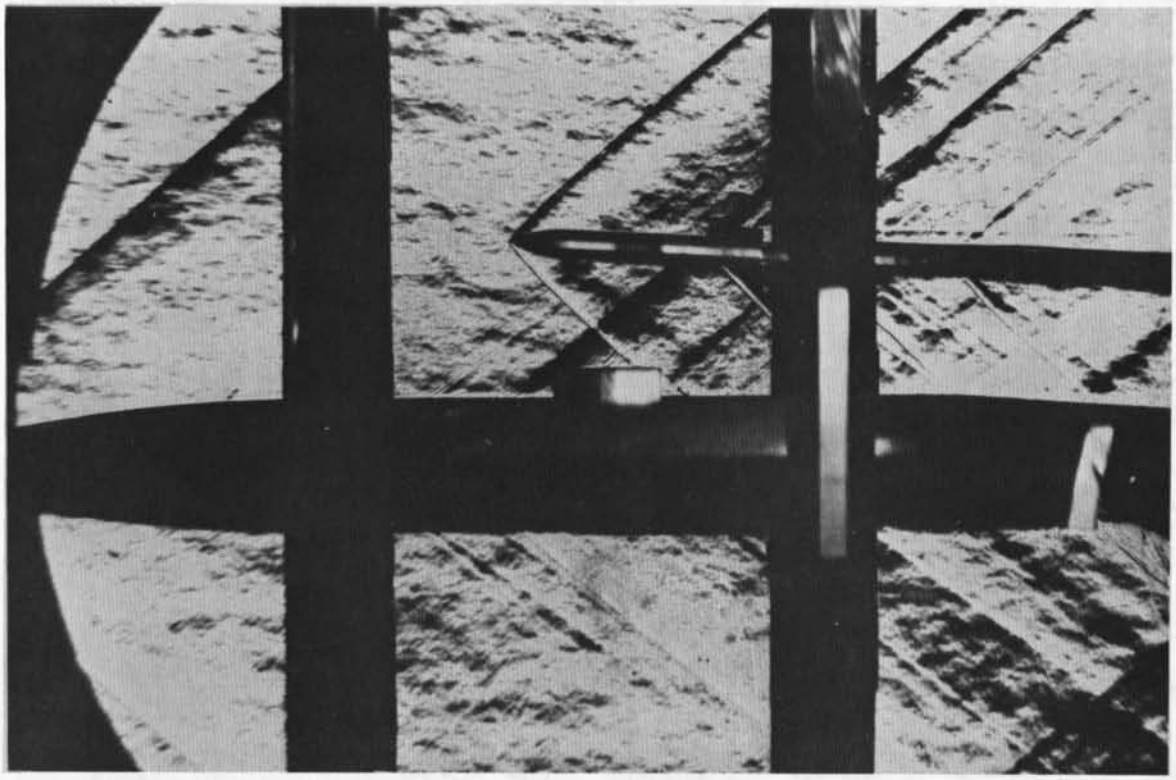

b. End of trajectory

Figure 20. Tunnel a schlieren photograph of the wing-body flow field, M_{∞} = 1.63.

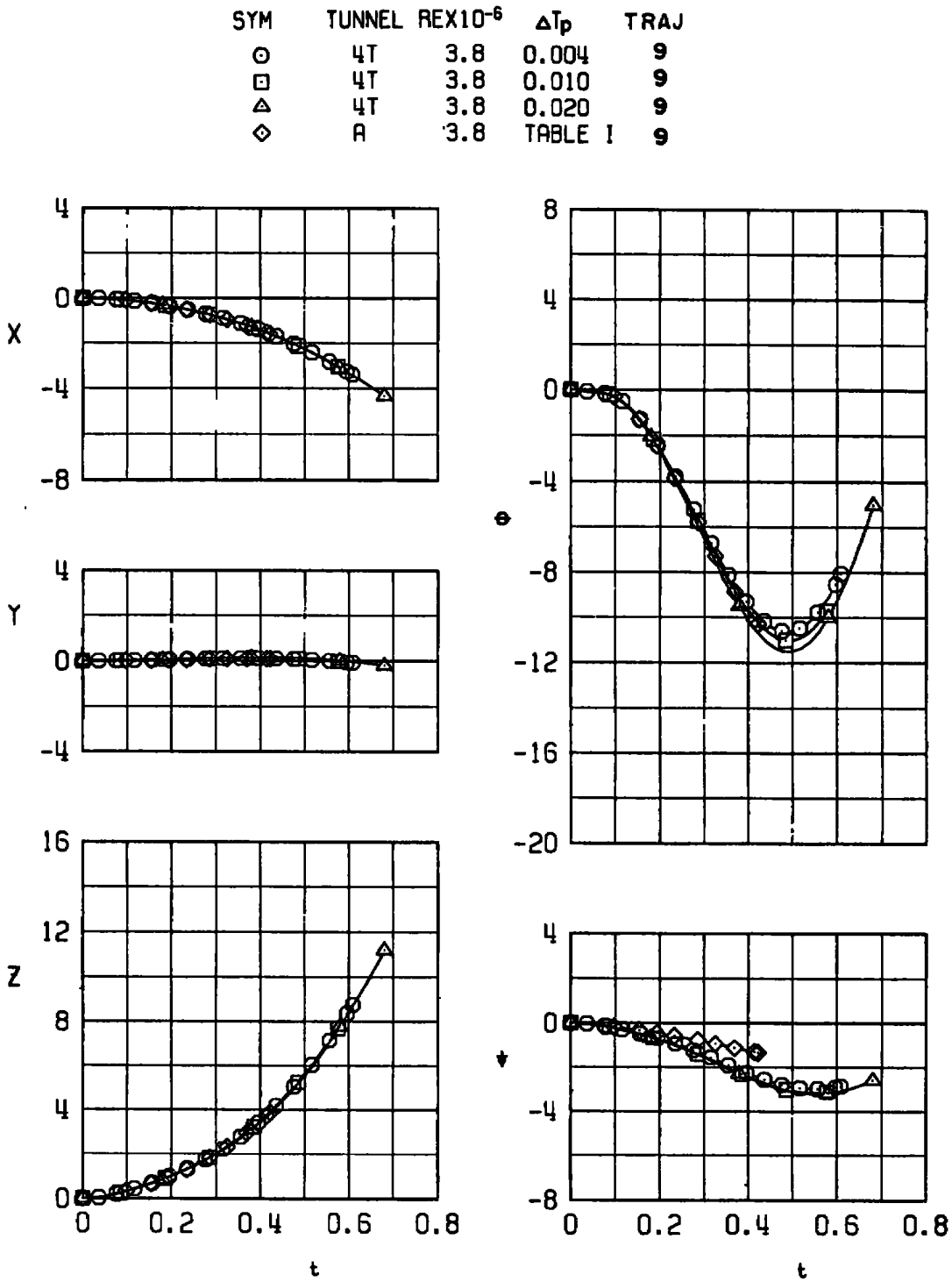

a. X_{L_1} = -1.5 ft, ω_m = 0

Figure 21. Separation trajectories with ejector force from the 1/3-semispan pylon station, M_∞ = 1.63.

SYM	TUNNEL	REX10^{-6}	ΔT_p	TRAJ
⊙	4T	3.8	0.010	8
◇	A	3.8	TABLE I	8

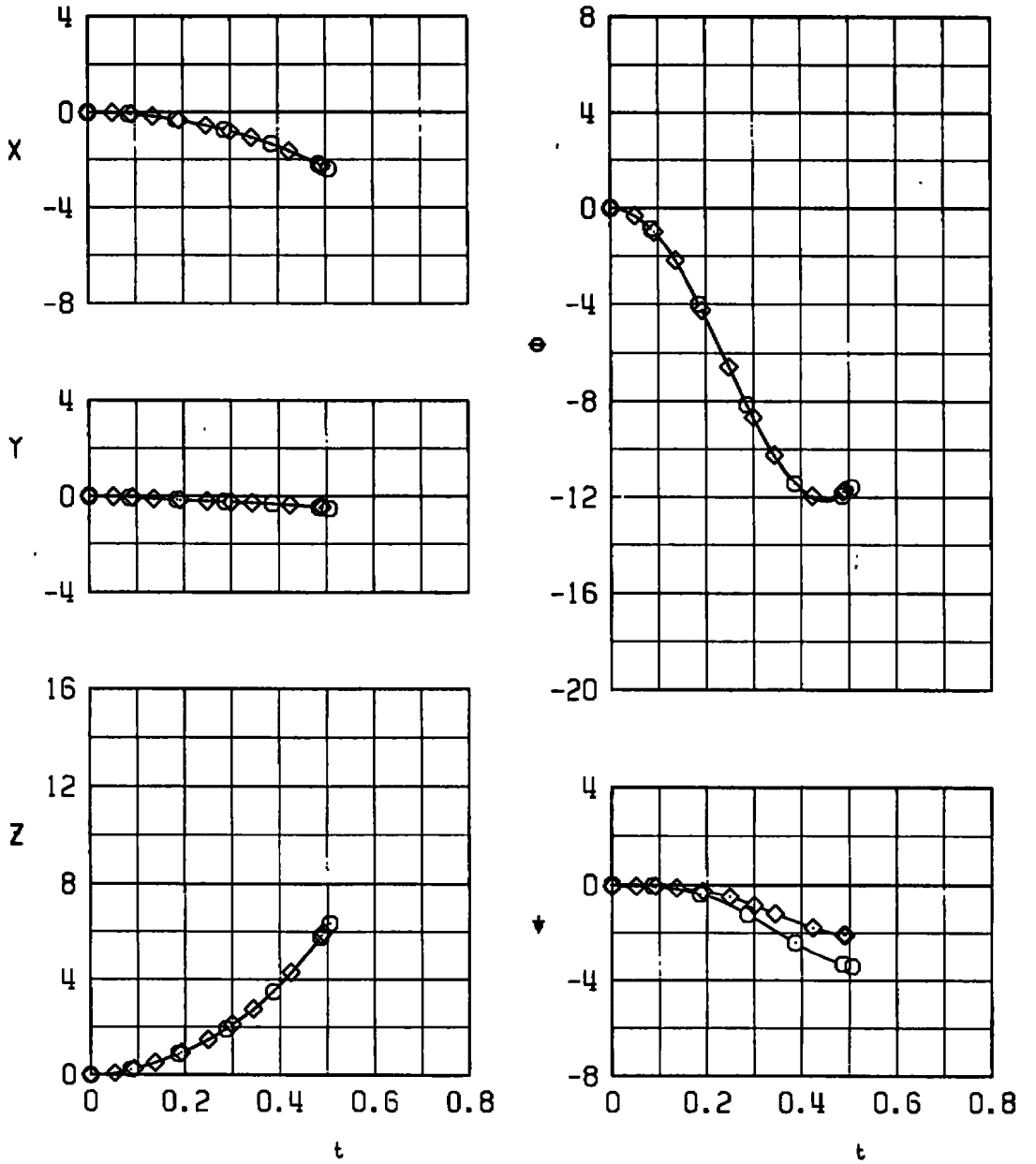

b. X_{L_1} = -0.5 ft, ω_m = 20 deg
Figure 21. Continued.

SYM	TUNNEL	REX10^{-6}	ΔT_p	TRAJ
⊙	4T	3.8	0.010	10
◇	A	3.8	TABLE I	10

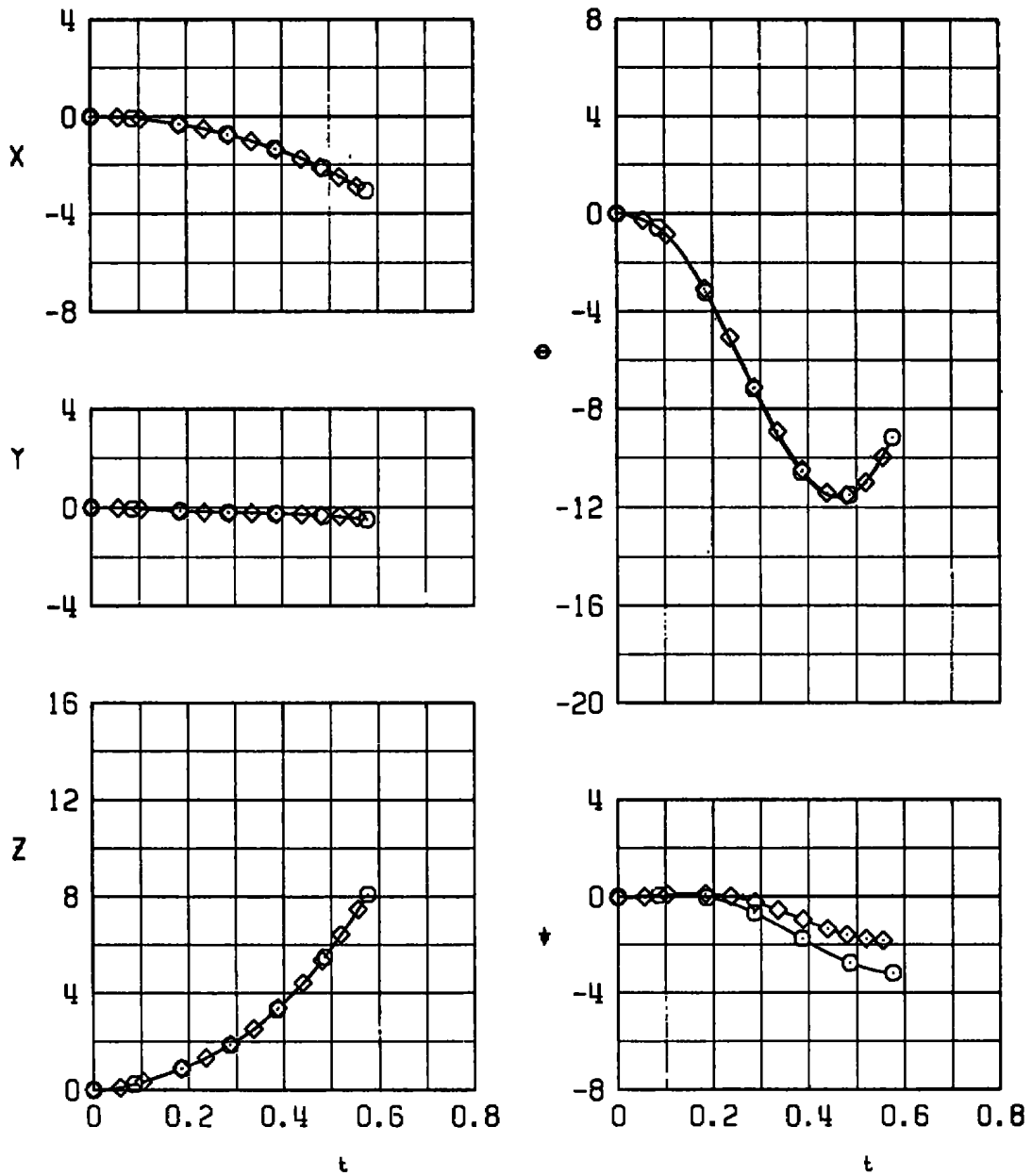

c. X_{L_1} = -1.0 ft, ω_m = 20 deg
Figure 21. Continued.

SYM	TUNNEL	REX10^{-6}	ΔT_p	TRAJ
⊙	4T	3.8	0.010	7
◇	A	3.8	TABLE I	7

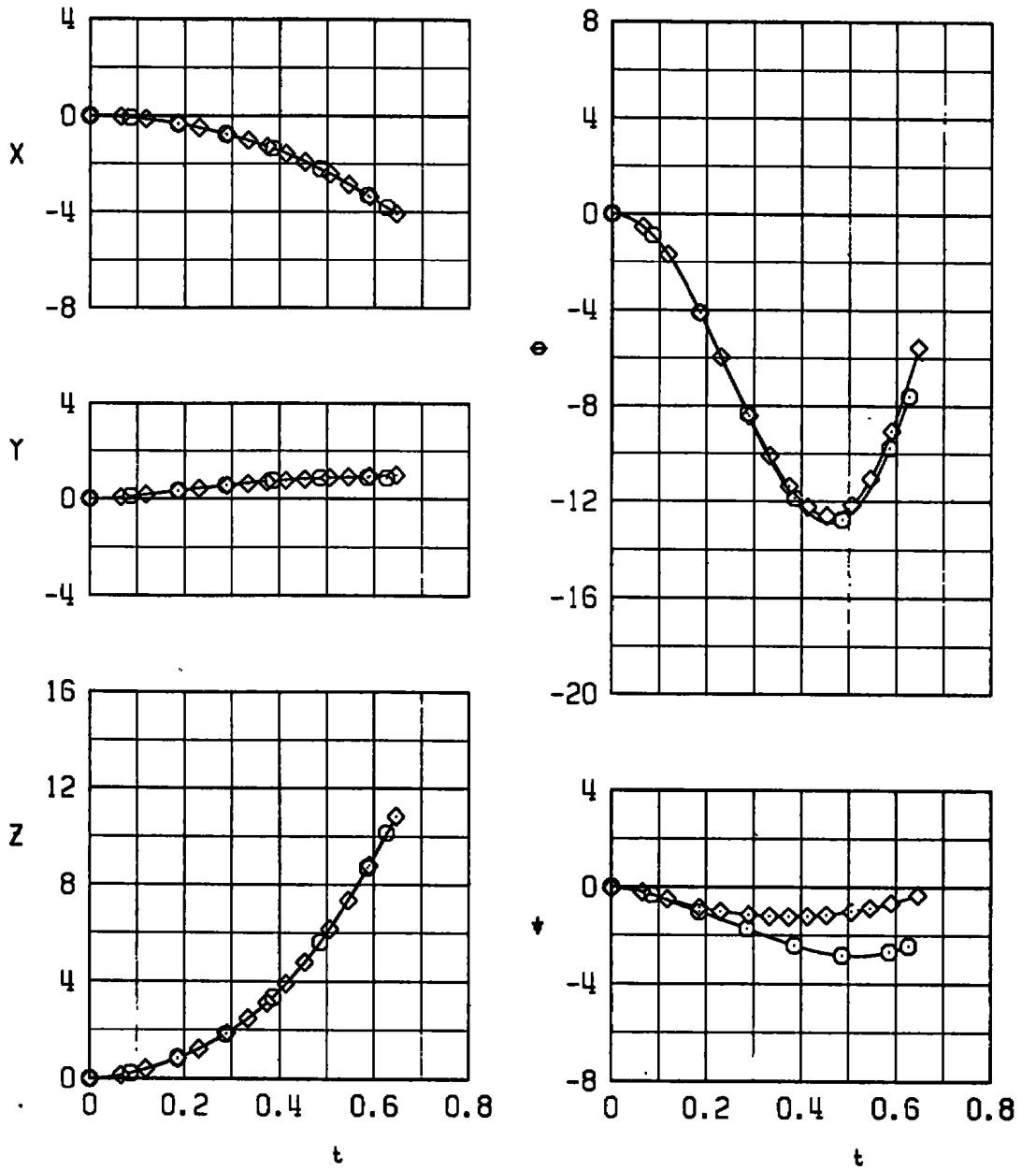

d. X_{L_1} = -0.50 ft, ω_m = -30 deg
Figure 21. Continued.

SYM	TUNNEL	REX10^{-6}	ΔT_p	TRAJ
⊙	4T	3.8	0.010	11
□	4T	5.0	0.004	11
◇	A	3.8	TABLE I	11

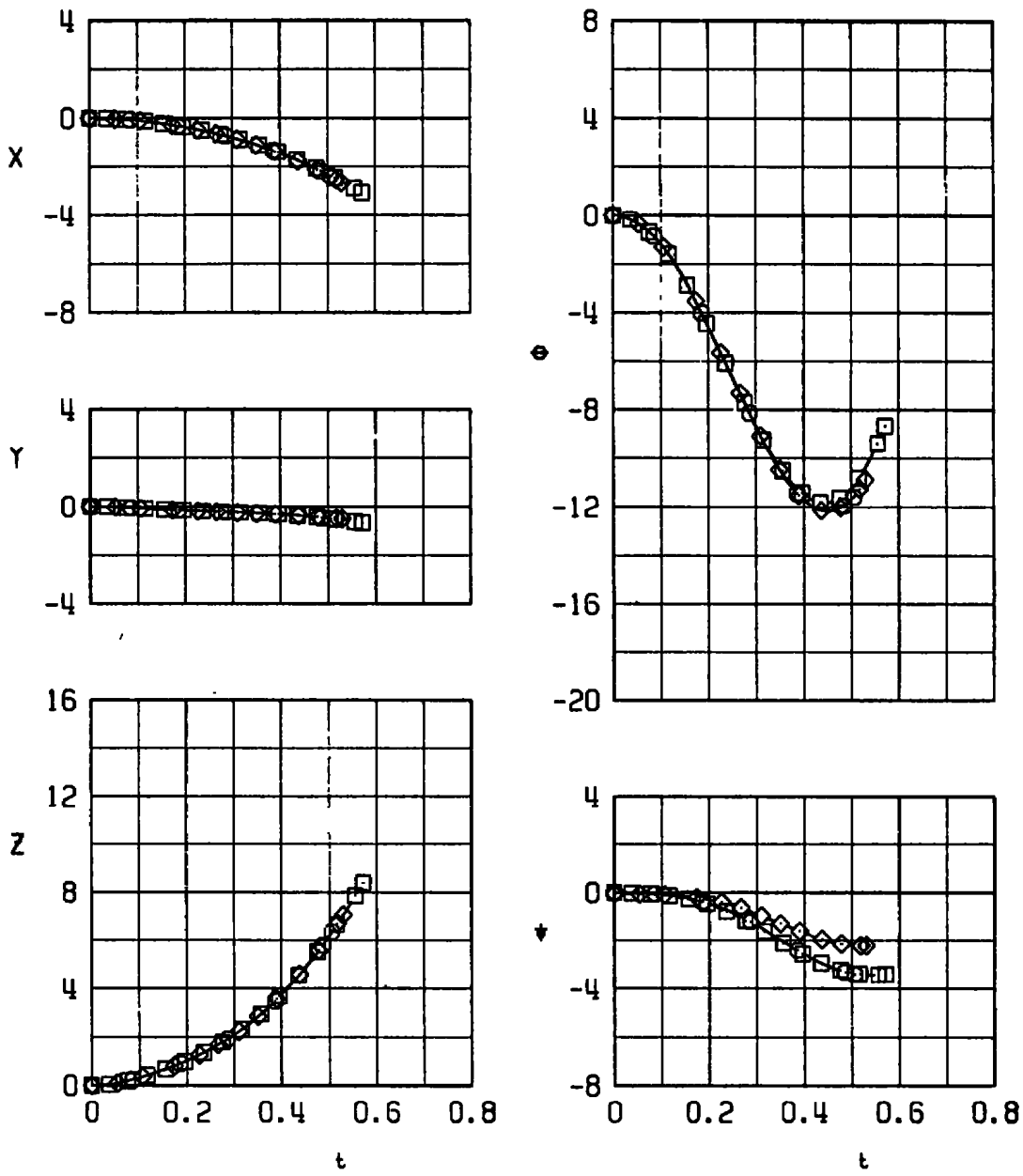

e. X_{L_1} = -0.5 ft, ω_m = 0

Figure 21. Concluded.

SYM	TUNNEL	ΔT_p	TRAJ
⊙	4T	0.010	9
⊡	4T	0.010	9

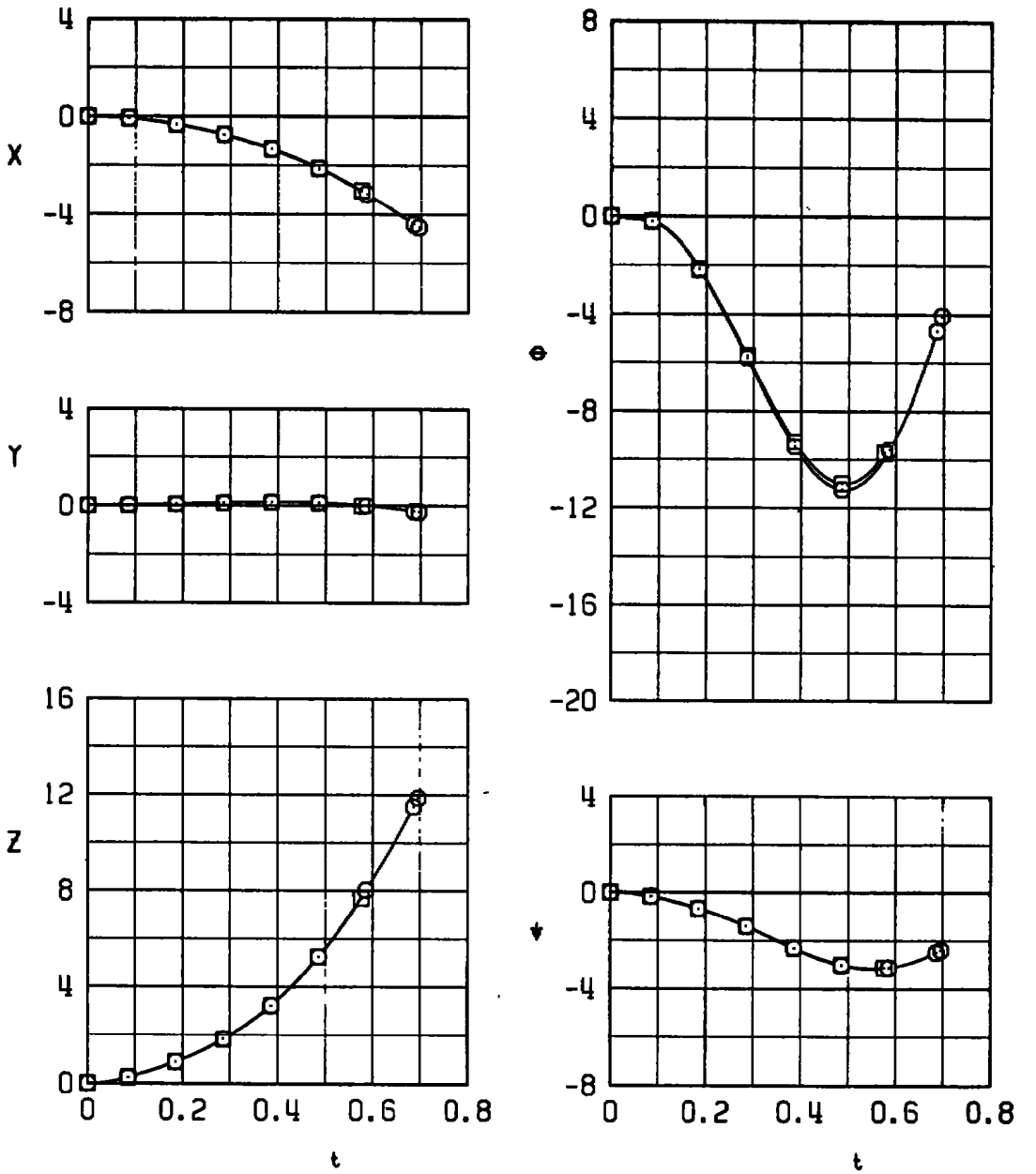

Figure 22. Separation trajectory repeatability from the 1/3-semispan pylon station, M_∞ = 1.63, Re/ft = 3.8 x 10^6.

Table 1. Trajectory Test Summary ($M_\infty = 1.63$)

Trajectory Number	Tunnel Conditions		Location		Trajectory Store Parameters (Tunnels A and 4T)								Tunnel A Trajectory Parameters										Tunnel 4T Trajectory Parameters				Run Ident Number	
	p_t	Re x 10^6	Station	Pylon	Ejector	X_{L_1}	ω_m	I_{xx}	I_{yy}	I_{zz}	X_{cg}	WT	Δt	Δt_p	$\Delta t_{p_{Limit}}$	C_{N_T}	C_{m_T}	C_{A_T}	C_{Y_T}	C_{n_T}	q_s	U_R	Δt_p	XINT	q_s	U_R	VKF	PWT
1	2,670	5.0	Free Stream	—	Yes	0	0	20	700	700	5.313	1,287	0.002	0.010	0.04	0.04	0.01	0.02	0.04	0.01	719	1,554	Var	Var	731	1,577	553	118 119
2	2,670	5.0	↓	—	No	0	0	↓	700	700	↓	↓	↓	↓	↓	↓	0.01	↓	↓	0.01	720	1,554	0.01	5	↓	↓	554	122
3	1,800	3.5	↓	—	Yes	-0.50	0	↓	70	70,000	↓	↓	↓	↓	↓	↓	0.05	↓	↓	0.05	718	1,553	0.01	5	↓	↓	918	238
4	1,800	3.5	↓	—	↓	-0.50	90	↓	70,000	70	↓	↓	↓	↓	↓	↓	0.01	↓	↓	0.01	715	↓	0.01	5	↓	↓	919	239
5	2,670	5.0	Fuselage ℄	Wedge	↓	0	0	↓	700	700	↓	↓	↓	↓	↓	↓	↓	↓	↓	↓	715	↓	Var	Var	↓	↓	650	147
6	2,630	5.0	Fuselage ℄	Wedge	↓	0.20	0	↓	↓	↓	↓	↓	↓	↓	↓	↓	↓	↓	↓	↓	712	↓	0.01	5	↓	↓	651	151
7	2,000	3.8	1/3-Left Wing	Swept	↓	-0.50	-30	↓	↓	↓	↓	↓	↓	↓	↓	↓	↓	↓	↓	↓	711	↓	0.01	↓	↓	↓	911	188
8	2,000	3.8	↓	↓	↓	-0.50	20	↓	↓	↓	↓	↓	↓	↓	↓	↓	↓	↓	↓	↓	722	↓	0.01	↓	↓	↓	912	193
9	2,000	3.8	↓	↓	↓	-1.50	0	↓	↓	↓	↓	↓	↓	↓	↓	↓	↓	↓	↓	↓	717	↓	Var	↓	↓	↓	743	186
10	2,670	5.0	↓	↓	↓	-1.00	20	↓	↓	↓	↓	↓	↓	↓	↓	↓	↓	↓	↓	↓	717	↓	0.01	↓	↓	↓	913	200
11	2,670	5.0	↓	↓	↓	-0.50	20	↓	↓	↓	↓	↓	0.004	0.020	0.08	↓	↓	↓	↓	↓	712	↓	Var	Var	↓	↓	914	201

$C_{\ell_p} = C_{m_q} = C_{n_r} = 0$

$S = 1.2272\ ft^2$

$b = c = 1.25\ ft$

Table 2. Aerodynamic Loads Test Summary ($M_\infty = 1.63$)

P_t, psfa	Re x 10^6	Station	Pylon	X_p, in.	Y_p, in.	Z_p, in.[a]	θ, deg	ψ, deg	Run Ident Number	
									PWT	VKF
2,620	5.0	Free Stream	---	---	---	---	0	0	111, 112 113, 114	---
2,640			---	---	---	---	---	---	115, 116	549, 550 806, 807
2,660		Fuselage ℄	Wedge	0	-1.00, 0, 1.00	0.05 to 8.00	0	0	161	556, 567, 579
2,660				-2					162, 165	558 565 577
2,670				-4					166	560 563 575
				0	-1.44, -0.44, 0.56			-5	167	616 627 639
				-2	-1.44	1.25 to 8.00			168	637
2,000	3.8				-1.44	0.05 to 1.25			170	637
					-0.44, 0.56	0.05 to 8.00			170	618, 625
				-4	-0.44, 0.56	0.05 to 8.00			171	620 623 635
				0	-1.00, 0, 1.00	0.69 to 5.44	-5	0	174	808 819 879
				-2	-1.00	0.69 to 5.44	-5	0	175	817

Table 2. Continued

p_t, psfa	Re x 10^6	Station	Pylon	X_p, in.	Y_p, in.	Z_p, in.[a]	θ, deg	ψ, deg	Run Ident Number	
									PWT	VKF
2,700	5.0	1/3-Left Wing	Swept	0	-1.00, 0, 1.00	0.15 to 8.00	0	0	203	512, 652, 663, 676
2,710	5.0	"	"	-2	"	"	"	"	204	654, 661, 674
2,710 / 1,800	5.0 / 3.4	"	"	-4	"	"	"	"	205	656, 659, 672
1,800	3.4	"	"	0	"	0.90 to 8.65	-7.5	"	208	495, 498, 920, 931, 932
"	"	"	"	-2	"	"	"	"	209	922, 929, 934
"	"	"	"	-4	"	"	"	"	210	924, 927, 936
"	"	"	"	0	1.17	3.15 to 8.65	"	-2	211	943
"	"	"	"	"	-1.00, 0, 1.00	1.79 to 9.29	-15	0	216	491, 974, 985, 986
"	"	"	"	"	-1.44, -0.44, 0.56	0.75 to 8.00	0	-5	218	492, 493, 494, 694, 718, 742
"	"	"	"	-2	"	"	"	"	219	692, 716, 740
"	"	"	"	-4	"	"	"	"	220	690, 714, 738

Table 2. Concluded

p_t, psfa	Re x 10^6	Station	Pylon	X_p, in.	Y_p, in.	Z_p, in.[a]	θ, deg	ψ, deg	Run Ident Number PWT	Run Ident Number VKF
1,800	3.4	1/3-Left Wing	Swept	0	-1.17, -0.17, 0.83	0.90 to 8.65	-7.5	-2	222	499, 502, 943, 944, 955
↓	↓	↓	↓	-2	↓	↓	↓	↓	223	941, 946, 953
↓	↓	↓	↓	-4	↓	↓	↓	↓	224	939, 948, 951
↓	↓	↓	↓	-4	-1.00	3.79 to 8.29	-15	0	226	990
↓	↓	↓	↓	-2	-1.00, 0	1.79 to 8.29	↓	↓	228	976, 988
↓	↓	↓	↓	-4	-1.00, 0	1.79 to 9.29	↓	↓	229	978, 990
↓	↓	↓	↓	0	-1.17, -0.17	↓	↓	-2	230	997, 1,009
↓	↓	↓	↓	-2	↓	↓	↓	↓	231	995, 1,007
↓	↓	↓	↓	-4	↓	↓	↓	↓	232	993, 1,005

[a]The schedule of Z_p values for each θ is as follows:

θ = 0: Z_p = 0.05, 0.10, 0.25, 0.50, 0.75, 1.00, 1.25, 1.50, 2.00, 2.50, 3.00, 3.50, 4.00, 4.50, 5.00, 6.00, 7.00, 8.00.

ψ or θ = -5: Z_p = 0.69, 0.94, 1.19, 1.44, 1.69, 1.94, 2.44, 2.94, 3.44, 3.94, 4.44, 4.94, 5.44.

θ = -7.5: Z_p = 0.90, 1.15, 1.40, 1.65, 1.90, 2.15, 2.65, 3.15, 3.65, 4.15, 4.65, 5.15, 5.65, 6.67, 7.65, 8.65

θ = -15: Z_p = 1.79, 2.04, 2.29, 2.54, 2.79, 3.29, 3.79, 4.29, 4.79, 5.29, 5.79, 6.29, 7.29, 8.29, 9.29.

Table 3. Flow-Field Test Summary (M_∞ = 1.65)

P_t, psfa	Re x 10^6	Station	X, in.	Y, in.	Z, in.	Run Ident Number PWT	Run Ident Number VKF
2,720	5.00	Free Stream	-17 to 25[a]	0	0	62 63	---
2,000	3.77	1/3-Left Wing	-17 to -26[b]	-3.25, -4.00, -4.75	1.37	74	88, 89, 90
↓	↓	↓	↓	↓	2.87	75 76	↓
↓	↓	↓	↓	↓	4.37	77 78	↓
2,720	5.00	↓	↓	↓	1.37	80	↓
↓	↓	↓	↓	↓	2.87	81 82 83	↓
↓	↓	↓	↓	-3.25, -4.00	4.37	84 85	↓
↓	↓	Fuselage ℄	-16 to -26[b]	-0.75, 0, 0.75	2.87	89	91, 92, 93
↓	↓	↓	↓	↓	4.37	90 91	↓
↓	↓	↓	↓	↓	5.87	92 93	↓

[a]Spaced in 2-in. increments.

[b]Spaced in 1-in. increments.

NOMENCLATURE

BL	Wing-body model buttock line from plane of symmetry, in. (see Fig. 5)
b	Store reference dimension for yawing-moment and rolling-moment coefficients, ft, full scale
$\bar{c}$	Store reference dimension for pitching-moment coefficient, ft, full scale
C_A	Store measured axial-force coefficient, axial force/$q_\infty S$
C_{A_T}	External input axial-force coefficient prediction tolerance
C_ℓ	Store measured rolling-moment coefficient, rolling moment/$q_\infty Sb$
C_{ℓ_p}	Store roll-damping derivative, per radian, $dC_\ell/d(pb/2V_\infty)$
C_m	Store measured pitching-moment coefficient, referenced to the store cg, pitching moment/$q_\infty S\bar{c}$
C_{m_q}	Store pitch-damping derivative, per radian, $dC_m/d(q\bar{c}/2V_\infty)$
C_{m_T}	External input pitching-moment coefficient predicition tolerance
C_N	Store measured normal-force coefficient, normal force/$q_\infty S$
C_{N_T}	External input normal-force coefficient prediction tolerance
C_n	Store measured yawing-moment coefficient. referenced to the store cg, yawing moment/$q_\infty Sb$
C_{n_r}	Store yaw-damping derivative, per radian, $dC_n/d(rb/2V_\infty)$
C_{n_T}	External input yawing-moment coefficient prediction tolerance
C_Y	Store measured side-force coefficient, side force/$q_\infty S$
C_{Y_T}	External input side-force coefficient prediction tolerance
FS	Wing-body model fuselage station from model nose, in. (see Fig. 5)
F_{Z1}	Forward ejector force, lb
I_{xx}	Full-scale store moment of inertia about the store X_B axis, slug-ft^2

I_{yy}	Full-scale store moment of inertia about the store Y_B axis, slug-ft^2
I_{zz}	Full-scale store moment of inertia about the store Z_B axis, slug-ft^2
M_∞	Free-stream Mach number
p	Store angular velocity about the Y_B axis, radians/sec
p_t	Free-stream total pressure, psfa
p_∞	Free-stream static pressure, psfa
q	Store angular velocity about the Y_B axis, radians/sec
q_s	Full-scale flight dynamic pressure at launch, lb/ft^2
q_∞	Free-stream dynamic pressure, psf
Re	Free-stream unit Reynolds number per foot
r	Store angular velocity about the Z_B axis, radians/sec
S	Store reference area, ft^2, full scale
TE	Ejector force cutoff time, sec
T_t	Free-stream total temperature, °R
t	Real trajectory time from initiation of trajectory, sec
Δt	Integration interval, sec
Δt_p	Prediction time interval, sec
$\Delta t_{p\,Limit}$	Maximum prediction time interval, sec
U_R	Total velocity of the store with respect to a space-fixed point at launch, ft/sec
V_∞	Free-stream velocity, ft/sec
WL	Wing-body model waterline from reference horizontal plane, in. (see Fig. 5)
WT	Full-scale store weight, lb

X	Separation distance of the store cg from the flight-axis system origin in the X_F direction, ft, full scale
X_{cg}	Axial distance from the store nose to the cg location, ft, full scale
X_{L_1}	Axial distance from the store cg to the forward ejector piston, ft, full scale
X_p	Separation distance of the store cg from the flight-axis system origin in the X_F direction, in., model scale
XINT	External input integer for adjusting integration interval
Y	Separation distance of the store cg from the flight-axis system origin in the Y_F direction, ft, full scale
Y_p	Separation distance of the store cg from the flight-axis system origin in the Y_F direction, in., model scale
Z	Separation distance of the store cg from the flight-axis system origin in the Z_F direction, ft, full scale
Z_p	Separation distance of the store cg from the flight-axis system origin in the Z_F direction, in., model scale
Z_T	Location of CTS roll axis from tunnel centerline, in.
α	Aircraft model angle of attack relative to the free-stream velocity vector, deg
α_{xy}	Angle between the projection of the local flow velocity vector in the X_F-Y_F plane and the X_F axis, deg
α_{xz}	Angle between the projection of the local flow velocity vector in the X_F-Z_F plane and the X_F axis, deg
θ	Angle between the store longitudinal (X_B) axis and its projection in the X_F-Y_F plane, positive when store nose is raised as seen by the pilot, deg
ϕ_m	Roll angle between the store model Y_B axis and the balance side-force direction, positive for clockwise rotation of the store model with respect to the balance, deg (see Fig. 10)
ψ	Angle between the projection of the store longitudinal (X_B) axis in the X_F-Y_F plane and the X_F axis, positive when the store nose is to the right as seen by the pilot, deg

ω_m Ejector piston line of action with respect to the store X_B-Z_B plane, positive for clockwise rotation when looking upstream, deg

LIGHT-AXIS SYSTEM DEFINITIONS

Coordinate Directions

X_F Parallel to the current aircraft flight path direction, positive forward as seen by the pilot

Y_F Perpendicular to the X_F and Z_F directions, positive to the right as seen by the pilot

Z_F Parallel to the aircraft plane of symmetry and perpendicular to the current aircraft flight path direction, positive downward as seen by the pilot

Origin

The flight-axis system origin is coincident with the store cg at release. The origin is fixed with respect to the aircraft and thus translates along the current aircraft flight path at the free-stream velocity. The coordinate axes rotate to maintain alignment of the X_F axis with the current aircraft flight path direction.

STORE BODY-AXIS SYSTEM DEFINITIONS

Coordinate Directions

X_B Parallel to the store longitudinal axis, positive direction is upstream at store release

Y_B Perpendicular to X_B and Z_B directions, positive direction is to the right looking upstream when the store is at zero yaw and roll angles

Z_B Perpendicular to the X_B direction and parallel to the X_F-Z_F plane when the store is at zero yaw and roll angles, positive direction is downward as seen by the pilot when the store is at zero pitch and roll angles

Origin

The store body-axis system origin is coincident with the store cg at all times. The X_B, Y_B, and Z_B coordinate axes rotate with the store in pitch, yaw, and roll so that mass moments of inertia about the three axes are not time-varying quantities.